TECHNICAL REPORT STANDARD TITLE PAGE

1. Report No.	2. Government Accession No.	3. Recipient's Catalog No.

4. Title and Subtitle	5. Report Date
SAR Calibration Technology Review	August 1981
	6. Performing Organization Code
7. Author(s)	8. Performing Organization Report No.
J. L. Walker and R. W. Larson	150400-7-F
9. Performing Organization Name and Address	10. Work Unit No.
Environmental Research Institute of Michigan Radar and Optics Division P. O. Box 8618 Ann Arbor, Michigan 48107	11. Contract or Grant No. NAS 9-16135
	13. Type of Report and Period Covered Final Report 29 May 1980 through 31 July 1981
12. Sponsoring Agency Name and Address NASA/Lyndon B. Johnson Space Center Houston, Texas 77058	14. Sponsoring Agency Code

15. Supplementary Notes

16. Abstract

This report presents a review of SAR calibration technology including a general description of the primary calibration techniques and some of the factors which affect the performance of calibrated SAR systems. The use of reference reflectors for measurement of the total system transfer function along with an on-board calibration signal generator for monitoring the temporal variations of the receiver to processor output is a practical approach for SAR calibration. However, preliminary error analysis and previous experimental measurements indicate that reflectivity measurement accuracies of better than 3 dB will be difficult to achieve. This is not adequate for many applications and, therefore, improved end-to-end SAR calibration techniques are required.

17. Key Words	18. Distribution Statement
Synthetic aperture radar Radar cross section Amplitude calibration Signal dependent noise Reference reflectors Clutter	

19. Security Classif. (of this report)	20. Security Classif. (of this page)	21. No. of Pages	22. Price
Unclassified	Unclassified	xi + 145	

FOREWORD

This is the final report for Contract NAS9-16135, Systems Analysis Support of Advanced Synthetic Aperture Radar Project sponsored by NASA Lyndon B. Johnson Space Center. The work reported here was performed by members of the Radar and Optics Division, ERIM under the direction of Dr. A. Kozma.

The principal investigator for the project was Dr. J.L. Walker. In addition, R.W. Larson contributed substantially to this work.

This contract was monitored by Dr. Kumar Krishen, NASA Lyndon B. Johnson Space Center, Houston, TX.

ACKNOWLEDGEMENTS

The authors gratefully acknowledge the support of the Radar and Optics Division Staff during this project. In particular, T. Lewis attended AdSAR design reviews, B. Thelen assisted with SAR analysis programs and made important contributions in the area of statistical error analysis. We also thank R. Shuchman for reviewing this report and providing helpful suggestions and R. Hamilton for his work in reviewing and editing the final draft.

PRECEDING PAGE BLANK NOT FILMED

TABLE OF CONTENTS

TABLE OF CONTENTS
(Concluded)

LIST OF FIGURES

LIST OF FIGURES
(Concluded)

LIST OF TABLES

1 INTRODUCTION

The use of synthetic aperture radar (SAR) for earth resource applications is motivated by the all-weather day/night operation of these systems and their capability of providing fine resolution microwave reflectivity data at long ranges. SAR systems have been used successfully for many years especially in military reconnaissance and target acquisition applications. These applications have primarily exploited the SAR image data to provide information related to the position, shape, and the relative reflectivity distribution of various scattering objects.

There are many other potential earth resource applications for problems in geology, agriculture, oceanography, and ice monitoring which require the capability of making absolute radar cross section measurements. In addition, when designing target acquisition radars, necessary inputs for most detection algorithms are the radar cross section characteristics of tactical targets and ground clutter. There exists only a limited amount of experimental data of this type. Moreover, the complexity and variety of targets and terrain types as well as the presence of both natural and cultural contaminating objects, make it very difficult to derive a useful theoretical model to predict microwave reflectivity in general. Therefore, it is necessary to depend heavily upon experimental measurements that can be obtained from a calibrated SAR, i.e, a SAR whose total transfer function (scene reflectivity to output image signal) is known.

In mid-1980, the Radar and Optics Division of ERIM initiated an effort under the sponsorship of NASA/JSC to provide systems analysis support for the joint JSC/JPL Advanced Synthetic Aperture Radar Project. The objective of this project was to develop and demonstrate new technology for future SAR systems. Accurate, absolute amplitude calibration was one of the key technology areas to be investigated. The Radar and Optics Division's role was to provide technical support

by attending design review meetings, providing technical critique and recommendations on the material presented at these meetings, and reviewing relevant SAR calibration technology. This report presents a summary of the work performed under this contract.

In Section 2, various potential applications of amplitude calibrated SAR systems are briefly described, along with estimates of calibration performance requirements. Section 3 presents a review of the basic SAR calibration problem and discusses some of the factors that affect our ability to calibrate a SAR. For background purposes and to establish consistent definitions of terms, various conventional SAR performance parameters are reviewed in Section 4 along with three additional parameters which are directly related to calibrated SAR systems. Techniques for calibrating a SAR are described in Section 5, important aspects that must be considered when designing a calibrated system are described in Section 6, and various error sources that affect reflectivity measurements are described in Section 7. A review of previous SAR calibration programs is presented in Section 8 along with some of the key results. During the early portion of this project, the Advanced SAR System specifications and design approach were reviewed. For completeness of this final report, a summary of these results is given in Section 9. Finally, Section 10 provides some recommendations for future SAR calibration work.

2
APPLICATIONS OF CALIBRATED SAR SYSTEMS

This section presents a brief overview of different applications for calibrated SAR data along with some representative references. Each of the various application areas mentioned has requirements for a SAR system that include a calibration capability. Calibration requirements include spatial accuracy, image aspect ratio, and other image parameter specifications in addition to amplitude calibration. The purpose of this brief discussion on applications is only to identify the disciplines and areas of study for which calibrated SAR data has been used or is required. The reader is referred to various references for detailed information, particularly the workshop reports [1,2] for extensive reference lists.

Calibration of SAR data is generally thought of in either a relative or absolute sense. In the relative sense, the earth scientist is interested in obtaining SAR images that are free of system effects. This means that differences in image intensity should be a function of target reflectivity only. System effects such as antenna gain, recorder gain, R^3 power loss, and change in effective resolution cell size are all corrected. Occasionally, the earth scientist also wants the natural target reflectivity (which is a function of incidence angle) to also be normalized within the image. This facilitates machine classification of the data.

Absolute calibration is necessary when SAR data from different passes or different days are to be compared. For example, if a soil moisture scientist wants to look at SAR images collected over a one-month period, absolute calibration is required. A geologist may require absolute calibrated data when comparing orthogonal-look-direction data.

Absolute amplitude calibration capability in a SAR system provides an additional dimension to the data. Information regarding the values of radar cross section (RCS) for a wide variety of objects becomes available for interpretation and classification when calibration is realized. Also, considerable information regarding values of the scattering coefficient σ° for a variety of terrain types becomes available. Classification of target types and terrain, in general categories, may prove to be possible. Also target scattering centers and calibrated distributions of terrain types can be measured to provide additional information for classification. Further, if calibrated dual-channel SARs are considered with orthogonal polarizations or different wavelengths, classification by polarization and/or wavelength scattering properties may provide yet another basis on which to classify targets and terrain types. It is thus clear that SAR calibration capability can be utilized for extending data exploitation.

Additionally, calibrated SAR data can be used to aid in the validation of diffuse terrain and sea radar backscatter models. It is realized that calibrated SAR measurements of every terrain feature of interest to the earth scientist are not possible.

A summary of SAR calibration requirements for various applications is included in Table 2.1. As indicated in the table, there are numerous specifications that have not, as yet, been determined. Thus, many more experiments are needed. With the availability of a calibrated SAR, a number of experiments can be defined to provide quantitative data with which to help determine the utility of calibrated data and calibration requirements for various remote sensing applications. Calibration performance parameters are described in more detail in Section 4.

Some of the important applications of calibrated SAR systems are discussed in the following paragraphs.

TABLE 2.1. SAR CALIBRATION REQUIREMENTS.

Values of uncertainty for various calibration parameters
(Uncertainty values in dB)

Calibration Performance Parameter	Application Areas: Clutter Statistics DoD	Target Signature	Soil Moisture	Crop Class.	Ice Class.	Geology	Oceanography	Agricultural (Forestry, Soils)
Reflectivity Measurement Accuracy	<1 dB	Best Achievable	<2 dB	<1 dB	TBD	NA	TBD	1-2 dB
Measurement Resolution (Relative) Single Chan	NA	(Estimated) (<3 dB)	<2 dB	~1 dB	<3 dB	TBD	<3 dB (sea truth required)	1 dB
Measuremen. Resolution (Relative) Multi-Channel:								
Polarization	NA	TBD	<2 dB	TBD	TBD	TBD	TBD	<2 dB
Frequency		TBD	<2 dB	TBD	TBD	TBD	TBD	<2 dB
Measurement Precision	Best	Best	1 dB	1 dB	TBD	TBD	TBD	1 dB
Spatial Resolution	3-5 m	Best	20 m	10 m	10 m	10 m	10 m	20 m

Clutter Statistics

To date, the objective of all SAR calibration programs conducted by ERIM has been to gather calibrated SAR data for use in calculating backscatter statistics for various types of terrain. Several such SAR calibration programs are discussed in Section 8. Histograms of data obtained with a calibrated SAR have been used to provide input to define radar clutter models [3-5]. Clutter models are utilized in radar system design for detectability criteria. Example results obtained are given in Appendix A.

Soil Moisture Determination

The ability to compute an absolute value of reflectivity σ° of a given area, made possible by calibrated data, can be utilized to determine a measure of soil moisture. Knowledge of the soil type greatly improves the accuracy in the estimated value of soil moisture. The absolute value of σ° of particular areas, obtained from a series of images over an extended time period, can be compared to obtain crop yield estimates based on soil moisture. Although there are many discussions of this application regarding the limitations based on "soil-moisture measurements", a carefully defined and conducted verification experiment using SAR is required to determine the achievable accuracy [6-8].

Target Classification

RCS measurements of a large class of targets (i.e., vehicles, ships) indicate some general trends. For example, the expected value of RCS, on the average, is larger for trucks than for tanks. Quantitative measures of the RCS values may be useful in a rough automatic classification scheme [9-10]. In addition, the measurement of the RCS of the component scattering centers that comprise a target signature may also be useful for target classification.

Crop Classification

Results of ground measurements of the σ° values of a large number of fields, with and without growing crops indicate a clustering by crop type. Periodic coverage, by SAR, of areas of interest and the comparison of the absolute values of σ° values can yield information on crop type and crop growth. The estimates are improved with the utilization of other a priori information such as season, rainfall, past crop history, etc. [11-16]

Oceanography

Absolute values of the σ° values for the sea can be utilized to obtain estimates of surface wind velocity, sea roughness, and (perhaps) wave heights [17-22]. Also, last but not least, a very important application for a calibrated SAR is for sea ice surveillance and ice classification [23-30].

3
SUMMARY OF THE SAR CALIBRATION PROBLEM

Some applications of SAR systems, as indicated in the previous section, require the measurement of radar cross section (RCS) of various scene elements. Depending on the application, the required measurements can be either the RCS associated with scattering centers of a specular target or the RCS per unit area (backscatter coefficient) σ° of diffuse terrain.

Generally, an estimate of the mean value of σ° is desired, although the higher-order statistics are sometimes of interest. As is well known, superimposed on the average terrain reflectivity is a noise-like granularity often referred to as coherent speckle. When there are a large number of small scatterers in a resolution cell, the amplitude of the SAR image is often modeled as a Rayleigh distribution witn the phase uniformly distributed between 0 and 2π. This model appears to be valid for coarse-resolution SARs when there are no large RCS point-like scatterers in the scene. Sometimes, Weibull or some other form of probability density function is more suitable. In addition, of course, macroscale reflectivity variations occur for typical farmland due to variations in soil moisture within a field or from field to field; the σ° statistics for such farmland are often of interest.

A SAR system provides an image whose power (squared-modulus of complex amplitude) varies as a function of the RCS of each resolution cell. This relationship between reflectivity and output image power is not generally known in an absolute sense unless the total system transfer function is carefully measured. In accordance with the general definition of the word calibrate (i.e., "to graduate a gauge of any kind with allowance for its irregularities so that the gauge can be used to provide an absolute measurement"), the calibration if a SAR is defined as the measurement of the total system transfer function so that the SAR output can be related to the reflectivity of the scene in an absolute sense.

It should be noted that, even if the radar could be calibrated to achieve a high degree of measurement accuracy, there is always the inherent statistical variation of the terrain reflectivity itself which implies that a large number of independent measurements may be required to estimate the average value of σ° with small variance. This should not be confused with the basic accuracy and precision of the calibrated SAR.

As is well known [31] from the radar range equation and simplified SAR models, the power P_I at the output of the image-formation processor is given by

$$P_I = \frac{P_T\, G^2(\theta)\, \lambda^2}{L\,(4\pi)^3\, R^4} H_R\, \sigma\,, \tag{3.1}$$

where P_T = average transmitter power,

$G(\theta)$ = antenna gain as a function of depression angle θ,

L = system losses (propagation losses, transmission line losses, radome losses),

λ = wavelength,

R = range,

H_R = receiver to processor output gain function (including the effects of azimuth and range compression), and

σ = radar cross section.

This can be rewritten in the form

$$P_I = K_p \frac{G^2(\theta)}{R^4} H_R\, \sigma\,, \tag{3.2}$$

where K_p is given by

$$K_p = \frac{P_T\, \lambda^2}{L(4\pi)^3}\,.$$

It is, therefore, conceptually straightforward to estimate σ from a SAR image if one has a knowledge of the total transfer function

$$H_S = K_p \frac{G^2(\theta)}{R^4} H_R \ . \tag{3.3}$$

The power, P_I, associated with the reflector response in the image is measured and σ is determined from H_S (P_I versus σ curve).

Similarly, for the case of diffuse terrain, the power P_I is measured over the particular image area A_C of interest (referenced to ground plane) and an estimate of σ° can be obtained from the relation

$$\sigma^\circ = H_S^{-1} \frac{P_I}{A_C} \ . \tag{3.4}$$

The SAR calibration process of determining the total system transfer function typically requires several measurement steps, as described in Section 5. In principle, the SAR calibration process is much like calibrating any measuring instrument. It consists of (1) collecting SAR data for some type of standard reference reflector field with known reflectivity, (2) performing measurements on the resulting imagery, and (3) calculating the system transfer function H_S.

As indicated in Figure 3.1, some applications require only a relative measurement of reflectivity, e.g., a comparison of the backscatter coefficient of one portion of the scene with respect to another portion. In this case, it is not necessary to calibrate the SAR in the sense of an absolute measurement of the total transfer function. The primary requirements for relative measurements are that the transfer function be stable i.e., not vary between successive measurements) and that the total system noise be sufficiently low to permit one to resolve small differences in reflectivity.

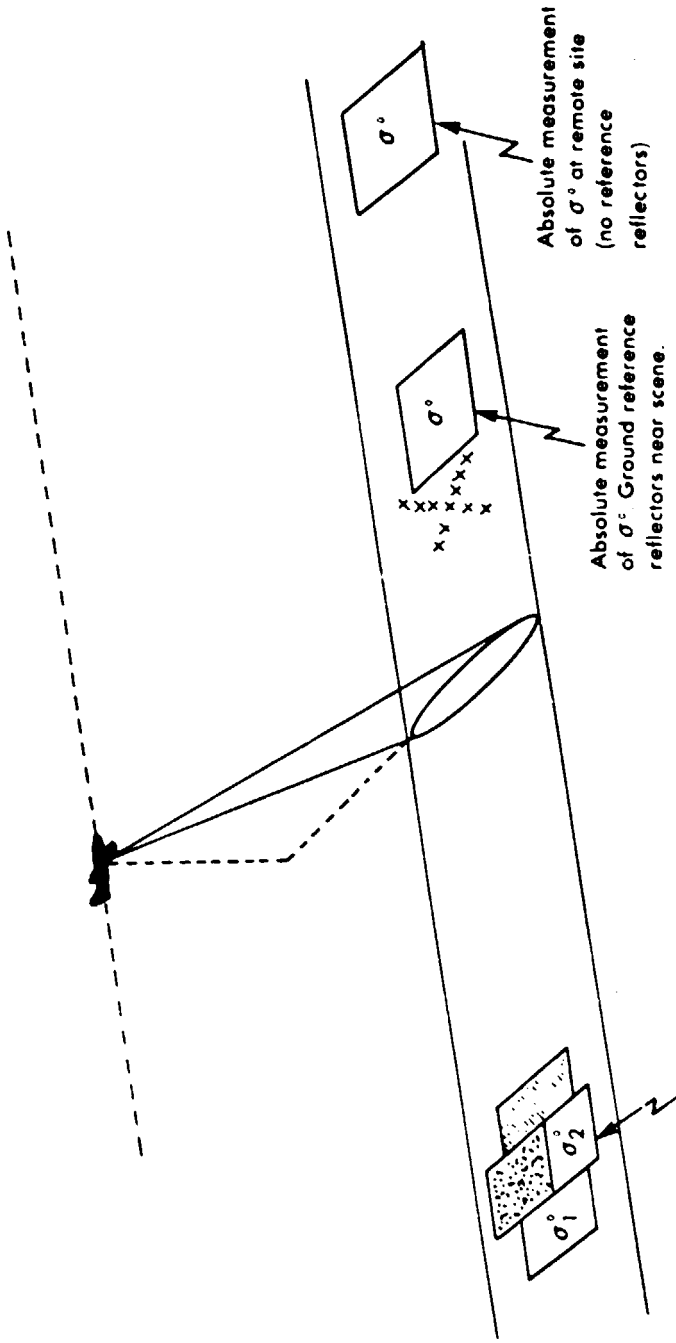

FIGURE 3.1. REFLECTIVITY MEASUREMENTS.

Similarly, for situations requiring an absolute measurement of reflectivity, but with reference reflectors of known RCS in or near the area to be measured, a complete explicit knowledge of the total transfer function is not necessary. The remaining case depicted in Figure 3.1 (i.e., absolute reflectivity measurements with no in-situ reference reflectors) requires complete system calibration as defined here.

There are a number of practical problems associated with SAR calibration which must be solved in order to have a system with sufficient accuracy and precision to be useful. First, there are difficulties in achieving reliable reflectivity references. Knowledge of the "true" value of reflectivity is limited by the accuracy of some other measurement device, whether it be anechoic chamber measurements or an auxiliary calibrated SAR, scatterometer, etc. In addition, other factors discussed in Section 7.1, such as reflector pointing errors and multipath effects, contribute to the overall uncertainty of the references to be used for SAR calibration.

There are uncertainties in virtually every part of the system, as indicated in Figure 3.2, which contribute to the total SAR calibration error. For example, errors in any of the parameters in the system transfer function, such as antenna gain as a function of depression angle, variation in system losses, transmitter power variations, etc. will all contribute to a reduction in reflectivity measurement accuracy. These errors are described in more detail in Section 7.3. Most of these errors can be minimized in a well-designed SAR system; however, transmitter power monitoring and a calibrated signal generator which injects controlled signals into the receiver for monitoring the receiver-processor gain are usually required. Unfortunately, the most serious factors are antenna gain uncertainties and geometry uncertainties which are not alleviated by on-board signal monitoring.

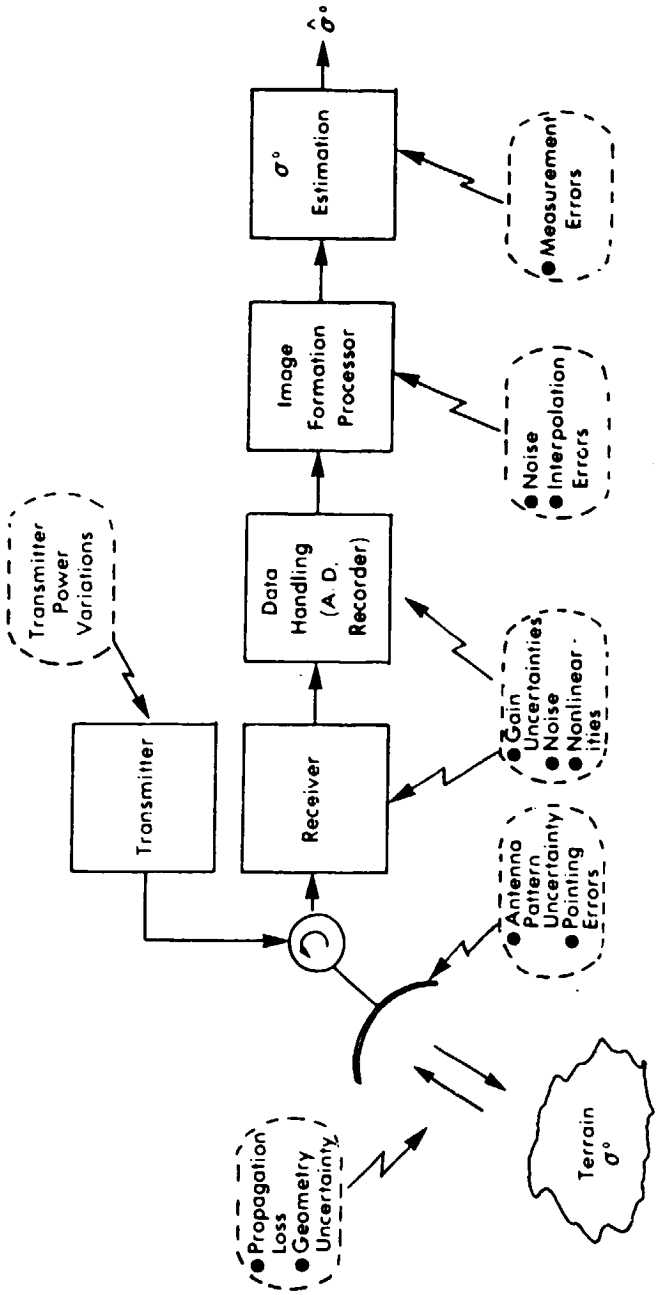

FIGURE 3.2. SAR CALIBRATION PROBLEM.

Various noise sources throughout the system also make it difficult to achieve accurate reflectivity measurements and even our ability to distinguish small differences in terrain reflectivity. As described in Section 4, the total noise consists of both additive noise (primarily receiver thermal noise) and signal dependent noise. Nonlinearities in the system are not only a significant source of signal dependent noise (intermodulation and saturation effects), but can also cause gain compression of large signals and small signal suppression [32-33].

Good system calibration imposes requirements for both well-designed, well-characterized (knowledge of errors, etc.) stable instrumentation and a methodology that provides for proper measurement, parameter monitoring, and periodic verification.

This section of the report has provided a brief summary of the SAR calibration problem. More detailed descriptions of SAR calibration techniques and system design considerations are presented in Sections 5 and 6, respectively.

4
CALIBRATED SAR PERFORMANCE PARAMETERS

For background purposes and to establish some common definitions, a set of parameters that describe the performance of calibrated SAR systems are described in this section.

The design of a SAR involves the detailed design of each of the major subsystems such as the antenna, transmitter, receiver, motion compensation, image-formation processor, etc. including the selection of the various hardware elements. Prior to undertaking this complex hardware design, it is important to establish specifications for each of the subsystems and to determine a consistent set of SAR system parameters (i.e., satisfy ambiguity constraints, radar range equation, etc.) so that the complete SAR system will meet its requirements. The requirements depend strongly on the particular application, such as ocean surveillance, crop classification, target acquisition, etc. Each type of application will lead to a set of user requirements, such as target size and cross section, terrain reflectivity specifications (max, min σ°), wavelength, polarization, etc. Many of the parameters necessary to completely specify a SAR system do not follow obviously from the user requirements, but must be established by means of utility studies involving experimentation, analysis, and experience.

The SAR system parameters can be partitioned into two categories. The first category consists of functional requirements. These are system parameters that define functions to be performed or methods to be used, e.g., mode of operation, polarization, wavelength, etc. The second category contains the system parameters related to performance. These are primarily image quality parameters.

In the past, it has been common to specify a SAR system primarily based on various military reconnaissance applications. These applications have led to a set of SAR specifications that emphasize target detectability and spatial resolution. There still is not universal agreement within the SAR community concerning a standard set of SAR performance parameters, although those listed in Table 4.1 have wide acceptance.

As discussed in Section 3, there are many applications for a calibrated SAR. These applications involve making various types of measurements of terrain reflectivity or RCS values. Consequently, additional performance parameters are needed to specify adequate performance for SARs, which are to be used for these applications. Table 4.2 lists three additional parameters which are directly related to calibrated SAR systems.

In the following sections, the conventional SAR performance parameters are first briefly reviewed, then, the three parameters which are appropriate for a calibrated SAR are described.

4.1 CONVENTIONAL SAR PERFORMANCE PARAMETERS

Mainlobe Width of Point Target Response

An important measure of SAR performance is related to the two-dimensional output function corresponding to a point target. This is often called the SAR impulse response. Ideally, this response would have a very narrow mainlobe and no sidelobes. In practice, this cannot be achieved and a typical SAR point target response will have the characteristics shown in Figure 4.1.

The response width is usually specified at the -3 dB level with respect to the mainlobe peak. In addition to the -3 dB level, lower secondary levels, e.g., -15 dB, can be specified to further bound the point target response width.

TABLE 4.1
TYPICAL SAR PERFORMANCE PARAMETERS

1. Mainlobe Width of Point-Target Response
2. Point-Target Response Envelope
3. Equivalent Noise Backscatter Coefficient (σ_n)
4. Dynamic Range
5. Spurious Response Level
6. Geometric Distortion

TABLE 4.2
ADDITIONAL PERFORMANCE PARAMETERS FOR
A CALIBRATED SAR

1. Reflectivity Measurement Accuracy
2. Reflectivity Measurement Resolution
3. Reflectivity Measurement Precision

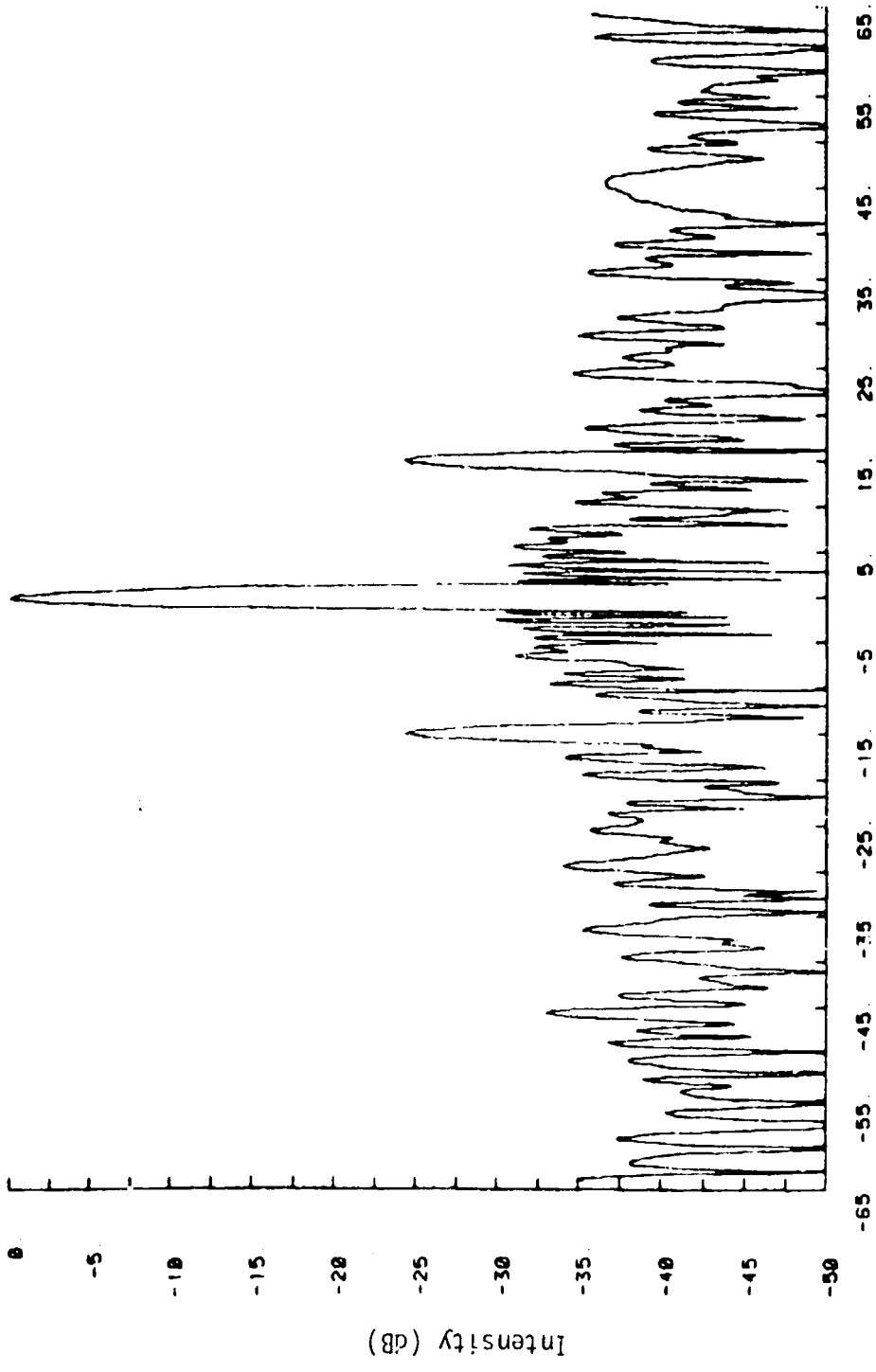

FIGURE 4.1. POINT-TARGET RESPONSE

The response width impacts the capability of the SAR to produce fine detail in the imagery. It is related to image resolution but the capability of a SAR (or any coherent imaging system) to distinguish closely-spaced point targets depends not only on the point target response width but also on the relative phases of the return signals associated with each point. As indicated in Figure 4.2, the resolvability of two point targets can be better or worse than the usual Rayleigh resolution criterion. Nevertheless, it is common practice in the SAR community to refer to the 3 dB widths in both the range and azimuth dimensions as the "resolution" of the system.

Point Target Response Envelope

This specification bounds the amplitude of the point-target response outside of the mainlobe. This is another way of specifying the acceptable peak values of both the near sidelobes (closer than 10 mainlobe widths from center) and the far sidelobes. Large near sidelobes are especially troublesome when attempting to image detailed cultural objects with many closely-spaced scattering centers while high peak sidelobes located far from the mainlobe appear as false targets.

Equivalent Noise Backscatter Coefficient

In the past, it was common to specify the Signal-to-Noise Ratio (SNR) and/or the Clutter-to-Noise Ratio (CNR) performance for a SAR, where N is the additive receiver thermal noise. In recent years, much more concern has been given to the fact that signal dependent noise sources (such as quantization and saturation effects, integrated sidelobes, and ambiguities) often impose a more severe limitation than receiver thermal noise in detecting either low radar cross section targets or slight variations in terrain reflectivity. Consequently, various types of total noise parameters have been defined. The equivalent total noise backscatter coefficient (σ°_{tn}) is representative.

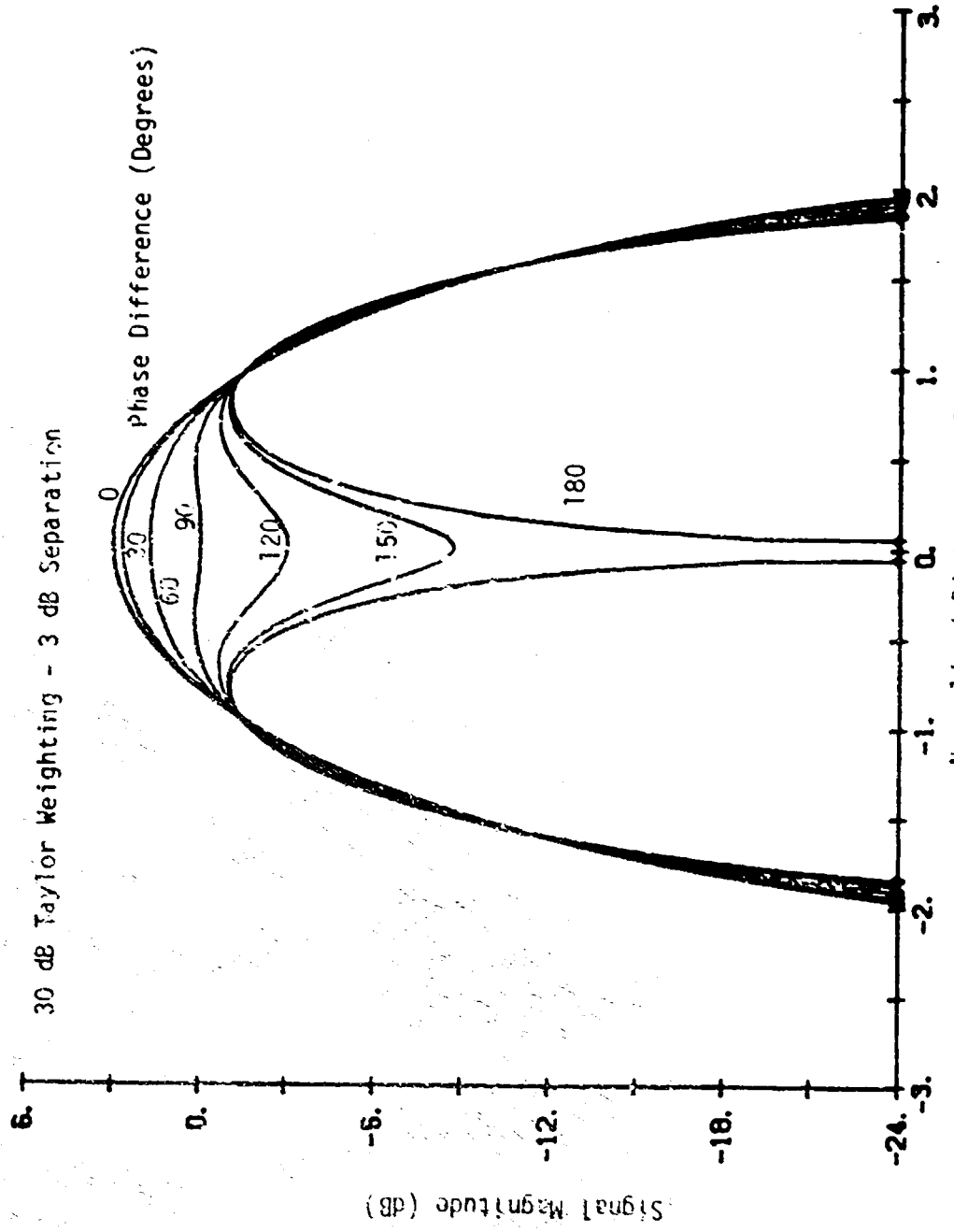

FIGURE 4.2. TWO-TARGET RESPONSE AS A FUNCTION OF RELATIVE TARGET PHASE

The total noise in the system can be expressed in terms of an effective backscatter coefficient (σ°_{tn}) which relates the noise level to an equivalent signal level corresponding to an actual radar return from a diffuse clutter region with a backscatter coefficient of σ°_{tn}. This parameter is given by the sum of both additive and signal-dependent noise components in the form:

$$\sigma^\circ_{tn} = \sigma^\circ_n + MNR\ \sigma^\circ_{avg}\ , \tag{4.1}$$

where σ°_n = the effective backscatter coefficient due to additive noise,

MNR = the multiplicative noise ratio, and

σ°_{avg} = the average backscatter coefficient of the illuminated scene.

The parameter σ°_n denotes the terrain backscatter coefficient which would produce the same mean image intensity as the system additive noise. The value of σ°_n can be reduced by decreasing the receiver noise figure and/or system losses, or by increasing antenna gain or transmitter power.

It is normally assumed that MNR is constant for a given SAR system. Contributions to MNR include the integrated sidelobe ratio (ISLR) of the point-target response function, range and Doppler ambiguity ratios, and various nonlinear distortions. In Section 6.4, some of the effects and sources of signal-dependent noise are discussed.

The effective backscatter of the total noise as a function of σ°_n, σ°_{av}, and MNR for typical ranges of these parameters is shown in Figures 4.3 through 4.5.

There are other related parameters which also have been used to specify the noise performance of a SAR. For example, SNR and CNR could be specified along with ISLR, ambiguities, A/D converter quantization, etc., although this removes the flexibility of the SAR designer in optimally budgeting noise contributions among the various sources.

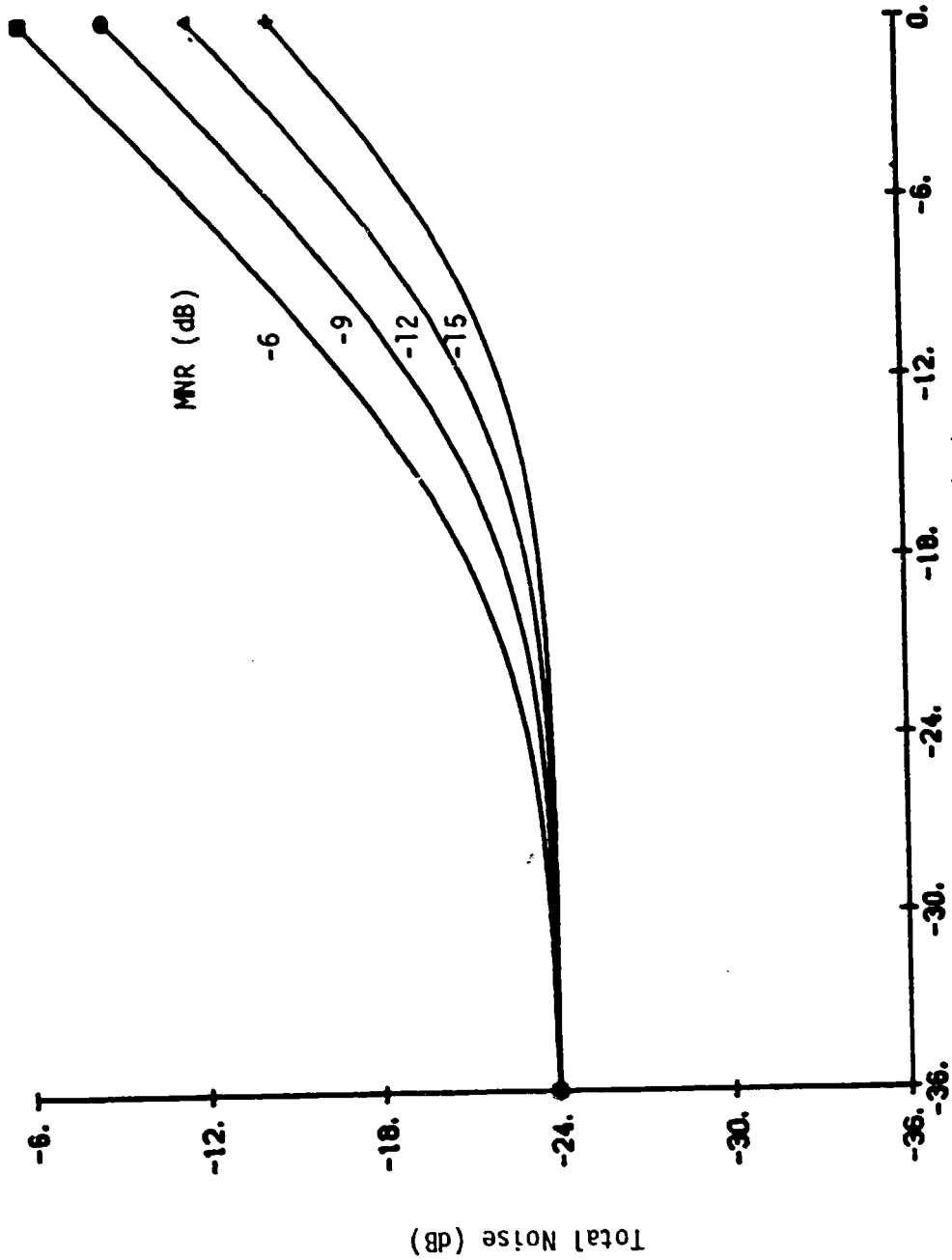

FIGURE 4.3. EFFECTIVE BACKSCATTER COEFFICIENT OF TOTAL NOISE FOR σ_n° = -24 dB

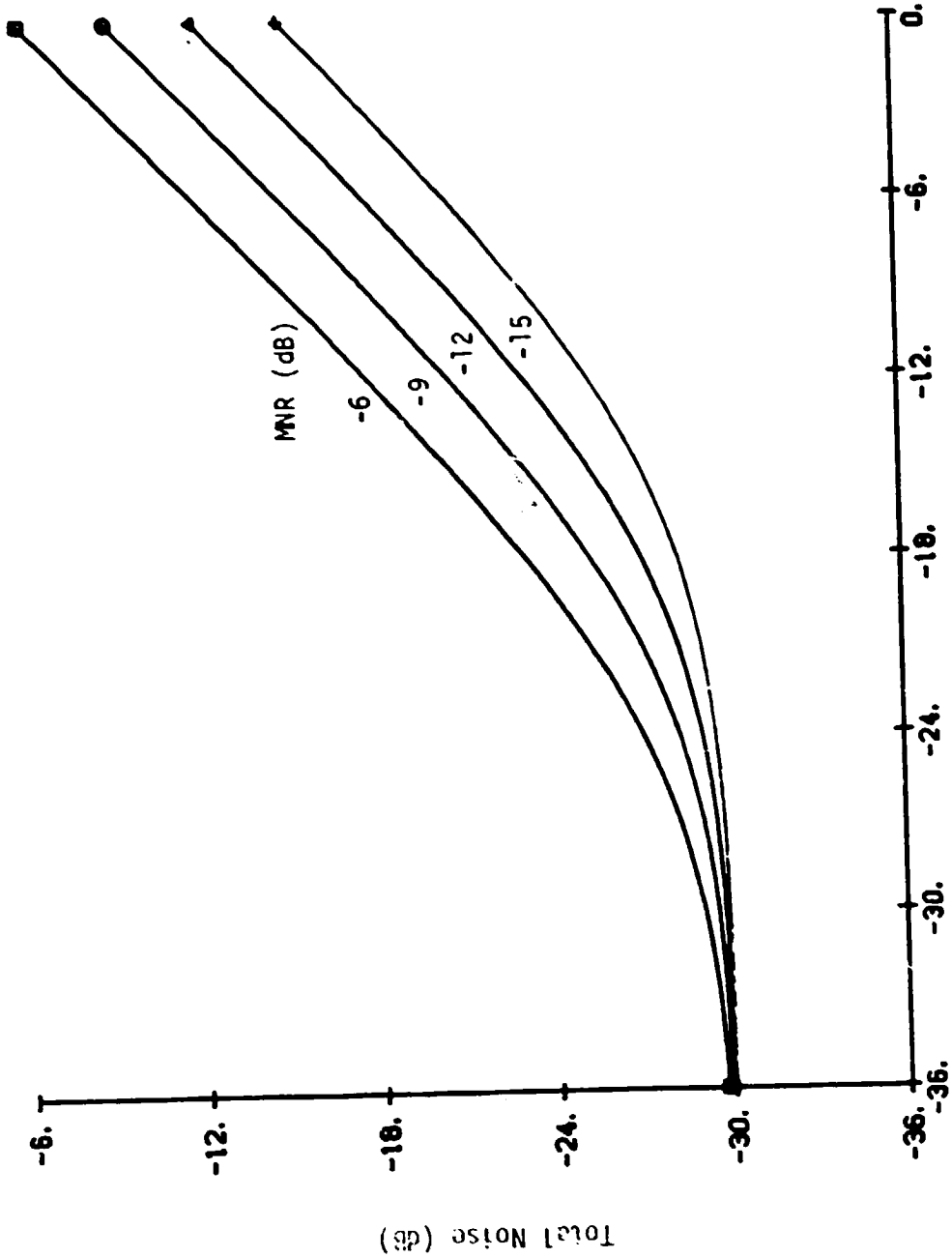

FIGURE 4.4. EFFECTIVE BACKSCATTER COEFFICIENT OF TOTAL NOISE FOR σ_n = -30 dB

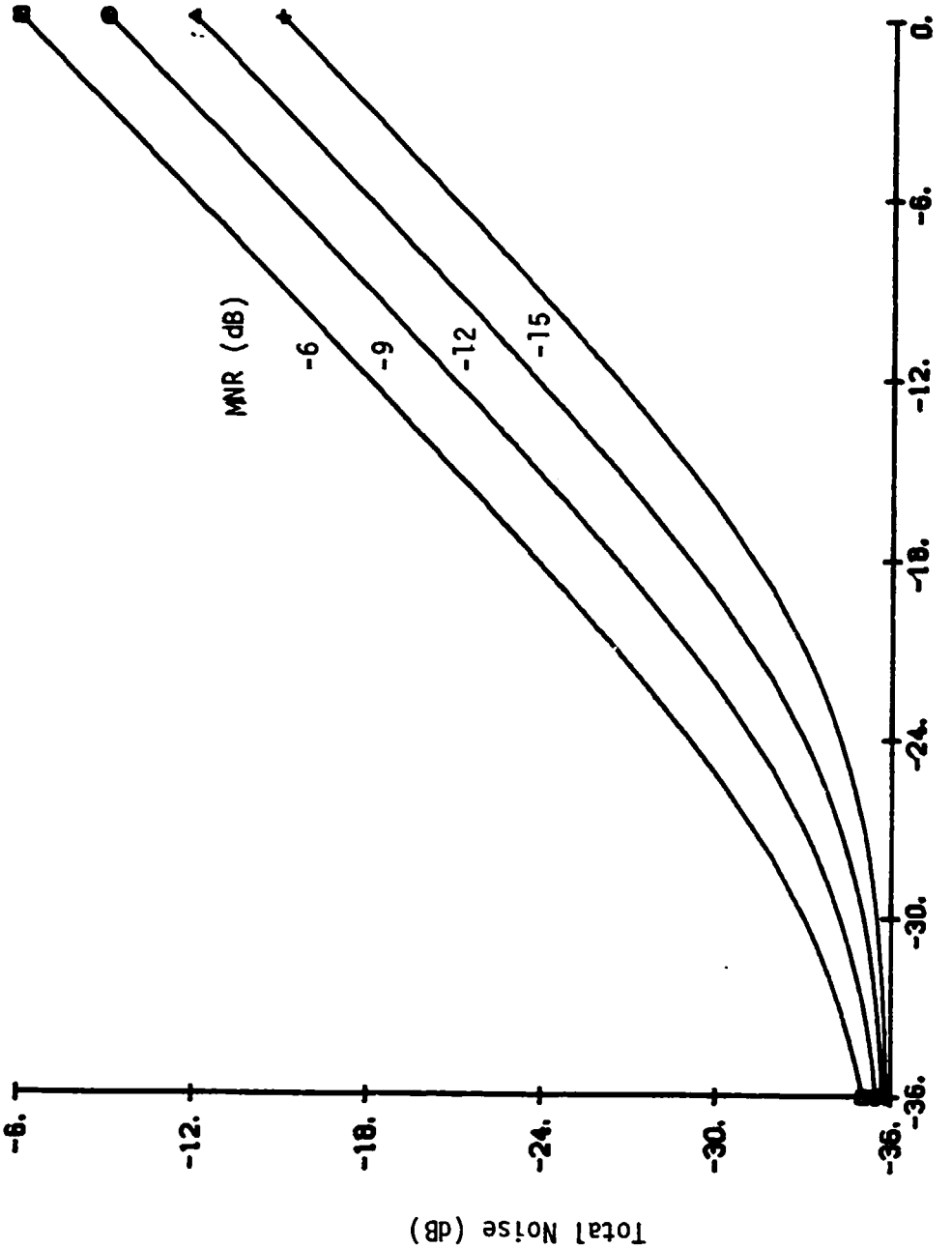

FIGURE 4.5. EFFECTIVE BACKSCATTER COEFFICIENT OF TOTAL NOISE FOR σ_n° = -36 dB

Image contrast is also used as a SAR performance parameter, as indicated in Figure 4.6. If the additive noise σ°_{n} is fixed, the contrast should improve as the average terrain backscatter coefficient (assume $\sigma^{\circ}_{av} = \sigma^{\circ}$) increases. However, as shown in Figure 4.7, the contrast is limited by the multiplicative noise coefficient. When attempting to image very low reflectivity terrain features in a low average return area, the image contrast is limited by the additive noise component as shown in Figure 4.8.

Dynamic Range

The dynamic range of a SAR system refers to the range of reflectivity values which result in detectable changes in the output image. There are a number of more specific definitions depending on whether point targets or diffuse clutter are assumed and whether the concern is with linear dynamic range or total dynamic range.

One common definition of dynamic range is the range of input radar cross sections of point targets for which the response mainlobe width and envelope image-quality specification are achieved. With this definition, a typical dynamic range for a SAR system is between 50 and 80 dB.

The dynamic range can also be defined as the ratio of peak usable output signal power to mean output noise power. Furthermore, peak usable output signal is defined as either the peak point target or mean clutter-image intensity for which linear operation is achieved.

Spurious Response Level

Spurious response level is an image quality parameter that accounts for undesirable artifacts in the image which are not included in any other performance parameter. Examples of spurious response are (1) intermodulation products resulting in false targets, (2) coherent signal leakages, (3) I/Q imbalance effects, etc.

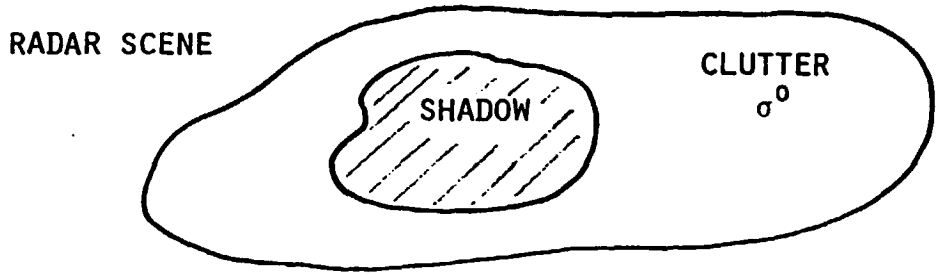

$$\text{CONTRAST} = \frac{\text{AVERAGE IMAGE INTENSITY OF CLUTTER}}{\text{AVERAGE IMAGE INTENSITY OF SHADOW}}$$

$$= \frac{\text{CLUTTER + TOTAL NOISE}}{\text{TOTAL NOISE}}$$

$$= \frac{\sigma^0 + \text{MNR} \cdot \sigma^0 + \sigma_n^0}{\text{MNR} \cdot \sigma^0 + \sigma_n^0}$$

FIGURE 4.6. SIMPLE TWO-PARAMETER CONTRAST MODEL

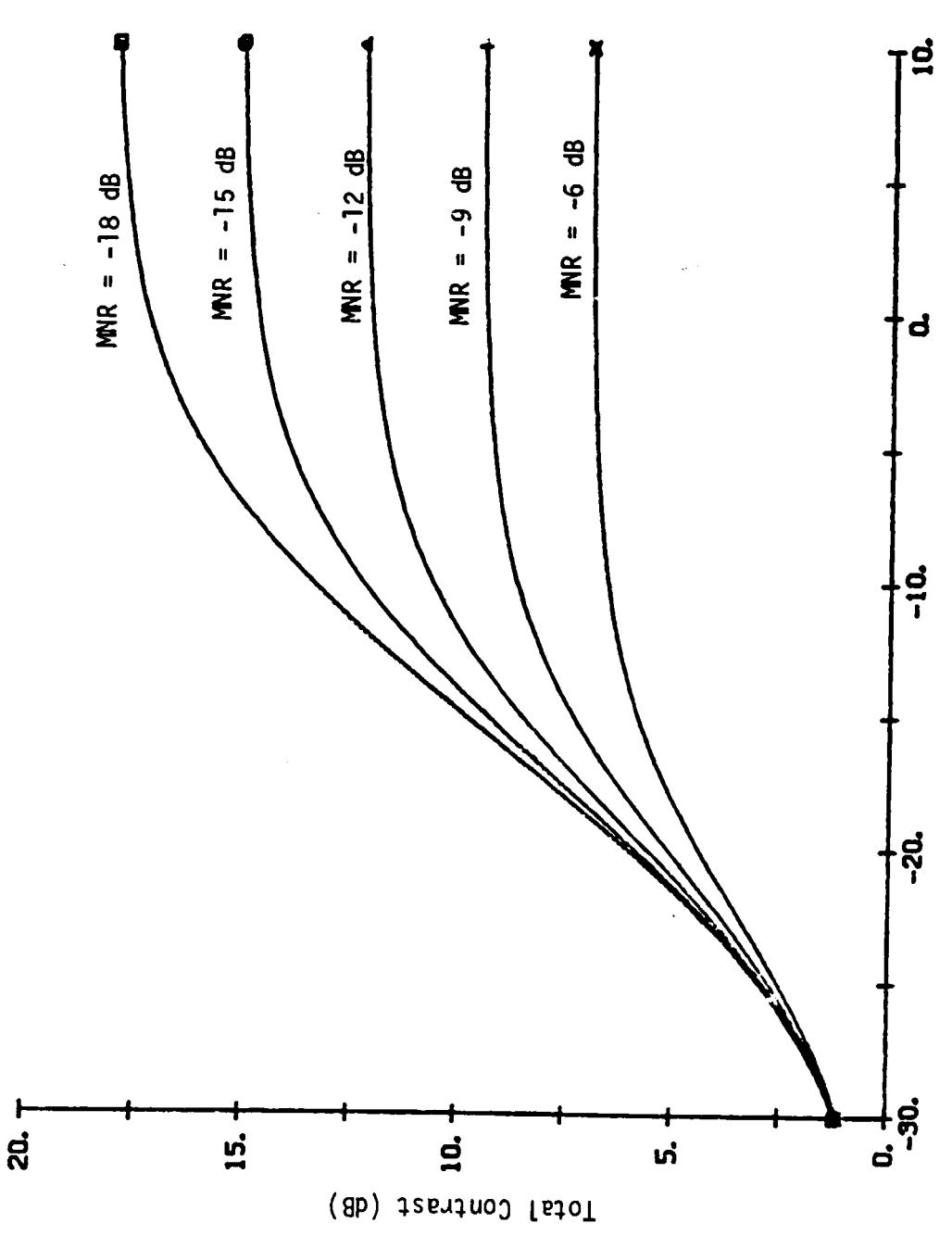

FIGURE 4.7. IMAGE CONTRAST VS TERRAIN BACKSCATTER COEFFICIENT (σ°) FOR σ_n° = -25 dB

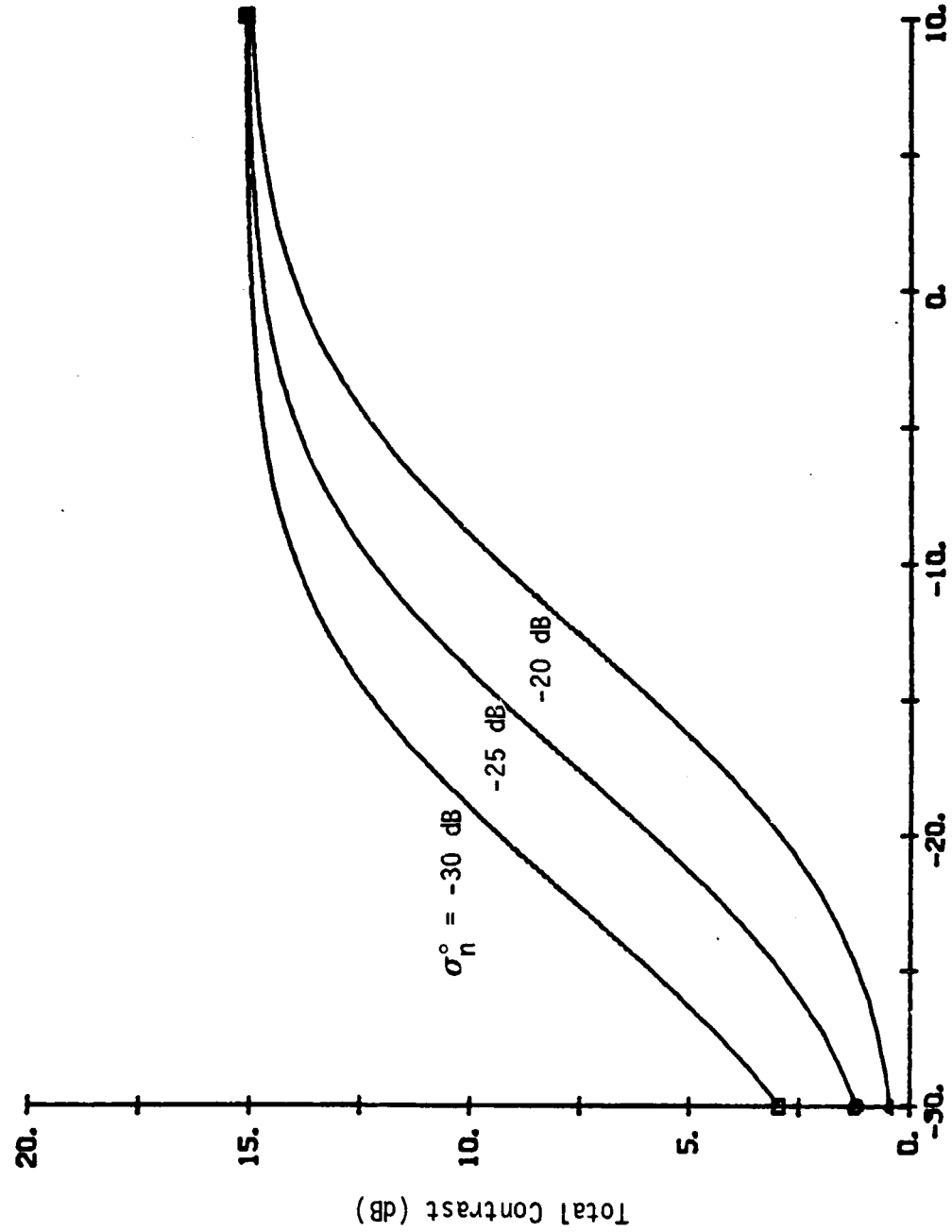

FIGURE 4.8. IMAGE CONTRAST VS TERRAIN BACKSCATTER COEFFICIENT (σ°) FOR MNR = -15 dB

Geometric Distortion

Geometric distortion is a measure of the spatially variant displacement error in the image. It represents a loss in relative accuracy in the locations of points in the image with respect to the actual location of the points in the scene. The total geometric distortion in the image includes both (1) deterministic effects due to ground-plane-to-slant-range-plane projection and (2) range curvature and various linear range phase errors due to navigation and motion measurement errors. Depending on the application, geometric distortion can be specified in terms of a maximum allowable spatial error or as a percentage of distance measured within the image.

4.2 ADDITIONAL CALIBRATED SAR PERFORMANCE PARAMETERS

Reflectivity Measurement Accuracy

Reflectivity Measurement Accuracy (RMA) is related to the absolute calibration of the SAR system. A good RMA value implies a low error between a measured value of reflectivity and the true value of reflectivity. The RMA is usually expressed in percent of the true value or in dB. That is,

$$\text{RMA} = \frac{\sigma^\circ - \hat{\sigma}^\circ}{\sigma^\circ} \quad \text{or} \quad 10 \log \frac{\hat{\sigma}_0}{\sigma_0} \ , \qquad (4.2)$$

where $\hat{\sigma}^\circ$ is the measured value of the backscatter coefficient and σ° is the "true" value. The "true" value is assumed to be the measured or calculated value of the best available accuracy, or some other accepted standard. As discussed in Section 6.1, the ability to determine the reflectivity measurement accuracy is limited by the availability of reliable and practical standards.

Reflectivity Measurement Resolution

The amplitudes of the backscattered signals from coherently illuminated terrain are distributed statistically and appear in the

imagery as a speckle pattern. When two or more homogeneous regions are being imaged, the question often arises as to whether or not the two regions have different backscatter coefficients.

Reflectivity Measurement Resolution (RMR) is a measure of the capability of the SAR system to detect and measure small differences in the backscatter coefficient of distributed clutter. Sometimes the closely related terms "Radiometric Resolution" or "Noise Equivalent $\Delta\sigma^\circ$" are used for this performance parameter. It is the fundamental performance metric for relative σ° measurements.

RMR can be defined as the minimum difference in backscatter coefficient ($\Delta\sigma^\circ$) that is measurable. A measurable Δ is defined as Δ such that the ratio of the RMS error between the actual difference (Δ) and the measured difference ($\hat{\Delta}$) to the actual difference is less than 1 percent. That is,

$$\frac{\sqrt{E(\Delta - \hat{\Delta})^2}}{\Delta} < 0.01, \tag{4.3}$$

where $\Delta = \overline{\sigma^\circ_2} - \overline{\sigma^\circ_1}$,

$\overline{\sigma^\circ_2}$ = mean backscatter coefficient of region 2,

$\overline{\sigma^\circ_1}$ = mean backscatter coefficient of region 1, and

$\hat{\Delta}$ = measured value of Δ.

Reflectivity Measurement Precision

The precision of any measurement process refers to the quality of coherence or repeatability of the measurement data and is a parameter that indicates the "closeness of agreement among repeated measurements". If a number of measurements of a standard reflector are made with a SAR system under fixed conditions, the dispersion in the measurements will indicate the reflectivity measurement precision

(RMP) of the system. RMP is usually expressed as the standard deviation of the set of measurement results.

A detailed and systematic analysis of the various factors that affect RMA, RMR, and RMP has not been completed. It is important to establish a statistical amplitude model of the SAR system so that the impact of system errors, total noise, and nonlinearities on the calibrated SAR performance parameters can be established.

In addition, a practical set of experimental measurement procedures must be developed to verify SAR performance in terms of RMA, RMR, and RMP. This will involve the design of test sites with appropriate reflectivity standards that are well characterized.

5
SAR CALIBRATION METHODOLOGY AND TECHNIQUES

Calibration as applied to a SAR system has been defined in Section 3 and can be summarized as follows. Absolute calibration implies that RCS values are to be estimated to within some absolute error bounds; relative calibration is a comparison of RCS values on a given image or on separate images. Overall system stability, that is, the capability to repeat measurements, is referred to as the precision of the measurements. The objective of calibration is to measure the system transfer function to permit the SAR output signal to be related to the reflectivity or radar cross section (RCS) values in the imaged scene.

The methodology which has been established as a guideline for SAR calibration can be summarized as: (1) provide for measurement of total system response (that is, from the scattering area to the output imagery), (2) provide methods for the monitoring of system response, (3) provide methods for calibration verification, and (4) provide for periodic verification of calibration accuracy. In addition, it is desirable to utilize the measurement results and analysis to obtain an estimate of error for various calibration measurements. These will be reviewed in Section 7.

A discussion of general calibration methodology and several basic techniques applicable to the calibration of a SAR system are included in this section. An example of the application of a calibration technique utilizing reflectors as calibration references and a calibration signal generator for system monitoring is given. Finally, an example of a procedure for verification and data gathering with a calibrated SAR is also given.

5.1 CALIBRATION TECHNIQUES

Following the guidelines of the SAR methodology given above, any SAR calibration method should include some appropriate technique or

approach for the measurement of total system transfer function. The measurement method must provide for a calibration reference to which the SAR absolute calibration is referred. Any method for SAR calibration must satisfy the following additional requirements: (1) provide for the monitoring and recording of particular SAR system parameters, (2) include an operational procedure for data gathering, and (3) include a calibration verification procedure.

The general calibration method should provide for a separate measurement of the SAR system antenna response. There are several techniques available for the measurement of antenna response; these will be described in a following section.

A partial list of techniques for the calibration of a SAR system is given in Table 5.1. The technique breakdown is done in the generic sense, with some indications for specifics given. The utilization of any of the suggested techniques will provide a measure of the total SAR system transfer function.

5.1.1 REFERENCE REFLECTOR TECHNIQUE

The first technique listed involves the measurement of the total SAR system transfer function using reference standards with calibrated reflectivity values, some examples are given. The relationship of SAR output power as a function of reflectivity value is obtained from the empirical data. These results are applicable at the particular ranges and depression angles for which the calibration data are obtained. If calibrated data are required at other ranges or depression angles, either (1) additional calibration data at the desired parameters must be obtained or (2) knowledge of the antenna and range response is required to apply calibration data to the desired parameter values.

TABLE 5.1
TECHNIQUES FOR DETERMINING TOTAL SYSTEM TRANSFER FUNCTION

1. Image Standard Reflectivity References

   Types

   - point-like reflectors
   - distributed scattering areas
   - active repeaters

   Determine reflectivity reference values

   - anechoic chamber
   - auxiliary calibrated instrumentation
     - scatterometer
     - SAR system
     - RCS range
   - calculated values

2. Determine Component Transfer Functions and Combine

   Make individual measurements of each subsystem

   - receiver, recorder, processor, etc.
   - antenna

   Calculate response of subsystems

   Combine to obtain total system transfer function

3. Image Scenes of Opportunity - which have "Known" Reflectivity Values

   Types

   - shadow regions
   - forest areas
   - desert

Reflectivity values used as calibration references must be measured as accurately as possible using a calibrated measurements facility; examples are given in Table 5.1. It is most desirable to utilize reflectivity references that will retain their calibrations over a long time period without requiring re-calibration of the reference. Point-like reflectors, such as corner reflectors, satisfy this requirement best. In addition to the measurements of the absolute value of each calibration reference reflector, the angular response must also be known. These data will be utilized to correct the RCS value of each reflector for variations in aspect angle during imaging with the SAR. In order to realize minimum error in the correction for aspect angle, accurate measurements of the orientation angles for each reflector must be made and recorded. Reflector design is discussed in Section 6.1.

There are a number of approaches that can be followed to calibrate the reference reflector or reflectivity areas. Careful and repeated measurements of various reflectors can be made in an anechoic chamber facility to calibrate each individual reflector. These reflectors are then installed in an area that can be imaged with the SAR system that is to be calibrated. If possible, the reflector area should be near the test site where measurements with the calibrated SAR are required. Auxiliary calibrated instrumentation can be utilized to calibrate particular areas for use as calibration references. For example, (1) scatterometers, ground-based or airborne, (2) short pulse, CW, or other calibrated RCS measurement instrumentation, or (3) another calibrated SAR could be utilized to provide the absolute calibration reference [34].

Error sources include uncertainties in (1) reference reflectivity values, (2) determination of imaging geometry, (3) antenna response, (4) output measurements, (5) uncompensated SAR vehicle attitudes, (6) transmitter power, and (7) temporal variation of transfer function. These errors will be described in more detail in Section 7.

5.1.2 COMPOSITE TRANSFER FUNCTION TECHNIQUE

The transfer function of each of the individual subsystems of the SAR system can be measured separately and the results combined to give total system response. A suitable measurement technique must be utilized to properly measure each system component. Since a number of separate measurements are required, the possibility for error is greater than for one single measurement of total system transfer function. Also, the results from individual measurements may not be combined properly; such problems as input-output matching, coupling or interaction between components and other effects may not be properly accounted for.

Although, in principle, the response of each SAR component (or some of them) can be determined from theoretical analysis, and the results combined to give total system response, the possibility for error is very great. Also, as discussed above, the problem in combining component responses is present.

5.1.3 SCENES OF OPPORTUNITY

A very few scenes have a limited and well documented range of scattering coefficients. These can be utilized for a calibration of sorts, but the potential for absolute error is quite high. There are a number of available references documentating measurements of the scattering coefficients of a variety of scenes; in particular, dry desert and forest areas have relatively small variances in the values of their scattering coefficients. This technique may be better than having no bounds at all on calibration; also, a series of measurements could demonstrate the precision performance for relative measurements.

5.2 ANTENNA PATTERN MEASUREMENTS

The SAR antenna response should be measured utilizing an antenna range to provide an accurate pattern reference. The in-flight

measurement techniques discussed here are designed to verify that the proximity of the SAR vehicle (airframe, radome, etc.) or the spacecraft launch or temperature effects, etc., have not distorted the antenna pattern. In addition, these techniques will provide a measure of the true, operational pattern of the SAR antenna.

Several techniques for the measurement of antenna response on the SAR vehicle are:

(1) use of calibrated reflectors across the swath,

(2) homogenous-terrain σ° measurements in range,

(3) non-homogenous-terrain average σ° measurements in range,

(4) incident-power calibrated receiver (gain measurement), and

(5) near-field measurements technique (installation mock-up required).

The reflector array method has been used in the flight measurements of dual polarization SAR antennas operating at X-band. This method requires a number of reflectors of equal RCS to be distributed across the range swath. The array is imaged a number of times so that reflectors are imaged at different depression angles (a number of measurements at each angle improves accuracy, of course). After correction for range differences, system range response, and aspect at each reflector, the resulting response is a measure of the 2-way antenna pattern. Results obtained from X-band low-depression-angle measurements were very consistent and provided a pattern over depression angles from 6° to 27° with an error of less than 2 dB standard deviation. Additional measurements of the reflector array with the SAR could reduce the 2 dB error. The reflector method is well suited for steep-depression-angle antenna response measurements, where minimum error from multi-path is encountered.

The uniform terrain method has been utilized with SEASAT-SAR and ERIM SAR data with satisfactory results; however, it is difficult to obtain homogenous terrain areas that fill the total swath width. Also, for aircraft measurements, the value of σ° changes with angle subtended across the swath.

An averaging technique to account for variations in σ° over non-homogenous (or homogenous) terrain is outlined in Figure 5.1. The procedure can be summarized as follows: First, obtain SAR data over an area of terrain having as nearly homogeneous scattering characteristics as possible. An area of 10-20 miles in length in a rural region would be satisfactory, avoiding cultural areas. Second, process the SAR data to obtain an image and divide the swath width into N range intervals corresponding to one degree increments in depression angle θ. Third, measure an average power $\langle P_n \rangle$ for each range interval over the total image length, consisting of M image pixels. Averages made over long paths at a given depression angle should result in an equal backscatter coefficient measurement from each range interval for non-homogeneous terrain. Little averaging is required for homogeneous terrain. Fourth, normalize the measured values of average power from each range interval for range variation across the swath ($1/R^3$ factor for the SAR system). Normalization to near range is convenient. After normalization for range, any variations in the values of average power across the swath should be due to the two-way antenna response. A measure of the relative antenna response across the swath is thus obtained. This method can be applied to data obtained over rural areas and would be particularly applicable to a spacecraft system where the total swath subtends a narrow angular extent so variation of σ° over the swath will be negligible. The accuracy of this method should be very good, but an analysis of the technique to obtain an error estimate is required.

The utilization of calibrated ground receivers is recommended for simultaneous pattern response and absolute gain measurements.

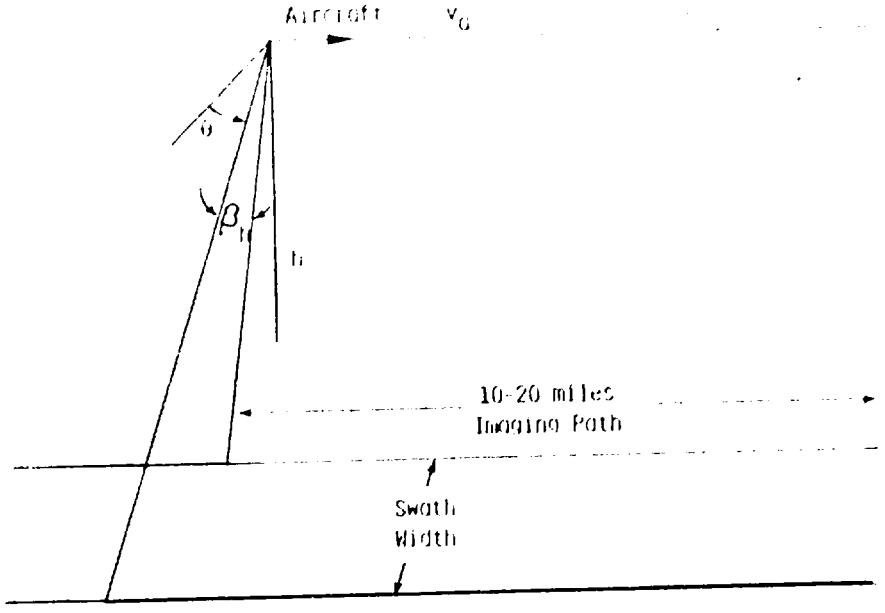

1. SAR Image of Non-homogeneous Terrain

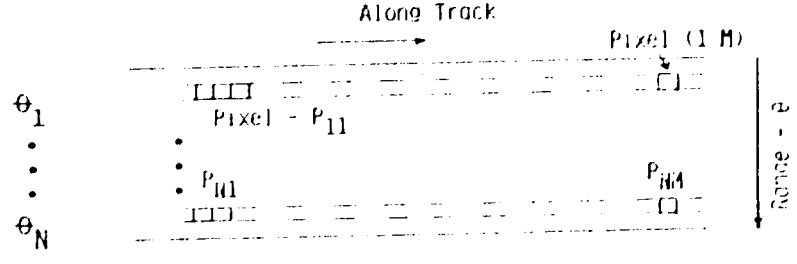

2. Power Measurements of Range Intervals Imagery

3. Average Power from Each Range Scan

$$\langle P_{11} \rangle = \frac{1}{M} \sum_{m=1}^{M} P_{1,m} \propto \sigma^0(\theta_1)$$

$$\vdots \qquad\qquad \vdots$$

$$\langle P_N \rangle = \frac{1}{M} \sum_{m=1}^{M} P_{N,m} \propto \sigma^0(\theta_N)$$

4. Correction for Range

$$\frac{1}{R^3}$$

5. Large Averages Should Result in Equal σ^0 Values:

$$\sigma^0(\theta_1) = \sigma^0(\theta_2) = \sigma^0(\theta_N)$$

6. Variations in σ^0 With θ Give the Two-way Antenna Responses

FIGURE 5.1. ANTENNA PATTERN MEASUREMENTS USING SAR DATA; AVERAGING OF NON-HOMOGENEOUS TERRAIN.

Although the receivers are more costly than precision reflectors, both gain and response (assuming several receivers) can be measured very accurately. The measurements described can be utilized for periodic checks of the response. This provides a measurement of the antenna gain as well as geometry and propagation factors.

A full-scale model of the aircraft antenna mounting structure can be constructed and antenna pattern measurements made on a far-field antenna range. Although the model construction can be expensive, the results should be very accurate. Spacecraft antenna patterns can be measured using a far-field range but without the mounting structure model, because the effects of mounting can be accounted for. Near-field measurement techniques have advantages in that the sidelobe levels and polarization isolation can be measured with best accuracy [35]. The capabilities of near-field measurement instrumentation tend to limit the maximum physical size of the antenna that can be measured, but techniques have been used (SEASAT antenna for example [36]) to overcome some of these limitations.

5.3 MONITORING OF SAR PARAMETERS

Provisions for the monitoring and recording of SAR parameters during calibration data gathering must be made as a part of any calibration technique that is utilized. A list of parameters to be measured is given in Table 5.2.

System monitoring requirements for calibration must be determined, primarily from a system error analysis. Important considerations include: (1) the instrumentation which needs to be included for the monitoring and recording of particular operational parameters such as (1) vehicle roll, pitch, and yaw data recorders for use in the calculation of SAR geometry for data reduction, (2) a signal generator for monitoring the temporal variation of system response, (3) a transmitter power monitor recorder, and (4) others.

TABLE 5.2
CALIBRATED SAR DATA COLLECTION
Parameters to be Measured

All Reference Reflectors

- Size
- Location
- Orientation Angle

SAR

- Power Transmitted
- Reference Power
- Antenna Depression Angle
- Drift Angle
- Roll Angle
- Velocity
- Altitude
- Range
- PRF Pulse Width
- Calibration Signals
- Range Delay
- Sweep Length
- NAV Parameters
- Bandwidth (range, azimuth)
- Processing Parameters

Measurements Prior to Data Collection

- Reflector Response (θ, ϕ)
- Antenna Response
- Reference Signal Generator Verification
- System Losses
- System Response

Measurements on SAR Data

- Output power for targets or scenes to be calibrated.
- Reference reflectors and calibration generator signals.
- Vehicle geometry; viewing aspect angle and range.
- Antenna and reflector responses.

(2) methods of recording parameters which are compatible with data analysis, and (3) specifications of measurements required on the calibration data. This latter would include (1) sample size, (2) number of samples, (3) how the measurements of the calibration reference reflectors are to be made and recorded, and (4) procedures for correction of aspect angle to reference reflectors using the geometry parameters recorded.

5.4 MEASUREMENT OF TOTAL SYSTEM TRANSFER FUNCTION

As an example of the measurement of total SAR system transfer function, the first calibration technique listed in Table 5.1 will be utilized. The various calibration programs that have been conducted by ERIM have utilized reflectors for the absolute RCS reference and a calibration signal generator for monitoring of the temporal variation in the H_R portion of the system transfer function. Also, instrumentation has been designed and utilized for the monitoring of important system parameters (such as (1) transmitter power, (2) aircraft roll, pitch, and yaw angles, and (3) reference signal generator power level). Finally, other system parameters, listed in Table 5.2, were recorded and utilized later during reduction of the calibrated SAR data. This approach requires the design, fabrication, and installation of reference reflector arrays for (1) measurement of the SAR system transfer function, and (2) SAR antenna response and calibration verification.

The calibration procedure is outlined in Figure 5.2. The reflector arrays are imaged with the SAR and the measured values of power P_I in the output image from the reflectors in the calibration array provide a measure of the total system transfer function H_S:

$$P_I = H_S \sigma \ . \qquad (5.1)$$

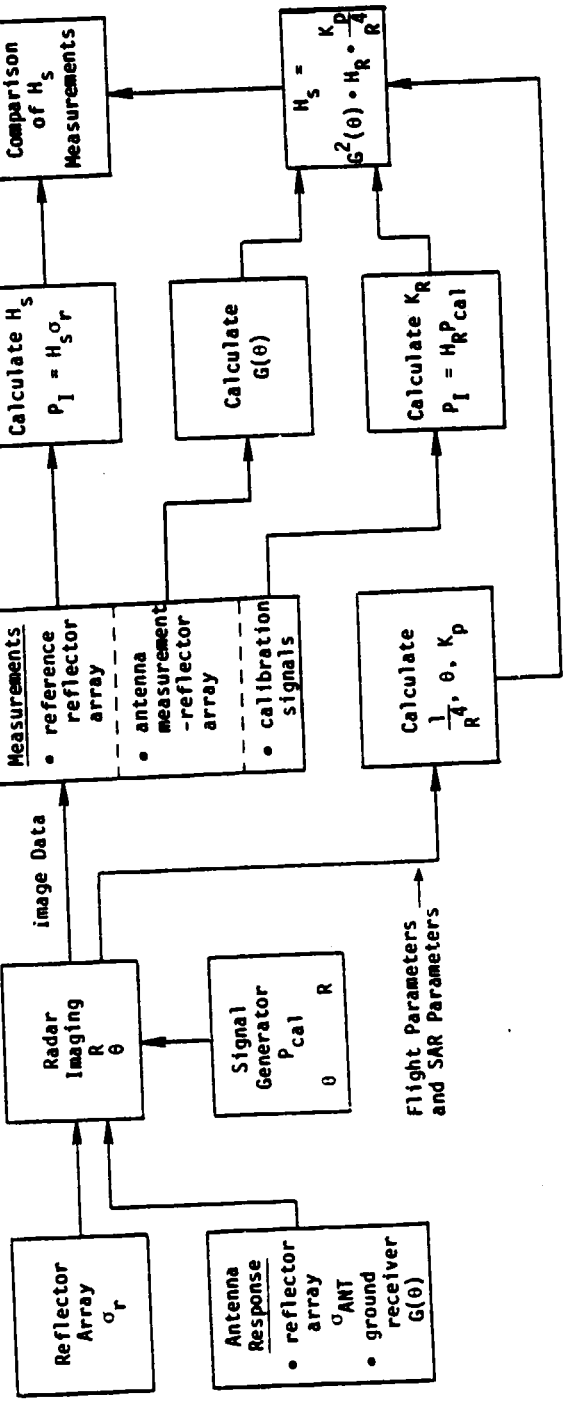

FIGURE 5.2. MEASUREMENT OF TOTAL SYSTEM TRANSFER FUNCTION.

Also, empirical results from SAR data of the antenna reflector array (or other antenna measurement techniques) provide data from which the antenna response $G(\theta)$ is obtained. A separate measurement with a calibrated ground receiver should be used to obtain measurements of the absolute gain of the antenna. And, recording of the flight and system parameters provides the imaging geometry $1/R^4$, θ, and K_p.

Measured values of the recorded signals from the calibration signal generator provide the system transfer function H_R, where H_R is the SAR system response from the SAR antenna terminals to the output image (Eq. 5.2) and is related to total SAR system response by Eq. 5.3.

$$P_I = H_R P_{cal} \tag{5.2}$$

$$H_s = K_p \frac{1}{R^4} G^2(\theta) H_R \tag{5.3}$$

The system transfer function measured using SAR data from reference reflectors is given by Eq. (5.1). Using Eq. (5.3) this can be written as

$$P_I = K_p \frac{1}{R^2} G^2(\theta) H_R \sigma_r , \tag{5.4}$$

where the output power P_I is obtained using data from measurements made with the calibration signal generator Eq. (5.2) is equated to the values from Eq. (5.4), to give

$$P_{cal} = K_p \frac{1}{R_1^4} G^2(\theta_1) \sigma_r \tag{5.5}$$

where system response H_R cancels for measurements obtained over a short time interva. Calibration can be verified with a verification of Eq. (5.5) using the measured values of K_p, R, and $G(\theta)$.

In summary, the calibration of a SAR requires that the total system transfer function be measured, that the antenna response be measured and verified on the SAR vehicle, and that system operating parameters be monitored and recorded. Several techniques for accomplishing these requirements have been discussed. The preferred technique for the measurement of total system transfer function is that utilizing reference reflectors. Similarly, a technique utilizing reference reflectors for the in-flight measurements of antenna response should provide the most accurate results. However, an averaging technique using SAR imagery of terrain can be utilized also. The transfer function of the SAR receiver-recorder-processor is monitored using a calibration signal generator, the requirements of which have been reviewed. Also, recording and monitoring of other system parameters are required.

5.5 UTILIZATION OF CALIBRATED SAR FOR REMOTE SITE DATA GATHERING

A calibration procedure utilizing reflectors and a calibration signal generator is outlined in Figure 5.3 for data gathering at a remote test site. Assuming that some time elapses after the measurement of the system transfer function, a verification test is usually required before a mission to obtain calibrated SAR data. The top block diagram in Figure 5.3 outlines the data gathering procedures to obtain verification of the system transfer function H_S.

The first step in the calibration procedure is to image the reference reflector array to obtain a verification of the SAR calibration. Measurements are made to determine (1) the total system transfer function H_S, (2) variations in the system response H_R, and (3) the system transfer function as given by Eq. (5.3) using the antenna response (measured during the calibration of the SAR) with the appropriate geometry ($1/R^4$ and θ). Calibration verification is then completed and, assuming no discrepancies were noted, the calibration in terms of the reference signal generator is obtained

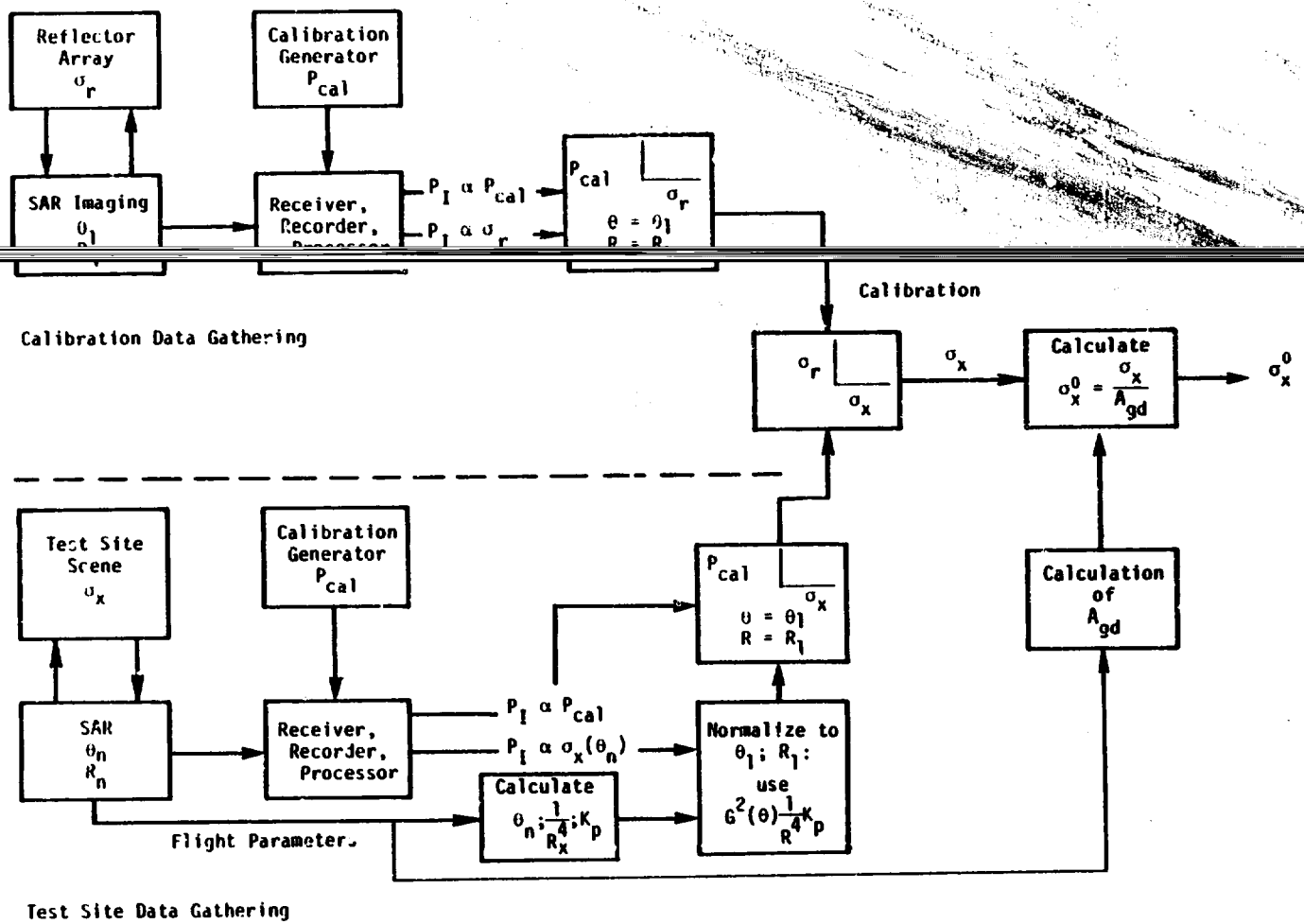

FIGURE 5.3. EXAMPLE OF CALIBRATION DATA GATHERING PROCEDURE.

(Eq. 5.5) for particular values of range R_1 and depression angle θ_1. This relationship is then utilized to calibrate the data obtained at a remote test site, again using P_{cal} measurements of H_R to determine any variations in H_R. Note that the signal generator power is at the receiver input; hence, the $1/R^4$ factor is used here.

At some time later, SAR data are obtained at the test site, "area x" depicted in the lower part of Figure 5.3. Received SAR signals from "area x" are processed to provide an output power P_I proportional to the power received from an RCS value σ_x at angle θ_n, that is

$$P_I = H_S \, \sigma_x \Big|_{\theta_n} . \tag{5.6}$$

The measured antenna response $g(\theta)$ is utilized with the geometry to normalize θ_n values to calibrated values at range R_1 and angle θ_1. The calibration look-up table provides absolute values for σ_x. System gain variations in H_R are accounted for by using measurements obtained from the signal generator source.

Output values are given in RCS per resolution area. If σ_x is from a "point" target, results from system performance measurements can correct for sidelobe response, noise, etc., to obtain a corrected RCS value. When distributed scattering areas are to be measured, imaging geometry parameters are used to compute the resolution area A_{gd} and the normalized scattering coefficient σ° is obtained from

$$\sigma_x = \sigma^\circ \, A_{gd} . \tag{5.7}$$

The verification experiment described for distributed scenes can be accomplished by following the procedure described in the paper

"An Unconventional Approach to Imaging Radar Calibration," by R. Fenner et al [34]. This paper describes the measurements necessary to provide a calibrated σ scene or area and for the simultaneous data gathering for verification demonstration. A Death Valley site is recommended as the experiment location.

6
CALIBRATED SAR SYSTEM DESIGN CONSIDERATIONS

In the design of a calibrated SAR system, there are a number of critical factors that must be considered, in addition to the basic SAR design requirements related to stability and compatibility with a particular calibration technique. These include: (1) the selection of reference reflector type and size, (2) reflector array design, (3) requirements for special instrumentation necessary for calibration (e.g., a calibration signal generator), and (4) the effects and sources of signal dependent noise. These aspects of calibrated SAR system design are briefly reviewed in this section.

6.1 REFERENCE REFLECTOR CONSIDERATIONS [37]

In order to satisfy the requirements for SAR calibration, reference reflectors or reflectivity areas having known values of RCS must be provided for use as absolute calibration "standards". The standard RCS reflectors are used to (1) measure the system transfer function by imaging an array of calibrated reflectors having a range of RCS values, (2) measure the antenna response in elevation (range) by imaging an array of reflectors of constant RCS values, and (3) provide the absolute values of RCS for calibration reference.

Considerations for reflectors to be used as SAR calibration references include the following:

1. Values of RCS versus size
2. Mechanical tolerances
3. Angular response
   a. Elevation
   b. Horizontal (along-track)
4. Variations in RCS
   a. Edge effects
   b. Mounting

5. Multi-path
   a. Bistatic RCS
   b. Mounting
6. Reflector type
   a. Cost
   b. Installation
   c. Weather
6. Siting of reflectors

Examples of a number of reflectors considered for calibration references are given in Figure 6.1, with expressions for the maximum RCS for each reflector type given in Figure 6.2. The reflector types considered included the following:

1. Luneberg lens
2. Top hat
3. Corner reflector
   a. Square
   b. Triangular
   c Round
4. Sphere
5. Flat plate

The angular response of a Luneberg lens reflector is given in Figure 6.3, along with the response of a triangular corner reflector for comparison. Clearly, the Luneberg lens provides a smooth RCS value over a wide angular range. The angular response width is important, due to siting accuracy requirements and imaging geometry requirements.

The Luneberg lens is best suited as a calibration reflector reference due to: (1) nearly uniform RCS over a 90° or greater aspect angle, (2) minimum multi-path problems, and (3) negligible "edge" effects and RCS ripple. However, Luneberg lenses are very costly and tend to be vulnerable to weather effects. Also, only low RCS

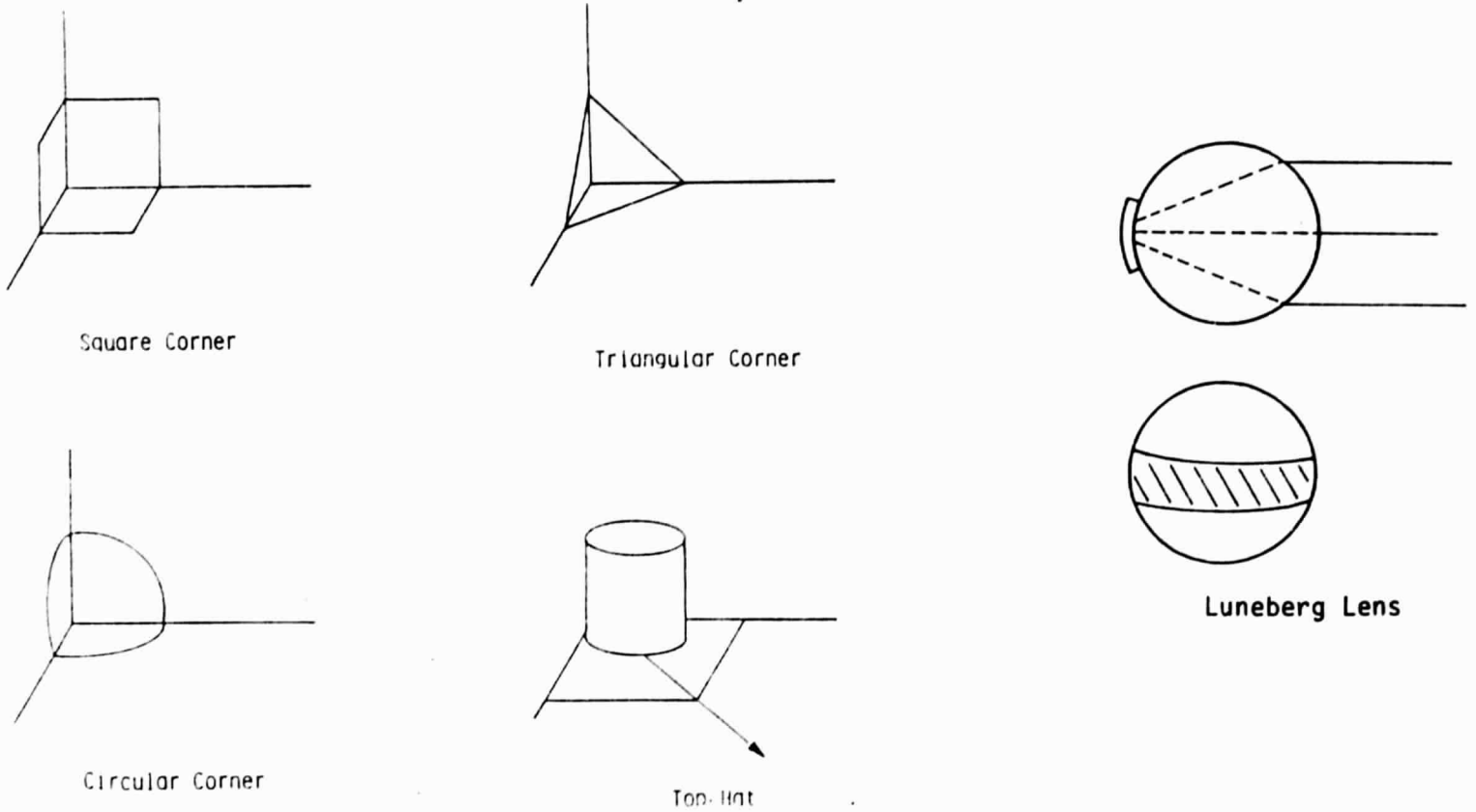

FIGURE 6.1. REFLECTOR TYPES SUITABLE FOR SAR CALIBRATION REFERENCES.

FIGURE 6.2. EQUATIONS FOR THE MAXIMUM RADAR CROSS SECTION OF REFLECTORS

- Triangular Corner

$$\sigma_{max} = \frac{4}{3}\pi\left(\frac{b^2}{\lambda}\right)^2$$

- Square Corner

$$\sigma_{max} = 37.7\left(\frac{b^2}{\lambda}\right)^2$$

- Circular Corner

$$\sigma_{max} = 15.611\left(\frac{b^2}{\lambda}\right)^2$$

- Top Hat

$$\sigma = \frac{8\pi h^2 r \sin\theta}{\lambda}$$

- Sphere

$$\sigma = \lambda r^2$$

- Flat Plate

$$\sigma_{max} = \frac{4\pi A^2}{\lambda^2}$$

- Luneberg Lens

$$\sigma = \frac{4\pi^3 a^4}{\lambda^2}$$

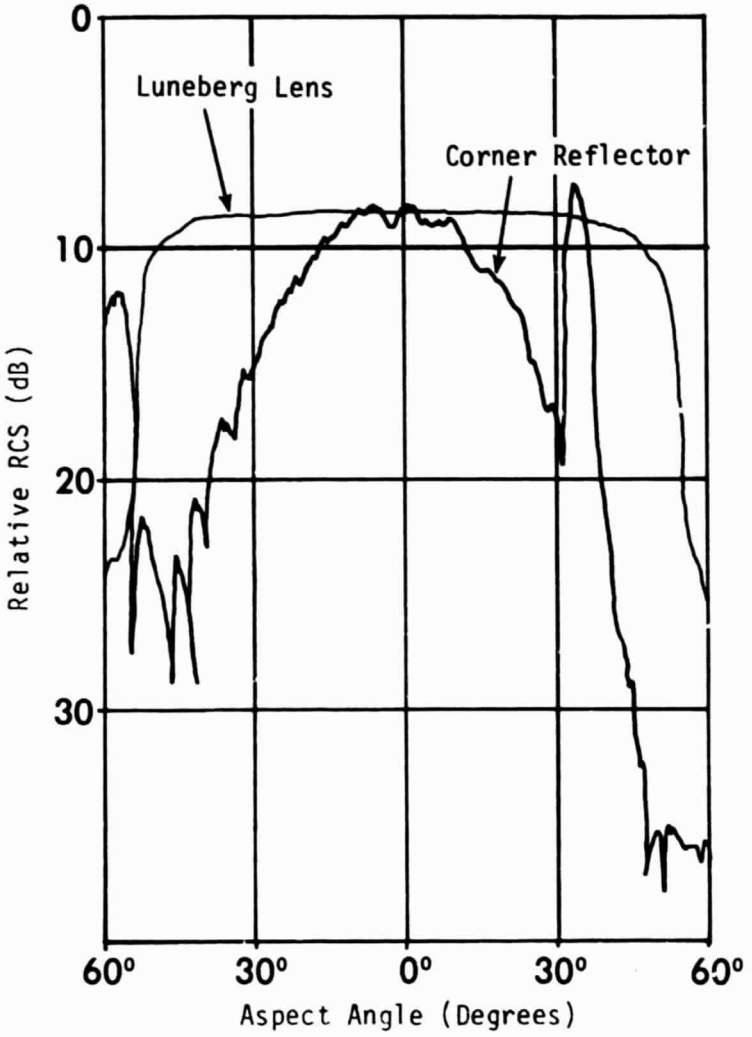

FIGURE 6.3. COMPARISON OF ANGULAR RESPONSE OF LUNEBERG LENS AND TRIANGULAR CORNER REFLECTOR.

values are available due to the cost, size, and weight. However, well-sited, low RCS, Luneberg lenses are excellent calibration references.

The geometries for the top hat reflector and corner reflector are given in Figures 6.4 and 6.5, respectively. The top hat reflector is very well-suited for small RCS values because the ground plane can be tilted to insure optimum aspect viewing from the SAR. The measured response is shown in Figure 6.6 for a 10 m^2 top hat. Note in Figure 6.4 that the viewing aspect is centered on the diagonal across the ground plane. This aspect reduces edge effects from the ground plane to a minimum; the ripple on the response is about 1 dB. The frequency dependency of the top hat can be seen from the equation given. The response of the top hat in azimuth (the ϕ angle) is constant over $\phi \pm 30^\circ$ about the diagonal.

Measured patterns showing the response of each corner reflector type (square, triangular, and circular) are given in Figure 6.7. The response measured in the plane including the peak RCS value for a 90° range of aspect angle is given in the figure. Each major division on the plot is 10°. The sharp peak on the right side is due to the flat plate as viewed from the bottom. The reflector is rotated 90° to a second sharp peak which is due to the dihedral when viewing the corner parallel to the lower side. The reflector is rotated through for values of θ from 0° to 90° to show the angular response through the peak, which is seen to occur 35° from the lower edge. In comparing the angular responses, it is seen that the triangular corner provides the largest beamwidth, but also has greater ripple in the region of interest. Since corrections in the RCS value for each reference reflector will be required due to variations in imaging viewing angle from the SAR, a smooth response will reduce the error contribution from this source.

Figure 6.8 gives the measured angular responses for square, triangular, and circular corner reflectors. The edge dimension for each

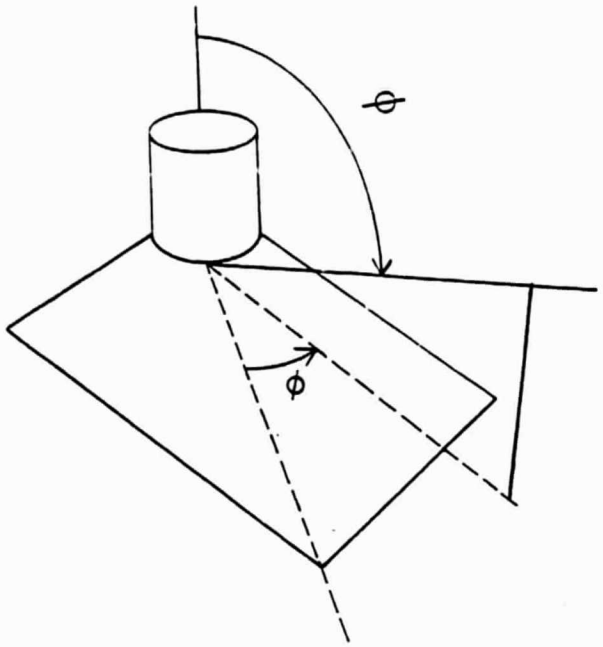

FIGURE 6.4. MEASUREMENT GEOMETRY FOR TOP HAT REFLECTOR.

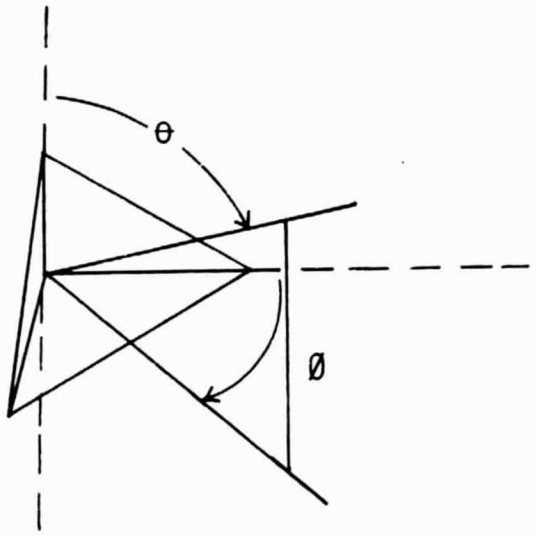

FIGURE 6.5. MEASUREMENT GEOMETRY FOR TRIANGULAR CORNER REFLECTOR.

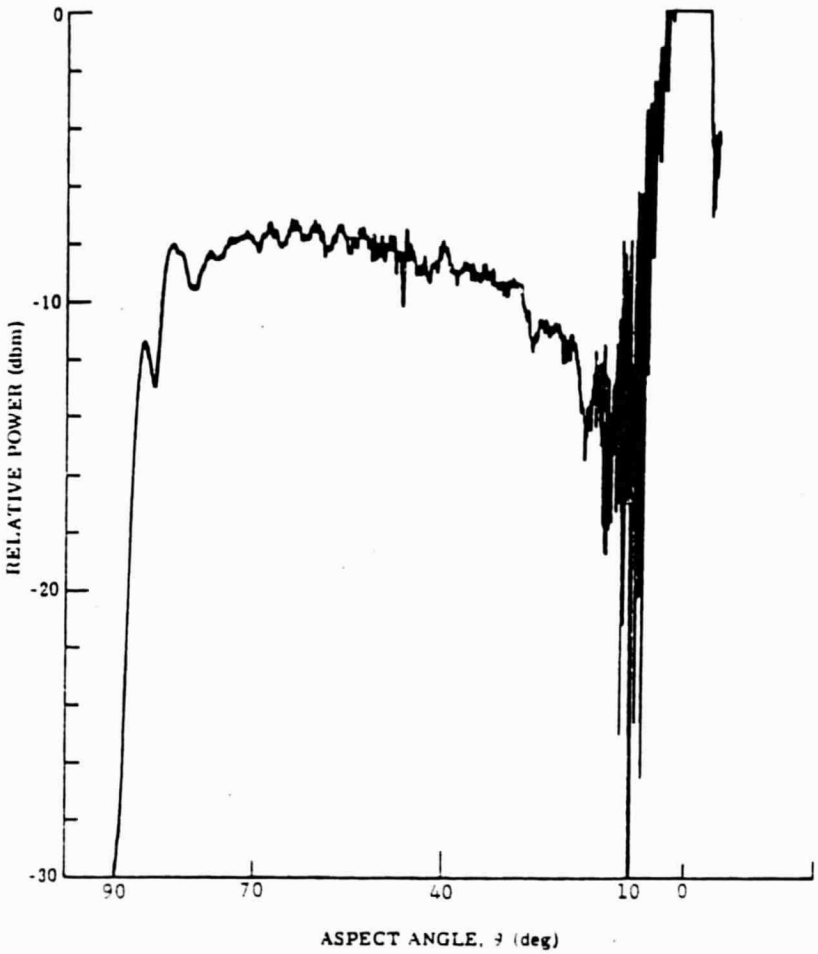

FIGURE 6.6. LOBING STRUCTURE FOR A 10 m^2 TOP HAT WITH ϕ = 90° (ACROSS CORNER).
(θ variable, E_ϕ polarization, f = 9.03 GHz)

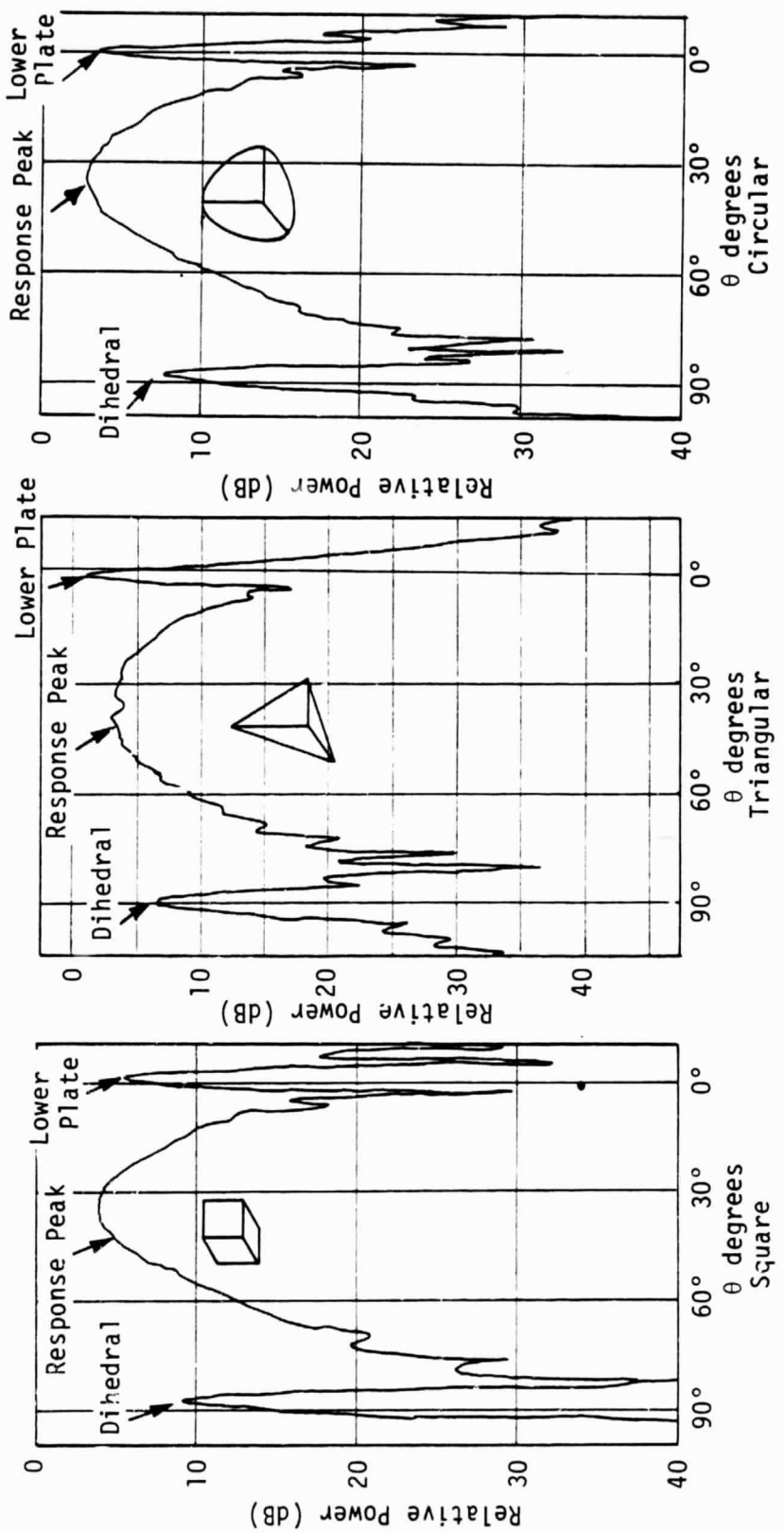

FIGURE 6.7. MEASURED ELEVATION RESPONSE FOR TRIHEDRAL REFLECTORS.

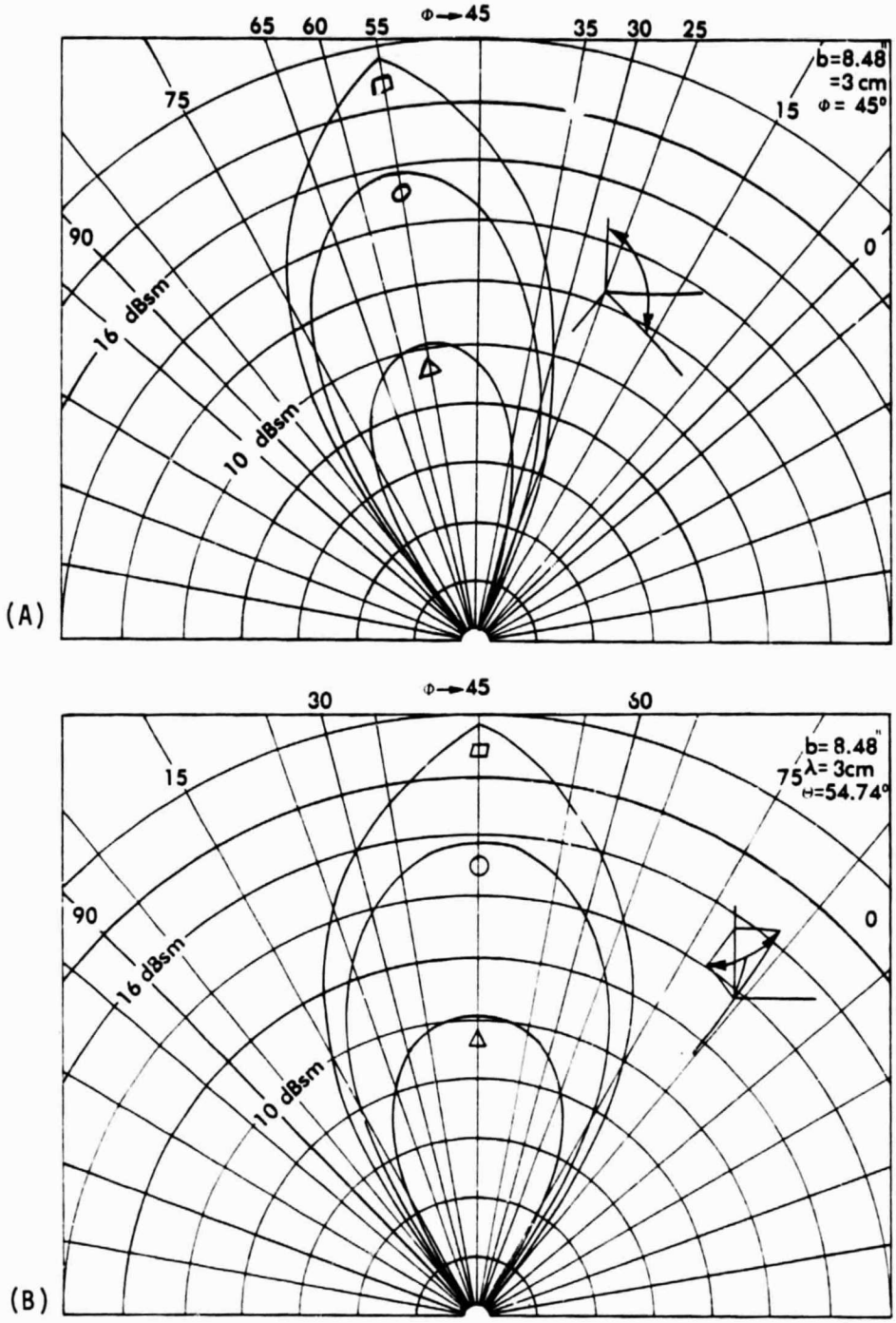

FIGURE 6.8. RCS OF TRIANGULAR, CIRCULAR AND SQUARE CORNERS.
(A - for a plane cut (ϕ = 45°)
(B - for a conical cut (θ = 54.74°)

reflector is 8.48 inches. Variation in RCS value is indicative of the area efficiency of the square corner, with the circular having medium efficiency and the triangular being least efficient. Each reflector has a peak response 35° above the flat side.

Figure 6.8a compares the response of the three reflector types as measured through the peak response ($\phi = 45°$) with $\theta = 90°$ being parallel to the flat base. The improved area efficiencies of the circular and square corners are reflected in the narrower response angles and larger RCS values as compared with the triangular reflector. Figure 6.8b gives a "horizontal" cut through the peak response ($\theta = 125°$) for $0 < \phi < 90°$.

Variations in the corner reflector RCS values as a function of frequency are illustrated with the measured and calculated values given in Table 6.1 and Table 6.2 for horizontal and vertical polarization. Also, calculated values of RCS (including edge effects) are given in each table; the calculated values are for horizontal polarization. It is seen that the variations in RCS value with frequency are larger for the smaller reflector size. This is due to the edge effects contributing to the total RCS; these effects are minimized in the square corner.

Mechanical or construction tolerances required to maintain a given precision in reflector RCS have been considered in considerable detail with results summarized in Figures 6.9 and 6.10. The geometry is illustrated in Figure 6.11 for triangular and square corners. It is seen that the angle tolerances for the square corner are slightly more severe than for the triangular, but not appreciably so.

As an example, if it is required to construct a square corner reflector having a measured RCS value within 1 dB of theoretical value (that is, $\Delta\sigma \leq 1$ dB), the lower curve in Figure 6.9 is used. If the reflector has a side dimension "a" of 10 inches, the angle $\Delta\alpha$ must be less than 1 degree. Using the same example for a triangular corner, it is seen that $\Delta\alpha$ must be less than 1.6 degrees.

TABLE 6.1
ON-AXIS MEASURED AND CALCULATED RCS
FOR A 6-IN. Δ CORNER

Frequency (MHz)	Measured (dBsm) Horiz. Pol.	Vert. Pol.	Calculated (dBsm) Corner and Edges
9250	3.67	4.47	2.31
9300	3.92	4.47	2.27
9325	5.17	4.87	2.27
9350	3.97	3.97	2.28
9375	5.17	4.47	2.30
9400	4.92	4.97	2.33
9450	5.82	5.97	2.43

TABLE 6.2
ON-AXIS MEASURED AND CALCULATED RCS
FOR A 11.5-IN. Δ CORNER

Frequency (MHz)	Measured (dBsm) Horiz. Pol.	Vert. Pol.	Calculated (dBsm) Corner and Edges
9250	13.67	14.67	14.16
9300	14.12	14.67	14.11
9325	15.27	15.67	14.12
9350	14.47	14.42	14.14
9375	15.77	14.72	14.18
9400	15.12	15.57	14.25
9450	15.77	15.67	14.42

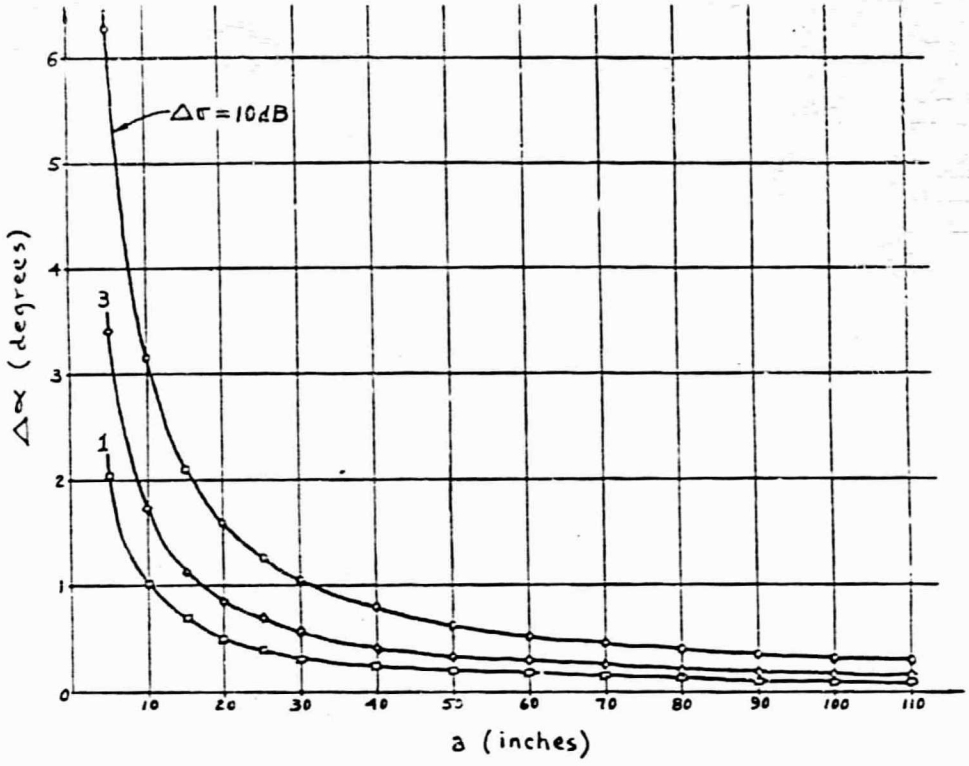

FIGURE 6.9. ANGULAR TOLERANCES FOR SQUARE CORNER REFLECTORS AT X-BAND.

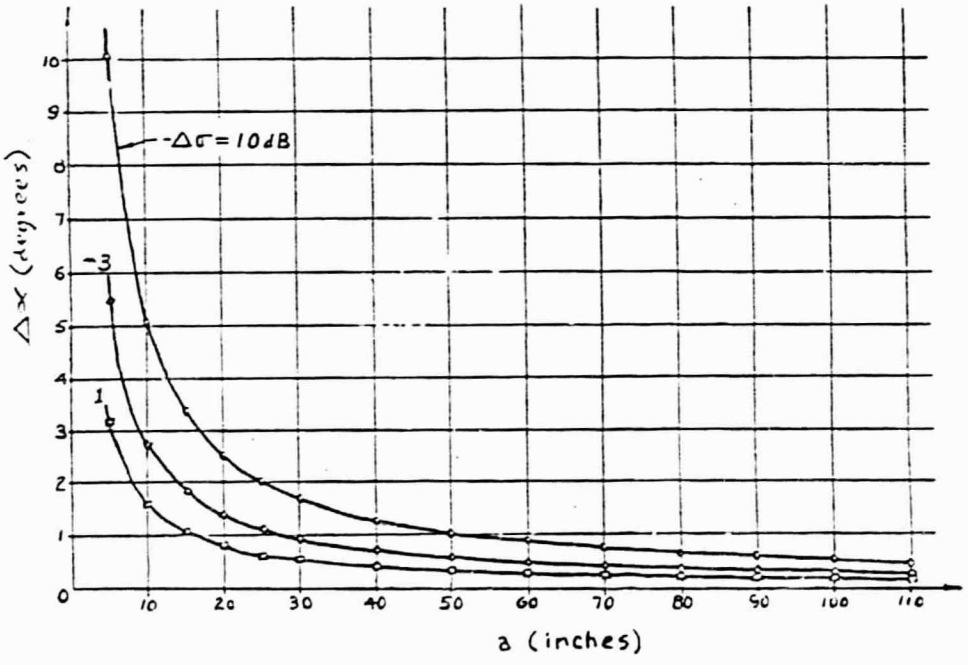

FIGURE 6.10. ANGULAR TOLERANCES FOR TRIANGULAR CORNER REFLECTORS AT X-BAND.

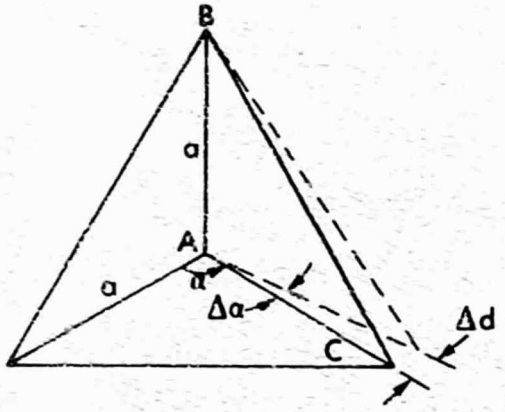

(a) Triangular Corner Reflector

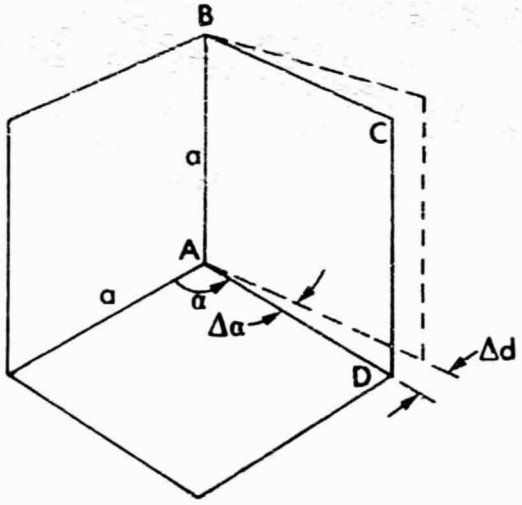

(b) Square Corner Reflector

FIGURE 6.11. ANGULAR ERROR GEOMETRY.

Multipath considerations are very important in selecting the orientation and siting of a reference reflector for calibration. The reflectors should be optimized for the particular radar imaging geometry. The general multipath geometries are illustrated in Figure 6.12. Sample calculations for typical assumed values of RCS, aspect angle, and multi-path reflection coefficients are given in Section 7. Use of an absorbing fence located to intercept the multipath radiation (the first Fresnel zone) reduces greatly the error due to multipath. Clearly, the bistatic RCS of a reference reflector is important in determining the magnitude of the error due to multipath. Bistatic RCS values for the rectangular and square corner are given in Figure 6.13.

Contributions to the RCS ripple due to edge effects are given in Table 6.3 for each of the three corner types. As may be seen from the data given, the edge-induced ripple becomes greater as the nominal reflector RCS value decreases. The square corner has the lowest error due to edge effects and multipath and is used as a calibration reference at low RCS values for 3 cm wavelength radar.

A sphere, when isolated, provides a very stable RCS reference. The RCS value is aspect-angle-independent and, for diameters larger than about 2 wavelengths, frequency-independent. However, the RCS is very sensitive to multipath effects. Also, large sphere diameters are required (for example, 3.56 meters to realize a 10 dBsm RCS value). Spheres are useful in anechoic chambers for very-low-value RCS references, but are not well suited for SAR calibration.

The flat plate also provides a very accurate RCS reference; however, the plate requires very precise orientation and, hence, is not considered a good reference for SAR calibration.

A summary of comparisons between corner reflector types is given in Table 6.4. It can be seen from the values given in the table that minimum error due to edge effects and multipath is obtained with the

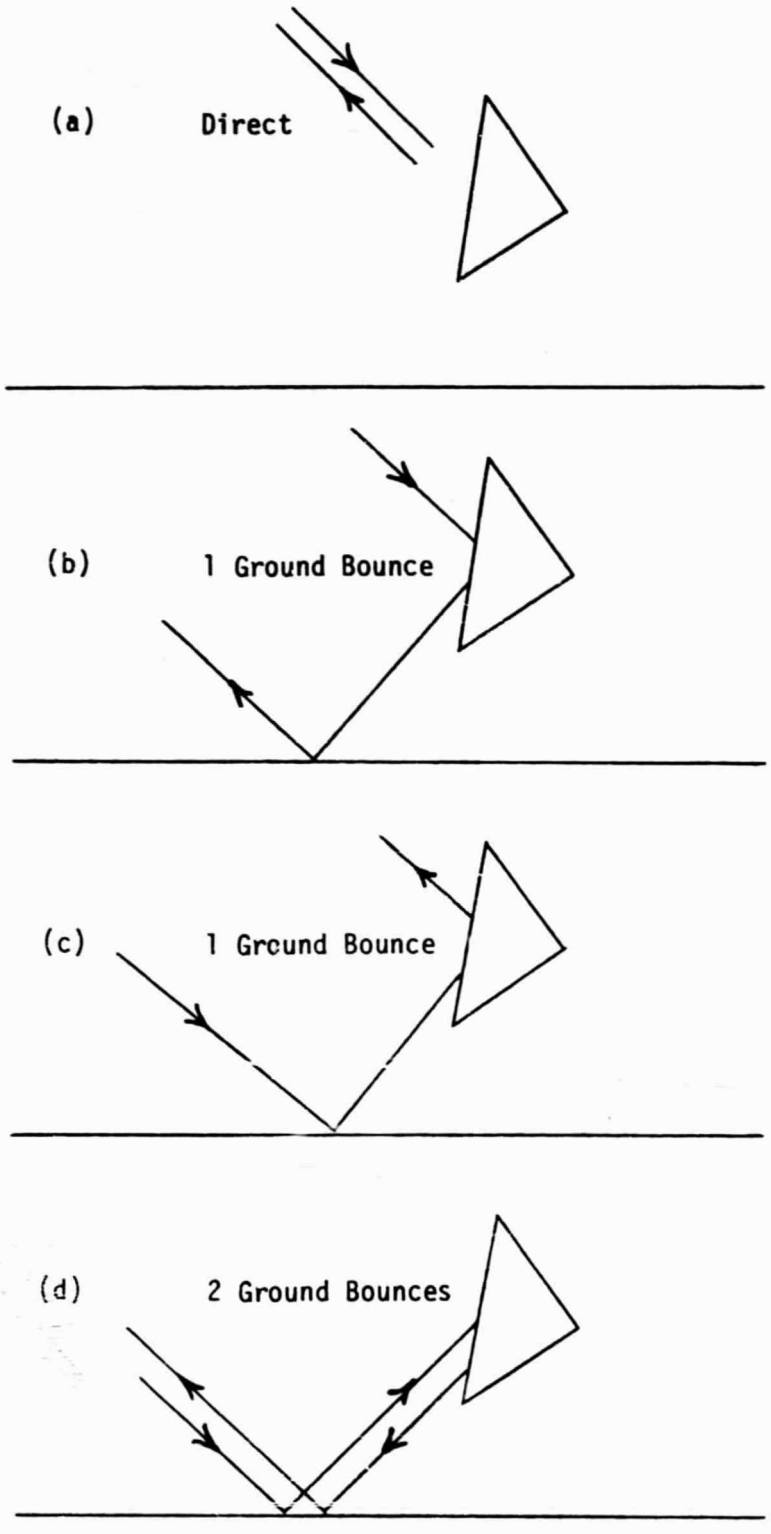

FIGURE 6.12. MULTIPATH GEOMETRY.

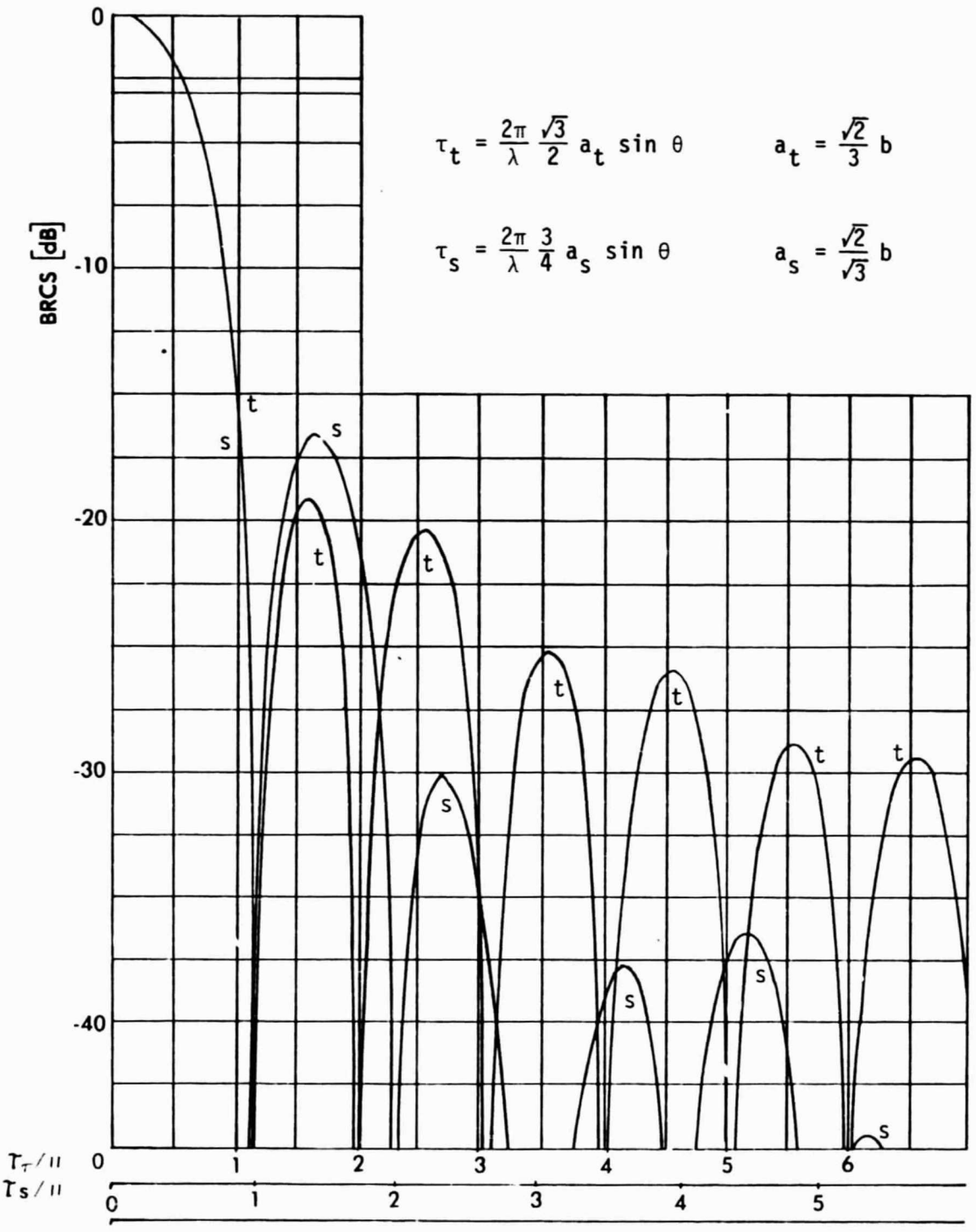

FIGURE 6.13. THE BISTATIC RADAR CROSS SECTION IN THE PLANE OF SYMMETRY FOR TRIANGULAR AND SQUARE CORNER REFLECTORS OF EQUAL PEAK EFFECTIVE AREA.

TABLE 6.3
EDGE-INDUCED RIPPLE

Normal RCS		10 GHz Peak-to-Peak Ripple			1 GHz Peak-to-Peak Ripple		
10 GHz	1 GHz	Triangular	Circular	Square	Triangular	Circular	Square
30 dBsm	10 dBsm	0.448 dB	0.031 dB	0.0063 dB	4.579 dB	0.987 dB	0.628 dB
20	0	0.797	0.074	0.0199	8.601	2.353	2.054
10	-10	1.419	0.175	0.0628	19.826	5.748	6.575
0	-20	2.536	0.416	0.1986	14.729	17.182	23.520

TABLE 6.4. COMPARISON OF CORNER REFLECTOR TYPES.

(Values given for 3 cm wavelength)

Reflector Type	RCS (dBsm)	Edge Dimension	Edge Effects P-P Ripple (dB)	Angular Response	Multipath Effects	Cost
Square Corner	0	7.5 cm	0.200	25° elevation	low	moderate
	10	13.4 cm	0.060	25° azimuth		
	20	23.7 cm	0.020			
	30	42.2 cm	0.006			
Triangular Corner	0	13.0 cm	2.500	40° elevation	high	moderate
	10	23.1 cm	1.400	50° azimuth		
	20	41.1 cm	0.800			
	30	73.0 cm	0.500			
Circular Corner	0	9.3 cm	0.420	30° elevation	moderate	high
	10	16.5 cm	0.175	40° azimuth		
	20	29.4 cm	0.074			
	30	52.3 cm	0.031			

square corner, when compared to other corner reflector types. However, the square corner provides the least value of angular coverage over which the RCS value is nearly uniform. Since the 25° angular response is adequate for SAR calibration applications, the square corner is preferred over the other corner reflector types for small RCS values. The conclusions regarding the selection of reflectors for calibration references for SAR systems can be summarized as follows:

1. Luneberg lens reflectors are best suited for low value RCS references (RCS < 0 dBsm); however, because of the large cost of the Luneberg lens, square corner reflectors and top hat reflectors provide a good compromise in accuracy versus cost.

2. Square corner reflectors are the best selection for intermediate RCS values (0 dBsm < RCS < 20 dBsm) due to low multipath effects, minimum edge effects, and cost considerations. Circular corners are slightly better than square in multipath ripple, but cost considerably more to construct.

3. Triangular reflectors are suitable for large RCS values (RCS > 20 dBsm).

4. Top hat reflectors are excellent for low RCS reference (RCS < 10 dBsm at 3 cm wavelength); however the cost is moderate to high.

5. Measured angular response patterns can be utilized for aspect-angle corrections.

6. Mechanical construction tolerances of the square corners are satisfied by using 0.25 inch aluminum stock with socket bolts used to fasten the three sides together. Also, all edges are tapered.

7. Multipath fences consisting of absorbing material should be used on flat ground to reduce multipath effects for depression angles less than approximately 20°; when sites permit,

installation of reflectors on hill tops reduces multipath effects.

6.2 REFLECTOR ARRAY DESIGN

Calibrated reflectors are utilized for (1) measurements of the total SAR system response, (2) in-flight measurements of the antenna pattern, and (3) calibration verification (if they provide absolute RCS reference values). Major considerations in the selection of reflectors for the SAR system response measurements include:

1. Minimum RCS value equal to the minimum detectable signal value. Maximum RCS adequate to saturate the SAR system at prescribed imaging ranges. At least three intermediate RCS values to establish response. Also, as many additional reflectors of equal value as possible to provide additional individual measurements for each RCS value.

2. Array extent to provide adequate spacing between large and smaller reflectors. At least twice the distance corresponding to a transmitted pulse length in range and twice the real aperture angular extent in along track direction.

3. Siting selected so as to maximize the signal-to-background (clutter) ratio, S/C. This implies careful attention to the σ° value of the terrain or surrounding area in order to maximum the S/C ratio:

$$\frac{S}{C} \alpha \frac{\sigma_r}{\sigma^\circ \rho_r \rho_a \csc \theta} \tag{6.1}$$

4. Siting considerations and selection of reflector locations to minimize multipath. The reflector location can be idealized as shown in Figure 6.12 to reduce multi-path. Also, when necessary, use of a fence consisting of absorbing material has been demonstrated to be very effective in reducing the multipath component.

Major considerations in the design of a reflector array for the in-flight measurement of vertical antenna response include:

(1) reflectors of equal RCS value spaced across the total imaged swath,

(2) reflector RCS value in the middle of the system linear response at the particular range to be used during imaging,

(3) signal-to-clutter ratios larger than 10 dB,

(4) multi-path precautions as cited above,

(5) reflectors spaced in azimuth (along track) to insure that system does not saturate due to multiple number of reflectors being imaged simultaneously, and

(6) adequate number of reflectors to provide at least 5 values for each depression angle value (the number of samples can be obtained by multiple passes).

6.3 CALIBRATION SIGNAL GENERATOR

The calibration signal generator provides the reference and monitoring source for the periodic verification of the SAR system transfer function. The basic requirements for calibration signal generation are:

(1) simulated signal received from a point reflector and/or from distributed scatterers,

(2) range-dependent signal,

(3) amplitude control, and

(4) automatic control capability.

A block diagram of a calibration signal generator is given in Figure 6.14. The input power can be obtained from the SAR signal waveform generator (transmitter amplifier input signal) to insure duplication of the transmitted waveform. A digital phase shifter,

FIGURE 6.14. CALIBRATION SIGNAL GENERATOR.

controlled by a signal generated with a programmed microprocessor, provides the azimuth signal history as a function of range and vehicle velocity. Velocity information can be obtained from the SAR system navigation and control system. Range can be selected by the particular microprocessor program to record calibration signals at a variety of different ranges; this provides a measure of uniformity over the processed range interval. Finally, the calibration signal power is coupled into the receive input through a variable, digitally controlled attenuator. The range of attenuator values can also be programmed in the microprocessor and must provide a range of signal levels from below the minimum detectable signal up to saturation. A system block diagram given in Figure 6.15 shows the location where the calibration signal is injected into the SAR receiver. Coupling is provided for with a directional coupler, as illustrated.

Calibration signals are recorded prior to, or immediately following, each data-gathering pass to provide a reference for each data set. If experience has demonstrated that a particular SAR system has the required long-term stability to satisfy error requirements, use of the signal generator can be less frequent.

Procedures for using the calibration signals, after the signals are recorded, include the following steps. First, the signals are processed through the SAR signal processor and the output values are recorded for each calibration signal. Care must be taken to insure that the processing of the calibration signals follows exactly that used for the SAR data (i.e., all system constants, bandwidths, and gain settings). Careful consideration must be given to the significance of the measurement of the calibration signal power. If the calibration signals are to be used to verify system response, all such measurements must be consistent. In addition, if the calibration signals are to be correlated with previously made calibration measurements from reference reflectors, these must be consistent also. For the calibration of point reflectors on the image, measurements of peak values of the calibration signals are required; for

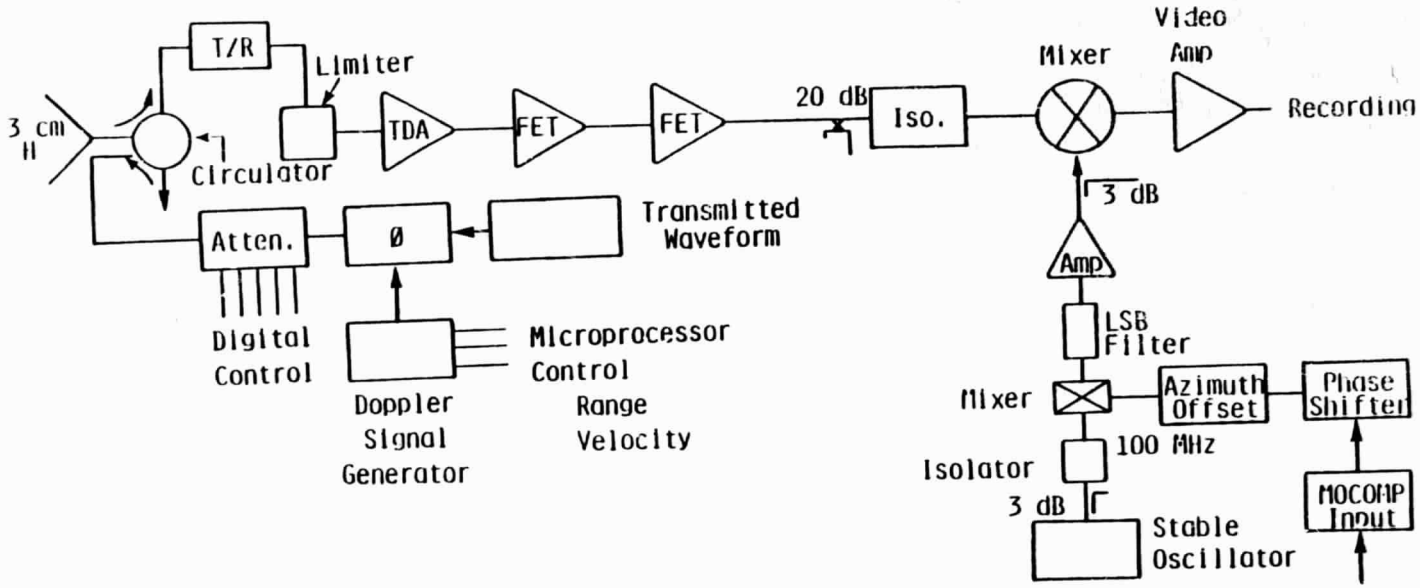

FIGURE 6.15. SAR RECEIVER BLOCK DIAGRAM WITH CALIBRATION SIGNAL GENERATOR.

calibration of distributed scatterers, further consideration is required.

System responses, as measured using calibration signal P_{cal} versus corresponding measured values of output power P_I, provide the transfer function of the system. These measured transfer functions are compared from time to time to monitor system stability from the antenna terminals to the image output and to obtain a measure of gain correction, if necessary.

Finally, it should be pointed out that a calibration signal generator satisfies a second important function, that of SAR system operational diagnostics. With a signal generator, the complete operation of the SAR can be (and usually is as standard operational procedure) checked out on the ground before each data-gathering mission. Systems having a real-time processor (RTP) on-board can use the simulated SAR return to verify proper operation up to the image output. Clearly, if the SAR system is not operating to specification for any reason, data gathering must be delayed until the system has been repaired. The calibration generator can be utilized to detect and identify system problems on the ground, thereby avoiding the gathering of non-calibrated data.

6.3.1 DESIGN REQUIREMENTS

The type of signal provided from the calibration signal generator will depend to a great extent on the particular SAR system to be used. Ideally, the response of the total SAR system is to be measured; this includes the receiver, recorder, and SAR signal processor.

As outlined above, the requirements that the calibration signal generator must satisfy include the following:

1. Provide a signal identical with that received from a point reflector and/or with that received from distributed

scatterers. This requires that the range and azimuth signal modulation be identical to that used in the SAR.

2. Provide compensation for variations in vehicle velocity and for range.

3. Have provisions for control of signal amplitude level into the receiver.

4. Generator power output should be coupled into the receiver input at, or near, the SAR antenna terminals.

5. Provide the capability to control signal power level and range to required values.

The requirements listed above provide for a complete capability to measure the SAR system response at any value of range, vehicle velocity, and signal power. Since the X-L SAR utilizes optical recording variations in the range and azimuth response must be monitored.

Requirements for a calibration signal generator for an all-digital SAR may be less demanding, after stability in range and azimuth has been demonstrated with results from response measurements. Factors that must be considered include:

(1) system gain as a function of range and azimuth, and

(2) overall short- and long-term stability.

Adequate system monitoring and calibration may be realized, for digital systems with verified stability, by using a single calibration reference. A single reference signal, perhaps with only noise modulation, may be adequate for system monitoring. These requirements and the resulting implications for calibration capability and error must be further analyzed to obtain optimum solutions.

The range power values from the calibration generator into the SAR receiver should provide a signal level from, or slightly below, minimum detectable signal up to the limiting level of the system.

Considerable care in the overall system design is required to avoid problems due to leakage into the receiver. Clearly, leakage signals can obscure calibration signals at some levels and, at worst, generate misleading information if the leakage is unrecognized as such.

All requirements for the most versatile calibration signal have been satisfied using a microprocessor-controlled generator. The block diagram of this system is given in Figure 6.14 and the requirements are listed in this section. The microprocessor is programmed to compute the azimuth Doppler history $\theta(x)$ as a function of range R_n and vehicle velocity input. Also, the program controls the digital microwave attenuator through a sequence of attenuation values.

6.4 SIGNAL-DEPENDENT NOISE

The lowest measurable signal level at the output of a SAR system is limited by the total system noise. As indicated in Section 4, this noise includes additive (signal-independent) noise as well as multiplicative (signal-dependent) noise sources. In a well-designed system, the additive noise is dominated by receiver thermal noise. Signal-dependent noise sources include integrated sidelobe energy of the point-target response, ambiguities, and intermodulation effects caused by system nonlinearities.

In this section, the effect of signal-dependent noise on the usable system dynamic range for distributed clutter measurements will be examined and two key sources of signal-dependent noise, namely, integrated sidelobes and quantization, will be reviewed.

6.4.1 DISTRIBUTED CLUTTER DYNAMIC RANGE

As defined in Section 4, the dynamic range of a SAR system for clutter measurements is the ratio of the maximum mean clutter image intensity for which linear operation is achieved to the mean output noise power. That is, clutter dynamic range (CDR) is given by

$$CDR = \frac{\sigma^{\circ}_{max}}{\sigma^{\circ}_{tn}}, \tag{6.2}$$

where σ°_{max} = maximum backscatter coefficient of terrain patch for linear operation and

σ°_{tn} = equivalent backscatter coefficient of total noise

The value of σ°_{max} depends on the area of the clutter region (A_C) and the maximum received RF power level permissible for linear operation. The peak received RF power level from a reflector with cross section σ is

$$P_R = \frac{P_T G^2}{L} \frac{\lambda^2}{(4\pi)^3 R^4} \sigma = K \sigma, \tag{6.3}$$

where definitions of parameters and example values are summarized in Table 6.5.

The RF power level corresponding to a distributed clutter region of area A_c and backscatter coefficient σ° is approximately

$$P_R = K A_c \sigma^{\circ} \sec \theta, \tag{6.4}$$

providing

$$A_c < A_s, \tag{6.5}$$

where A_s is the area of the total illuminated scene. That is,

$$A_s = L_a L_R, \tag{6.6}$$

where L_a and L_R represent the dimensions of the illuminated scene in azimuth and range respectively and are given by

$$L_a = \frac{\lambda R}{d_a} \text{ and} \tag{6.7}$$

$$L_R = \frac{cT_p}{2}. \tag{6.8}$$

TABLE 6.5
EXAMPLE SAR PARAMETER VALUES

Symbol	Definition	Example Value (X-Band Channel of X-L SAR)
P_T	Peak transmitter power	500 watts
G	Antenna gain	28 dB
L	Total system losses	8.9 dB
λ	Wavelength	0.032 m
T_p	Transmitted pulse length	2.7 μsec
d_a	Antenna azimuth length	1.52 m
R	Slant range	5400 m
P_R	Received RF power level	
P_{max}	Maximum P_R for linear operation	-70 dB

Therefore, the maximum backscatter coefficient for linear operation is

$$\sigma^{\circ}_{max} = \frac{P_{max}}{K A_c \sec \theta} . \tag{6.9}$$

For the homogeneous clutter case wherein the entire illuminated scene has the same backscatter coefficient ($A_c = A_s$), it turns out that

$$\sigma^{\circ}_{max} = {}^{\circ}_{av}, \tag{6.10}$$

which implies that the clutter dynamic range is given by

$$CDR = \frac{\sigma^{\circ}_{max}}{\sigma^{\circ}_{tn}} = \frac{\sigma^{\circ}_{av}}{\sigma^{\circ}_{n} + MNR\ \sigma^{\circ}_{av}} \tag{6.11}$$

or

$$CDR = \frac{1}{MNR} \tag{6.12}$$

for a SAR system in which the total noise is dominated by signal-dependent noise.

In general, the clutter dynamic range is given by

$$CDR = \frac{P_{max}}{K \sec \theta} \frac{1}{A_c} \frac{1}{\sigma^{\circ}_{tn}} . \tag{6.13}$$

For the example values given in Table 6.5, the clutter dynamic range varies between 9 dB and 51.5 dB for values of A_c ranging from A_s to the limiting case of the area of a resolution cell (assuming $\sigma^{\circ}_{av} = -15$ dB).

6.4.2 INTEGRATED SIDELOBES

An important source of signal-dependent noise is the integrated sidelobe energy of the system impulse response. Even though the peak

value of the sidelobes may be down more than 25 dB or so relative to the peak of the mainlobe in a well-designed SAR system, the total integrated energy contained in the sidelobes is often significant and may reduce image contrast and reflectivity measurement accuracy.

For example, the sidelobes of the responses to a very large reflector can be observed in the lower left corner of the SAR image shown in Figure 6.16. Every element in the scene has approximately the same relative sidelobe response, which tends to distribute energy from one portion of the image to adjacent portions and, hence, affect the accuracy of reflectivity measurements.

Integrated sidelobe effects are of particular concern when attempting to measure a patch of terrain with a relatively low backscatter coefficient which is surrounded either by terrain with a high backscatter coefficient or other large reflectors. Since integrated sidelobes represent a type of signal dependent noise, increasing the transmitter power will, of course, not alleviate the problem.

As is well known, these sidelobes can be controlled by proper amplitude weighting of the coherent processing aperture and by minimizing phase errors. Phase errors [31, 38] which vary over the processing aperture tend to remove energy from the mainlobe and redistribute it into the sidelobes. Phase errors which vary approximately sinusoidally tend to concentrate this energy at distances from the mainlobe which are proportional to the frequencies of the phase-error variations (sometimes called paired echoes [39]). Random, broadband phase errors distribute the energy over many sidelobes; this effect may extend far from the mainlobe. These high-frequency, random phase errors are of primary concern in calibrated SAR system design.

There are numerous sources of this type of phase error in a SAR system, such as uncompensated motions of the SAR vehicle, local oscillator and transmitter phase instabilities, interpolation errors associated with digital processors, etc. In designing a SAR system, a maximum acceptable high-frequency phase error for the total system

FIGURE 6.16. SAR IMAGERY INCLUDING EXAMPLES OF IMPULSE RESPONSE SIDELOBES. (X-band, HH polarization)

is first established, then a phase error budgeting procedure is carried out to allocate a portion of the total phase error to each of the contributing sources, in order to establish appropriate component design specifications.

Figures 6.17 and 6.18 show two examples of the effects of high-frequency gaussian random phase errors for the case of relatively large errors (6° and 60° rms). The decrease in mainlobe amplitude and increase in sidelobe level can be readily observed.

A detailed analysis of the effects of general types of phase errors is a very difficult problem. For the purposes of this report, an approximate expression which indicates the increase in sidelobe energy caused by high-frequency gaussian random phase errors will be derived.

Either the range or azimuth channel of a SAR can be represented by the Fourier transform relation

$$\left|g(x)\right|^2 = \left| \int_{-B/2}^{B/2} w(f)\, e^{j\phi_\varepsilon(f)}\, e^{j2\pi fx}\, df \right|^2, \qquad (6.14)$$

where $g(x)$ = complex impulse response,
x = image spatial coordinate,
f = signal spatial frequency over coherent aperture,
$w(f)$ = aperture weighting function, and
$\phi_\varepsilon(f)$ = phase error.

If it is assumed that the phase error can be modeled by a stationary Gaussian random process with zero mean and autocorrelation function $R_\phi(f)$, then the expected value of the image intensity can be written as

$$E\left|g(x)\right|^2 = \int_{-\infty}^{\infty}\int_{-\infty}^{\infty} w(f)\bar{w}(f')\, e^{-[R_\phi(0)-R_\phi(f-f')]}\, e^{-j2\pi x(f-f')}\, df\, df'. \qquad (6.15)$$

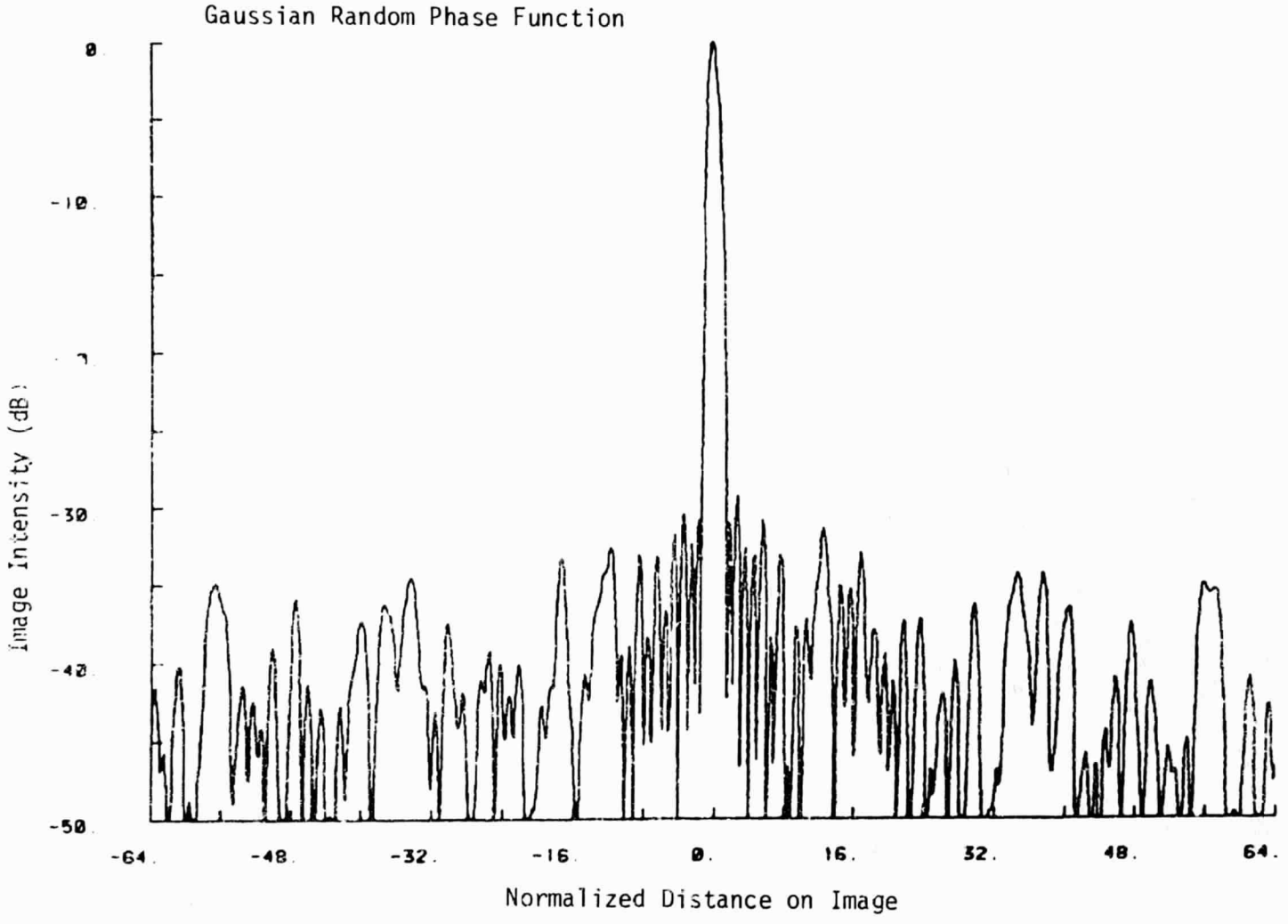

FIGURE 6.17. POINT-TARGET RESPONSE SHOWING EFFECT OF 6° RMS PHASE ERROR

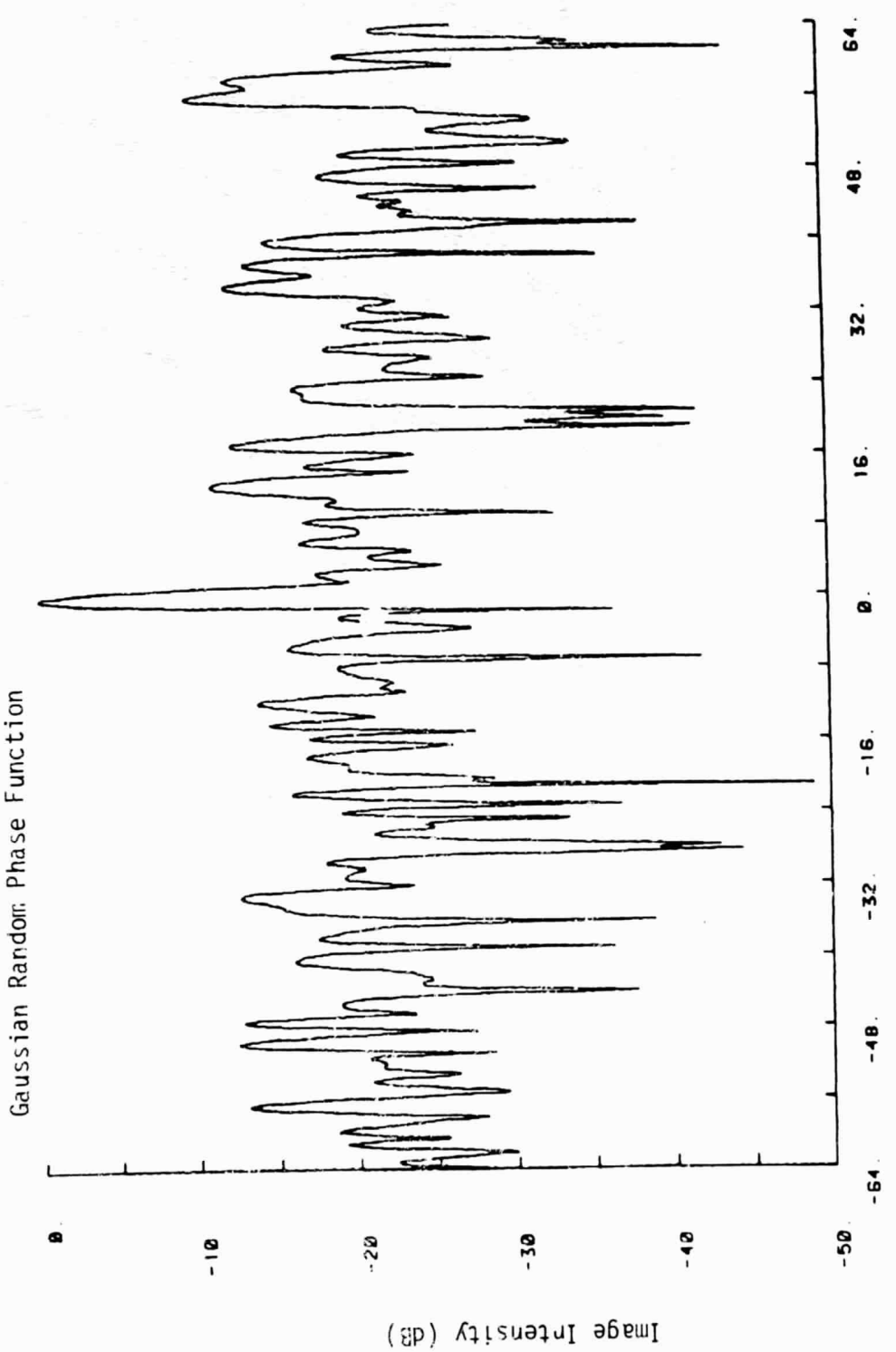

FIGURE 6.18. POINT-TARGET RESPONSE SHOWING EFFECT OF 60° RMS PHASE ERROR

Defining new variables, $p = f - f'$ and $p' = -f'$, the above equation can be rewritten as

$$E\left|g(x)\right|^2 = \int_{-\infty}^{\infty} [w(p) * \bar{w}(-p)]\, e^{-[R_\phi(0)-R_\phi(p)]} \, e^{-j2\pi xp}\, dp. \qquad (6.16)$$

In most situations, the autocorrelation function of the high-frequency phase errors is concentrated about the origin. That is,

$$R_\phi(p) \approx 0 \quad \text{for} \quad p \; > \text{processing aperture length.}$$

Therefore, for values of x within the mainlobe of the SAR system impulse response,

$$E\left|g(x)\right|^2 = e^{-\sigma_\phi^2}\left|g_o(x)\right|^2 \text{ for } |x| < \rho, \qquad (6.17)$$

where $g_o(x)$ = error-free impulse response,

ρ = 3 dB width of mainlobe, and

$\sigma_\phi^2 = R_\phi(0)$ = variance of ϕ_ε.

The reduction in mainlobe energy (MLE), as seen from Eq. (6.17), is

$$\text{Reduction in MLE} = e^{-\sigma_\phi^2}.$$

This implies that the increase in the sidelobe energy (ISLE) of the impulse response is

$$\text{ISLE} = 1 - e^{-\sigma_\phi^2}. \qquad (6.18)$$

Therefore, the ratio of the increase in integrated sidelobe energy to actual mainlobe energy is approximately equal to the variance of the phase error. A typical SAR design requirement is that this ratio

be approximately -15 dB, which implies that the corresponding RMS value be about 1.4 degrees.

An alternate approach for studying the impact of impulse response sidelobes on SAR performance has been developed by Bayma [40]. This approach involves examining the response of a SAR to a uniform clutter and shadow (no-return) boundary -- sometimes called the single-step response. That is, let

$$s_0(x) = \begin{cases} 1, & x < 0 \\ 0, & \text{otherwise}, \end{cases} \tag{6.19}$$

where $s_0(x)$ is the one-dimensional terrain reflectivity.

The mean response to this reflectivity step is given by

$$E\left|s(y)\right|^2 = E\left|h(x)\right|^2 * s_0(x)$$

$$= \int_{-\infty}^{x} E\left|h(x)\right|^2 dx, \tag{6.20}$$

where $h(x)$ is the phase-error-contaminated SAR system impulse response. The transition of the response between the uniform clutter and the no-return region is a function of both the impulse response mainlobe width and the sidelobe level. The depth of the response in the no-return region is determined by the integrated sidelobe ratio.

Figure 6.19 shows the response for an unweighted aperture with no phase errors. In Figure 6.20, the results for a 35 dB Taylor-weighted aperture with four different levels of random phase error are shown. Other examples of single-step responses and also double-step responses can be found in Reference [40].

Other ways in which sidelobes of the SAR impulse response affect the performance of calibrated SAR systems are discussed in Section 7.1 of this report.

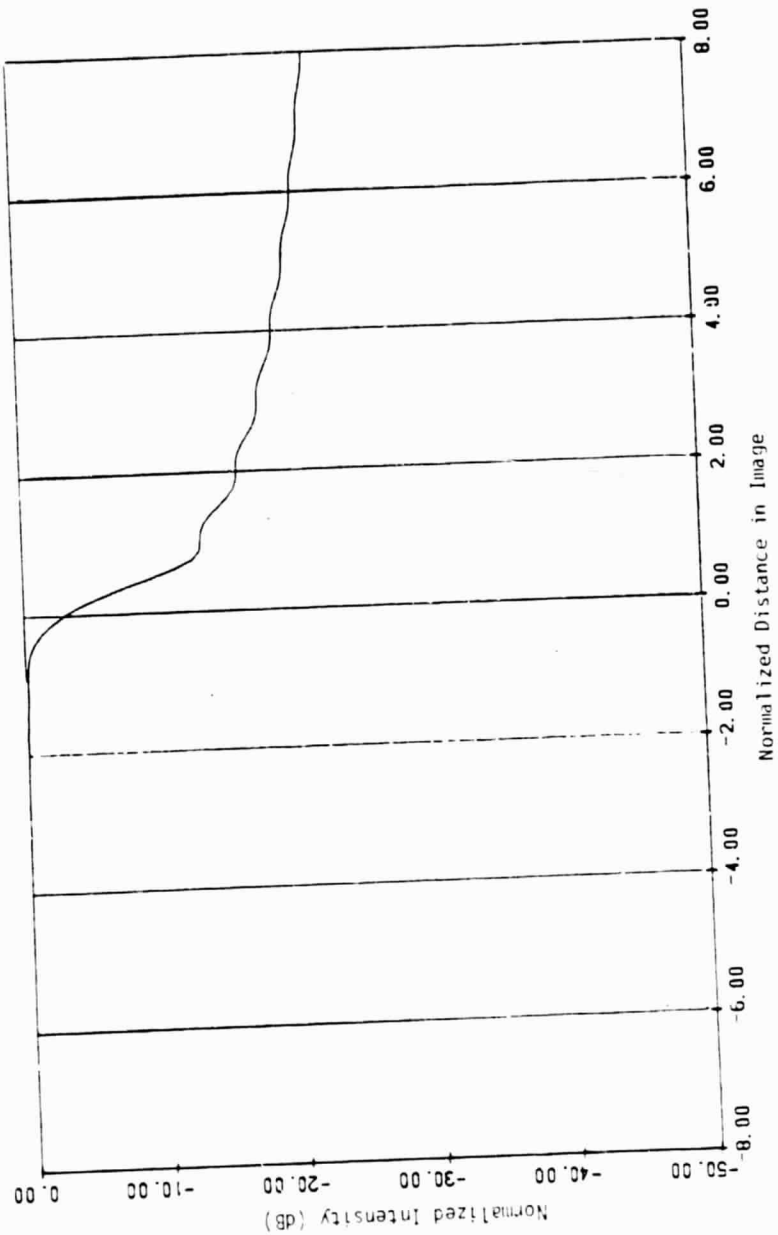

FIGURE 6.19. SINGLE-STEP RESPONSE FOR UNIFORM APERTURE.

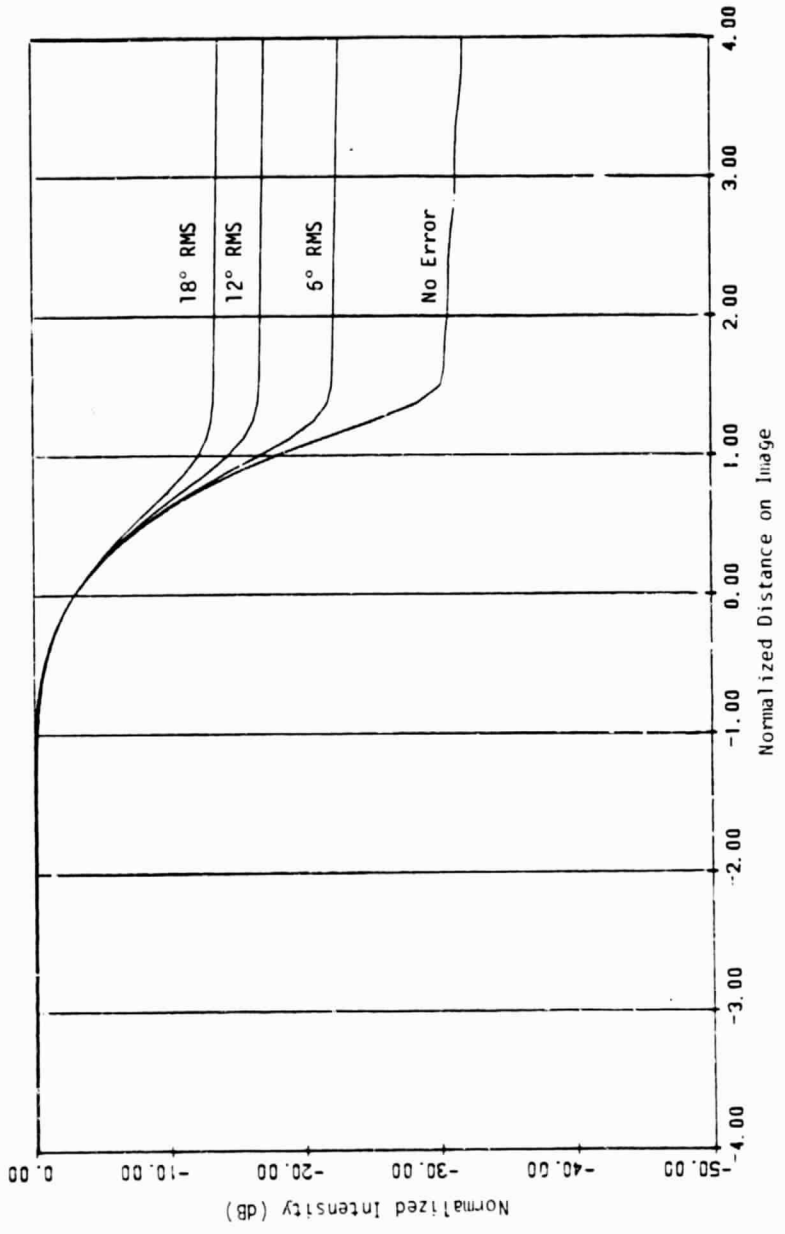

FIGURE 6.20. SINGLE-STEP RESPONSE FOR 35 dB TAYLOR-WEIGHTED APERTURE WITH RANDOM PHASE ERRORS (16 CYCLES/APERTURE).

6.4.3 QUANTIZATION NOISE

In modern SAR systems using digital recording of the phase history data, the quantization inherent in the A/D converter is often a significant source of signal-dependent noise. Quantization noise can be the largest single contributor to signal dependent noise in a well-designed SAR system. This is because data-handling-rate constraints imposed by either data links or tape recorders tend to restrict resolution or swath width. Therefore, a reasonable system design decision is to budget relatively small amounts of signal-dependent noise to all sources other than SAR phase history quantization and use the smallest quantized word length (A/D converter output) which is consistent with image quality requirements.

The questions of concern here are: (1) what is the signal-dependent noise contribution due to quantization and (2) what is the optimum input level for an A/D converter?

The effects of sampling and quantizing SAR phase history signals have been investigated from a number of viewpoints [41-47]. Typically, it is assumed that the phase history signal can be modeled as a sample function of a zero-mean Gaussian random process. It is also assumed that the signal is sampled only slightly above the Nyquist rate, so that the samples are uncorrelated.

As described by Bayma [42], if x is the input to a quantizer and y the output as indicated in Figure 6.21, then the portion of the output signal which is correlated with x is

$$\hat{y} = ax, \tag{6.21}$$

where a is the equivalent linear gain of the quantizer chosen to minimize the mean square error. The remaining (uncorrelated) portion of the output signal is denoted by e_y, where the mean square error is given by

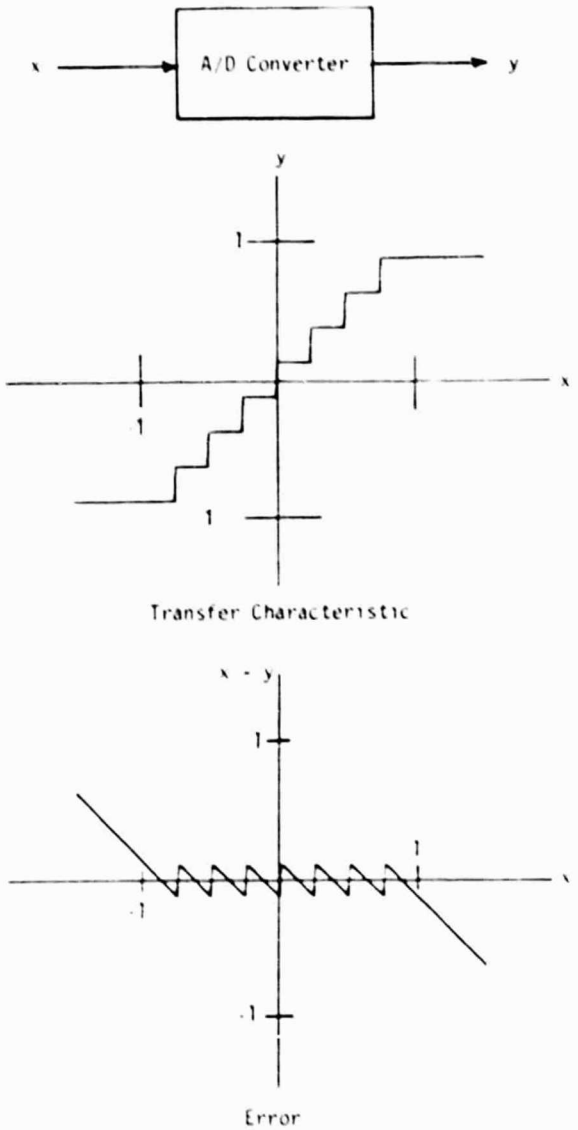

FIGURE 6.21. QUANTIZER CHARACTERISTICS.

$$\text{var } (e_y) = E(y - \hat{y})^2 \tag{6.22}$$

and, therefore,

$$\text{var } (y) = \text{var } (\hat{y}) + \text{var } (e_y). \tag{6.23}$$

The SNR of the quantizer is then given by

$$\text{SNR} = \frac{\text{var } (\hat{y})}{\text{var } (e_y)} \tag{6.24}$$

and the multiplicative noise ratio (MNR) associated with the quantizer is just the reciprocal of the quantizer SNR.

The effective gain (a) of a quantizer is shown as a function of input signal level for various word sizes in Figure 6.22. For small input signals (less than quantizer step size), the effective gain can become arbitrarily large while, for large signals, the gain is compressed due to quantizer saturation.

The SNR of the quantizer is presented in Figure 6.23. The optimum input signal levels resulting in maximum output SNR can be seen. These are consistent with the results of Max [41]. For input signal levels below the optimum value, the effective quantization noise is constant, which implies that the SNR should increase proportionally with the input signal. The SNR decreases quite rapidly for input signals larger than the optimum value, resulting from saturation-induced noise.

The contribution to the system MNR (which is the reciprocal of the A/D converter SNR) is given below, assuming optimum adjustment of input signal level.

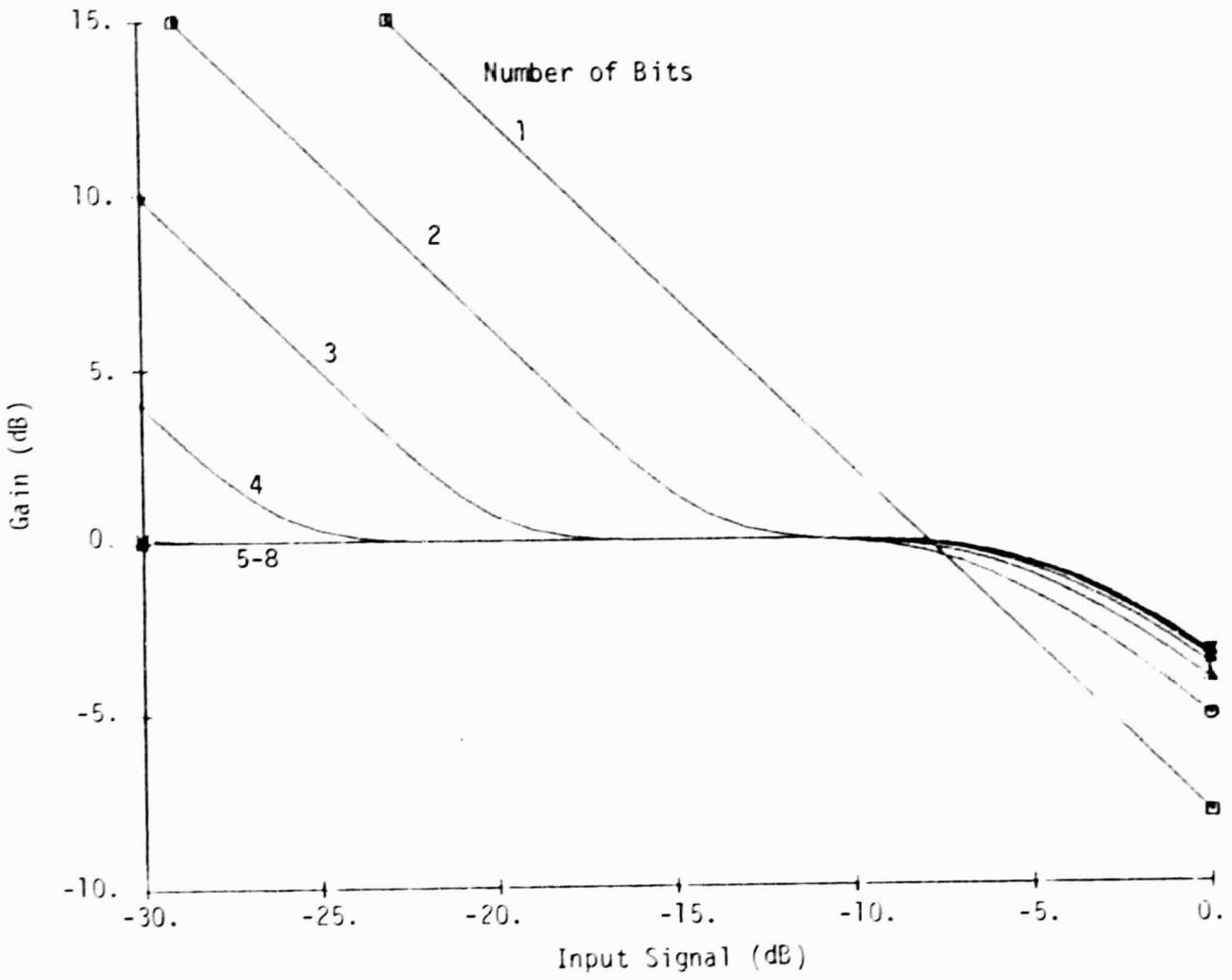

FIGURE 6.22. QUANTIZER GAIN AS A FUNCTION OF INPUT SIGNAL LEVEL AND WORD SIZE

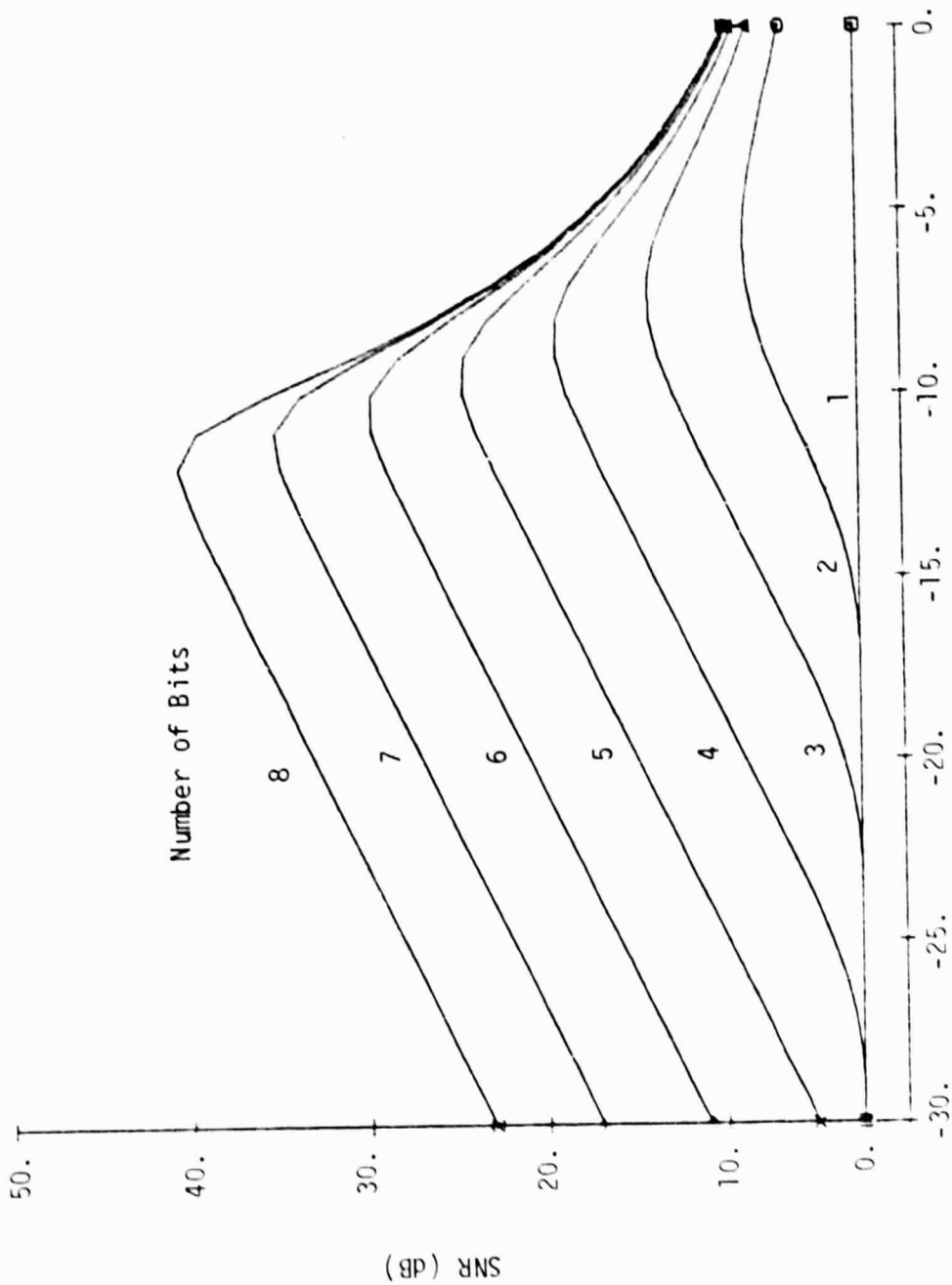

FIGURE 6.23. QUANTIZER SNR AS A FUNCTION OF INPUT SIGNAL LEVEL AND WORD SIZE

A/D Converter MNR (dB)	Number of Bits
- 2.4	1
- 8.7	2
-14.1	3
-19.3	4
-24.5	5
-29.8	6
-35.2	7
-40.5	8

It is necessary to use some type of automatic gain control in order to maintain the optimum A/D converter input level. If this is not done, the quantization noise will be larger and will vary as a function of the input signal level.

7
CALIBRATION ERROR CONSIDERATIONS

The reflectivity measurement accuracy of a SAR system is affected by the uncertainty in knowing the system transfer function and by the presence of total system noise. This section will examine some of the error sources that contribute to system transfer function uncertainty and the resulting impact on measurement accuracy. Since the total accuracy depends to a great extent on the particular SAR calibration scenario, i.e., availability of reference reflectors and whether or not they are located at the same depression angle as the area to be measured, a summary of the errors associated with each scenario is also included in this section.

7.1 REFERENCE REFLECTOR ERRORS

As described previously, reference reflectors play a key role in the SAR calibration process, since they are often used for measurement of the total system response, in-flight measurement of the antenna pattern or, at least, for verification of calibrated SAR performance. This section will summarize the sources of error in the RCS of a reference reflector, i.e., the difference in the measured RCS and the actual RCS.

The primary reference reflector error sources are listed in Table 7.1. Uncertainty in knowing the orientation angle relative to the radar line-of-sight is often the largest contribution to the total reference reflector error. The RCS of corner reflectors not only decreases with departures from the axis of symmetry but ripples in the angular response also occur (Section 6.1). Experience has shown that the azimuth (horizontal) orientation and the elevation (vertical) orientation of field-deployed reflectors can be estimated to within $\pm 2^\circ$ and $\pm 1^\circ$ respectively. If a correction is made for the estimated angular response of the reflector, it should be possible to estimate the RCS of a reference reflector to within ± 1 dBsm of the "true" values with a 90 percent confidence level.

TABLE 7.1
REFERENCE REFLECTOR ERROR SOURCES

1. Orientation Angle Uncertainty (azimuth and elevation)
2. Multipath Effects
3. Clutter in Resolution Cell
4. Energy in Sidelobes
5. Interpolation Error
6. Edge Effects
7. Mechanical Variations

Multipath Effects

The effective RCS of a reference reflector located above a ground plane will be modified due to reflections involving both the reference reflector and the ground plane. The proper choice of reflector type, as reviewed in Section 6.1, can minimize but not completely eliminate these multipath effects.

The total effective RCS of a corner reflector above a ground plane (Figure 6.12) is given by

$$\sigma_r = \left[\sqrt{\sigma_D} + 2\rho_s \sqrt{\sigma_1}\, e^{j\phi_1} + \rho_s^2 \sqrt{\sigma_2}\, e^{j\phi_2}\right]^2, \qquad (7.1)$$

where σ_D = RCS due to direct path,

σ_1 = RCS for one-ground-bounce path,

σ_2 = RCS for two-ground-bounce path,

ρ_s = amplitude reflection coefficient of ground plane,

ϕ_1 = relative phase of one-bounce returns, and

ϕ_2 = relative phase of two-bounce returns.

Depending on the relative phases (ϕ_1 and ϕ_2), the contribution of multipath may be either positive or negative with respect to the direct return RCS. Generally, multipath contributions are significant only in the case of low grazing angles and relatively smooth reflecting surfaces, i.e., large ρ_s. In order to obtain a quantitative estimate of the multipath contribution, specific reflector types, mounting geometries, and ground-plane bistatic reflectivity coefficients must be considered. Errors induced by multistatic effects have been examined in previous measurements programs and standard deviations of RCS measurements of about 1 dB are typical.

As an example of multipath effects, consider the first two terms in the above expression for the RCS of a reflector. These correspond

to the one-bounce situation in Figure 6.12(a, b, c). The computed values for the maximum and minimum RCS for 10 dBsm square and triangular corners are given in Table 7.2.

Clutter in Resolution Cell

The measurement of the RCS of a reflector is corrupted by the surrounding clutter and total noise background. This section will examine the error caused by the background.

The measured RCS of the reference reflector can be written as

$$\sigma_r = \left[\sqrt{\sigma_r} \; \sqrt{\sigma_b} \; e^{j\phi_b}\right]^2, \tag{7.2}$$

where σ_r = RCS of reference reflector,

σ_b = RCS of background (clutter plus noise in resolution cell),

ϕ_b = Phase of background relative to reference reflector return.

The above equation assumes that the signals add coherently and that ϕ_b is uniformly distributed between 0 and 2π.

The probability distribution for total return signal can be calculated and, subsequently, the mean and standard deviation can be determined. For present purposes, it can be observed that the approximate average of the measured RCS is $\sigma_r + \sigma_b$ and the maximum and minimum values are $(\sqrt{\sigma_r} + \sqrt{\sigma_b})^2$ and $(\sqrt{\sigma_r} - \sqrt{\sigma_b})^2$, respectively. This implies that the background causes an average 3 dB error in the measured RCS for a 0 dB signal-to-background ratio ($\sigma_r/\sigma_b = 1$). The error will, of course, be reduced by using a larger RCS reference reflector and using more than one reflector.

Energy in Sidelobes

Another source of error that occurs when using point-like reference reflectors for SAR calibration is related to the decrease in

TABLE 7.2
VARIATION IN REFLECTOR VALUE DUE TO MULTIPATH

	Square	Triangular
Reflector size: σ_o	10 dBsm	10 dBsm
Reflection Coefficient: ρ_s (short grass)	- 8 dB	- 8 dB
Wavelength	3.2 cm	3.2 cm
Edge dimension	13.4 cm	23.1 cm
Depression Angle	12°	12°
Bistatic RCS: σ_1 (from Figure 6.12)	0.18 m^2	0.72 m^2
Variation in σ_r		
Max. value	10.6 dBsm	11.66 dBsm
Min. value	9.24 dBsm	7.9 dBsm

energy of the mainlobe of the point target response and the attendant increase in sidelobe energy caused by system phase errors. In addition to the contribution to signal-dependent noise as described in Section 6.4.2, this effect can also result in an error in estimating the backscatter coefficient of terrain when point-like reflectors are used as calibration references.

If the effects of total system noise are ignored, a typical estimator for the reflectivity of a patch of terrain is

$$\sigma_T = \bar{P}_{IT} \frac{\sigma_r}{P_r}, \tag{7.3}$$

where $\bar{P}_{IT}$ = average power over the terrain patch (measured on the image),

σ_r = RCS of reference reflector, and

P_r = peak power response from reference reflectors.

The σ_r/P_r ratio is assumed to represent the total system transfer function and, hence, allow SAR image measurements to be related to absolute cross sections.

In the presence of phase errors, the peak of the reference reflector response is reduced; if ignored, this effect would lead to an erroneously high estimate of terrain reflectivity. Therefore, it is usually better to attempt to measure the total energy of the reference reflector response, i.e., mainlobe and sidelobes. In practice, to avoid contamination by background terrain clutter and system noise, only the near sidelobes are included in the actual measurement.

Interpolation Errors

In SAR systems involving digital recording and image formation processing, the point-target response is not a continuous parameter function, but is known only at discrete sample positions. Typically,

sampling ratios between 1 and 2 samples per mainlobe width (3 dB) are used. This implies that, in order to estimate either the peak power or total energy of the reference reflector response, some form of interpolation must be incorporated as part of the measurement algorithm. The choice of interpolation function, the number of sample points to be used, and the resulting error are still currently being studied.

Edge Effects and Mechanical Variations

There are numerous other mechanical construction factors which affect the uncertainty in knowing the RCS of a reference reflector. These include not only the edge effects and construction tolerances described previously but also posts and other mounting hardware which can contribute returns that add coherently to the main return to either increase or decrease the total RCS.

7.2 ESTIMATION OF σ° USING IN-SITU REFERENCE REFLECTORS

In order to illustrate the impact of reference reflector errors, one of the simplest SAR calibration situations will be examined, namely, the estimation of σ° using in-situ reference reflectors. That is, reference reflectors are located in or very near a region of terrain whose backscatter coefficient σ° is to be estimated.

The basic procedure is to select an area in the SAR image which encompasses the terrain region of interest and to measure the average power over this area. An absolute reflectivity is estimated by multiplying this terrain power by the ratio of the estimated reference reflector cross section to the power of the reflector response. The accuracy can be improved by using a number of reference reflectors and averaging their responses.

If the only statistic to be extracted from the SAR image data is the mean value of σ°, the average value of the total system noise can be subtracted from the average of the measured terrain response.

One way to estimate the total noise is to measure the power in the image data for a "no-return" area. Typically, this area can be either a large shadow, smooth water, or some other specially designed surface.

Using this procedure, an estimate of σ° is given by

$$\hat{\sigma}^\circ = (\bar{P}_{IT} - \bar{P}_{IN}) \frac{\sigma_R}{\bar{P}_{IR}} \frac{\cos\theta}{\rho_a \rho_r}, \tag{7.4}$$

where $\bar{P}_{IT}$ = average terrain power in the image overall sample resolution cells,

$\bar{P}_{IN}$ = average power in the image associated with sample resolution cells in the no-return area,

σ_R = estimated cross section of reference reflectors, and

$\bar{P}_{IR}$ = average of reference reflector power responses in the image.

That is,

$$\bar{P}_{IR} = \frac{1}{N_R} \sum_{i=1}^{N_R} H_s \, \sigma_{ri}, \tag{7.5}$$

where N_R = total number of reference reflectors,

σ_{ri} = actual cross section of the i^{th} reference reflector, and,

H_s = system transfer function (Section 3).

As discussed in the previous section, the estimated cross section σ_r of the reference reflectors will be in error because of orientation uncertainties, multipath, etc. Furthermore, it is assumed that the power responses from both the terrain and the no-return area being measured are independent and identically distributed exponential random variables. As an additional simplication, it is assumed that the effective backscatter coefficient of the so-called no-return area is zero.

The expected value and variance of the estimate for σ° can be derived from the results for the quotient of two random variables [48] and are given by the approximate expressions

$$E(\hat{\sigma}^\circ) = \sigma^\circ + \frac{\sigma^\circ}{\sigma_r^2} \frac{V(\sigma_{ri})}{N_R} \text{ and} \tag{7.6}$$

$$V(\hat{\sigma}^\circ) = \frac{(\sigma^\circ + \sigma^\circ_{tn})^2}{N_T} + \frac{(\sigma^\circ_{tn})^2}{N_N} + \frac{(\sigma^\circ)^2}{N_R} \frac{V(\sigma_{ri})}{\sigma_r^2}, \tag{7.7}$$

where N_T = number of terrain cells being averaged,

N_N = number of no-return area cells being averaged, and

$V(\sigma_{ri})$ = variance of reference reflector cross section.

By analyzing the reference reflector errors described previously for specific situations, an estimate of the square of the coefficient of variation $V(\sigma_{ri})/\sigma_r^2$ can be determined. This value, along with an estimate of the equivalent backscatter coefficient for total noise (σ°_{tn}), can then be used to calculate the expected value and variance of the estimate for various σ° levels.

For the case of a sufficiently large number of reference reflectors N_R, the expected value of the σ° estimate becomes unbiased, i.e.,

$$E(\hat{\sigma}^\circ) = \sigma^\circ \tag{7.8}$$

and the variance reduces to

$$V(\hat{\sigma}^\circ) = \frac{(\sigma^\circ + \sigma^\circ_{tn})^2}{N_T} + \frac{(\sigma^\circ_{tn})^2}{N_N}. \tag{7.9}$$

7.3 TRANSFER FUNCTION ERRORS

Instrumentation for the monitoring and recording of particular system-operation parameters has been described in a previous section of this report. In this section, the errors associated with the measurements of each of the system parameters will be summarized.

For quantitative measurements on the SAR data, the measured parameter is the power P_I in the output imagery obtained from processing SAR data. The general expression for P_I given in Section 3 is repeated here for convenience:

$$P_I = \frac{P_T \lambda^2}{R^4 L} G^2(\theta) H_R \sigma. \qquad (7.10)$$

Output Power Measurements

The output image obtained from processing SAR data is presented in either an analog or digital format. Considering the analog system first, measurements of output power from the SAR are made in an optical signal processor. Experience has demonstrated that power measurements can be made with an uncertainty of approximately 1 dB. Contributions to this uncertainty include (1) variations in transmission losses through signal film and liquid gate in the optical processor, (2) variations in the illumination source, and (3) uncertainties in the reading of the output meter.

When SAR image data are in a digital format, the measurement of output power is made using an array of samples defining the area of interest. The peak response may not be included within the sample; an interpolation function will give the peak value and the location of the peak. The error in peak value will depend upon (1) the interpolation spacing, (2) the quantization levels used, (3) data format, linear or log, and (4) the statistics of the data to be measured. Typical values for measurement error have been calculated to be less

than ±0.5 dB and can be less if more samples are used in the estimate. All of the above error estimates assume a signal-to-noise ratio of about 7 dB or greater. Measurement error will increase for small signal values due to contamination by noise.

The details of the approach for the measurement of the output parameter P_I; for (1) calibration reference reflectors, (2) antenna response, (3) calibration signals, and (4) the test site area of interest, will affect greatly the uncertainties in the final calibration accuracy. The important factors will clearly be the number of independent samples, signal-to-noise ratio, and methods of estimation. These considerations are outlined in an example given in Section 7.2.

Transmitter Power P_T

In the measurement of transmitter power, two errors must be considered, (1) the absolute value, and (2) the repeatability or precision of the measurements. Absolute calibration uncertainty is estimated to be ±0.25 percent and instrumentation uncertainty is less than 1 percent, based on manufacturers' specifications. An additional error of approximately 0.25 dB is due to uncertainties in the directional coupler and estimates of loss for transmission lines. Using a commercial power meter and a precision directional coupler with an X-band SAR, the uncertainties in average power measurements are about 0.3 dB. This error includes uncertainties in pulse width and pulse repetition rate.

Antenna Gain $G(\theta)$

The antenna gain appears in the radar equation as a squared factor; hence, any uncertainties are doubled in value. Careful measurements in antenna response made on a far-field antenna range can have errors as small as ±0.5 dB in the main-lobe region. Estimates in the sidelobe levels can have considerably greater error, depending on signal level. The largest uncertainty is introduced by placing

the antenna in a radome surrounded by the structure of the aircraft frame. Results of measurements obtained in previous SAR calibration efforts give approximately ±2 dB uncertainty in antenna gain within the 10 dB contour of the mainlobe. Measurements made, during flight, of the antenna response have increasing error at lower depression angles due to multipath, so that the error could increase to as much as 4 dB for depression angles less than approximately 15°.

For spacecraft SAR antennas, the structural environment does not result in appreciable error; however, thermal variations cause deformation of the aperture surface, resulting in gain variations. Also, if the antenna is deployed in space, a verification of the operational gain and response is desirable.

Receiver, Recorder, and Processor H_R

Temporal variations in the receiver, recorder, and processor portion of the system transfer function can be monitored, if necessary, using a calibration signal generator. Results of measurements reported over a period of 10 days showed uncertainties in compensated values of H_R of less than 2 dB for a SAR system utilizing film recording and optical processing. A large percent of this residual uncertainty is due to error in the measurement of P_I. Gain compensation factors (normalization of total gain) required were as large as 3 dB.

Long term gain stability performance of less than ±1 dB is anticipated from new SAR systems using digital recorders and processors.

Calibration Signal Generator P_{ref}

The power for the calibration signal generator is obtained through a directional coupler from the transmitter driver. The signal is modulated with the proper time-bandwidth Doppler history (appropriate for the particular range and velocity) by a digital phase shifter. Amplitude is then controlled by a digital attenuator,

and the calibration signal is coupled into the receiver through a directional coupler. A second directional coupler is used to provide a power-level monitoring point prior to the adjustable attenuator. Measurements of the attenuation steps showed a standard deviation of approximately ±0.2 dB, or less, depending on the number of attenuation elements programmed in the "on" position at any given setting. Using the same value of standard deviation for transmitter power (0.3 dB), the overall standard deviation for the calibration generator power is less than ±0.5 dB.

Geometry

Three operational geometry parameters must be measured and utilized in the calibration of SAR data: (1) range R, (2) altitude h, and (3) antenna pointing angle reference θ. These factors are utilized for calculating

(1) range factor $1/R^3$,
(2) depression angle $\theta = h/R$, and
(3) reference angle for antenna gain: $G(\theta_0 - \theta)$.

Range estimates are made based on measurements of delay time. Uncertainties of less than 0.1 μsec have been demonstrated with the ERIM X-L SAR system. Uncertainties in the altitude can vary from 1 percent to several percent depending upon altitude and topological ground information available. Spacecraft ephemeris data can be very accurate after a large number of orbits have been observed.

Error in the radar range equation due to range uncertainties will be less than 0.2 dB for a typical aircraft SAR situation. Uncertainties in calculated depression angle will be less than 0.5° for $\theta <$ 40° and less than 1.5° for 40° $< \theta <$ 60° for aircraft-type geometry.

Error in depression angle results in uncertainties in the value of resolution area ($A_{gd} = \rho_a \rho_r \csc \theta$) calculated to determine values of σ^o for distributed areas. Uncertainties in A_{gd} at

steep depression angles ($\theta > 50^\circ$) can be as large as 0.5 dB, with uncertainties less than 0.2 dB for shallow depression angles.

Pointing angle and computed values of θ are used with the measured antenna response to determine antenna gain value. Pointing accuracy of the X-band SAR antenna in the ERIM aircraft has been measured to within an uncertainty of about 0.1°. Aircraft pitch and roll can be monitored to within a 0.1° uncertainty. Combining all angle error estimates, an uncertainty in antenna angle ($\theta_0 - \theta$) of 3° or less can be expected at steep depression angles, with uncertainties of between 1 to 2° at shallow depression angles. If these errors occur at angles about the beam maximum, the resulting uncertainty in antenna gain will be 1 dB or less for a 12° beamwidth antenna. However, if the angle is a half beamwidth or more from the antenna peak, uncertainties as large at 3-4 dB or more can result.

Uncertainty values for the ERIM X-band SAR (1974) are given in Table 7.3. Estimates of the expected capability of the future ERIM X-band SAR are also given.

Losses L

The total system loss factor L includes transmission line, propagation, and radome losses. Measurements of the transmission line losses are made between (1) the transmitter output amplifier to the antenna terminals (antenna losses are included in the gain factor) and (2) between the antenna terminals and receiver input. These measurements can be made within a maximum uncertainty of 0.1 dB. It is important to check these values periodically. Included in the measurement are losses in the rotating joint, circulator, TR protection, and several waveguide junctions. Variation in any of these due to vibration, aging, etc., can result in a significant change in loss.

For operational wavelengths longer than approximatey 5 cm, published values of propagation losses are adequate. For wavelengths shorter than approximately 5 cm, propagation loss should be based on

TABLE 7.3
ESTIMATES OF SAR PARAMETER UNCERTAINTIES

SAR Parameter	Error Estimate (1974 ERIM X-Band SAR)	Error Estimate (Future SAR)
Transmitter Power	0.3 dB	< 0.1 dB
Antenna Gain	± 2 dB	< ± 1 dB
Output Power Measurements	1 dB	< 0.5 dB
σ_{ref}	± 2 dB	± 1 dB
Receiver	1.3 dB	< 0.5 dB
H_R		
Recorder-Processor		
Calibration Signal Generator	0.5 dB	0.1–0.2 dB
Geometry		
R	1 percent	< 1 percent
$\theta_d < 50^\circ$	$< 1^\circ$	
$\theta_d > 50^\circ$	$< 2^\circ$	
$\theta_d \sim 70^\circ$	3°	
A_{gd}	0.1–0.3 dB	
Pointing Accuracy	0.1° azimuth, 1°	$< 0.2^\circ$
Losses (no rain) (atmosphere and transmission line)	0.12 dB	0.12 dB

published data that are related to temperature, humidity, and pressure measurements. For aircraft operation in clear weather, at wavelengths of 3 cm or longer, published values will provide estimates of propagation with a maximum uncertainty of approximately 0.02 dB. For moderate rainfall (6 mm/hr), total attenuation can exceed 3 dB with an uncertainty of 0.3 dB or more. Several dB uncertainty could be introduced due to a heavy rainfall, but these conditions are very isolated. Backscatter from rain can increase the effective system noise by a considerable amount, but should be a limiting factor during only a very small percentage of operational time [49-56].

Losses due to transmission through the aircraft radome are negligible except when the radome is wet; during these periods, calibration data could be seriously degraded. Operation in rain or clouds, such that the radome is wet, should be avoided by a change in altitude or flight path.

7.4 SAR CALIBRATION SCENARIO

Measurement uncertainties that contribute to the error in the calibration of a SAR system are dependent upon the particular SAR calibration scenario. Table 7.4 includes a list of SAR parameters with a table of several calibration scenarios considered in this section. Particular SAR parameters that contribute to the measurement error for each of the scenarios are indicated in the table. Using the values for parameter uncertainties listed in Table 7.3, an estimate of the total uncertainties in the reflectivity measurements for each scenario has been calculated using statistical methods [48]. These values were calculated, using error estimates appropriate for the 1974 ERIM X-band SAR and for a future SAR, and are included in Table 7.4. The first four calibration scenarios listed are for single-channel operation. Two examples are for a calibration reflector array co-located with the test area, and two examples consider a remote test area. Two additional scenarios for relative calibration

TABLE 7.4. SAR CALIBRATION SCENARIOS.

(Parameters contributing major error sources for each scenario are indicated)

SAR Parameter	I Single Pass $\theta = \theta_1$ at Reflectors and Test Site	II Remote Site $\theta = \theta_1$ at Reflectors and Remote Site	III Single Pass $\theta = \theta_1$ Reflectors $\theta = \theta_n$ Test Site	IV Remote Site $\theta = \theta_1$ Reflectors $\theta = \theta_n$ Remote Site	V Relative Single Channel θ_1	V Relative Single Channel θ_1 to θ_n	V Relative Two-Channel
Power	X	X	X	X	X	X	X
Antenna			X	X		X	X
Meas.-Image	X	X	X	X	X	X	X
σ_r	X	X	X	X			X
Receiver	short term	long term	short term	long term			X
Recorder / Processor	X	X	X	X	X		X
Calibration Signal Generator		X		X			X
Geometry							
θ			X	X		X	X
R			X	X		X	X
$\theta < 50°$							
$\theta > 50°$			X	X		X	X
$\theta \simeq 80°$							
Total Error: 1974 X-band	3.6 dB	5.2 dB	5.0 dB	5.7 dB	2.8 dB	4.29 dB	6.4 dB
Future	2.2 dB	3.9 dB	3.7 dB	4.1 dB	2.0 dB	3.00 dB	5.0 dB

are included. Each of the SAR calibration scenarios is discussed in this section. As pointed out elsewhere in this report, measurement uncertainties can be reduced by increasing the number of samples. Practical considerations, such as the cost of additional flight time and additional reference reflectors, etc. tend to limit the number of measurement samples. However, consideration of the statistical sampling patterns in the analysis of the SAR imagery from test sites can minimize uncertainties.

7.4.1 SINGLE CHANNEL

Case I

The first scenario requires that calibration reflector arrays be located near the test area such that both the reflector array and the test area can be imaged on a single pass. This is the scenario used in the example given in Section 7.2. The imaging geometry is such that both reflectors and test area are imaged at the same range and depression angles. For this situation, all system parameters are identical for both the calibration and test site data, except for (1) short-term variations in transmitter power and receiver-recorder-processor and (2) errors in output measurements. The measured ratio of the power P_{I_r} from a reference reflector to the received power P_{I_x} from the test area σ_x is equal to the ratio of the RCS values:

$$\frac{P_{I_r}}{P_{I_x}} = \frac{\sigma_r}{\sigma_x} . \tag{7.11}$$

The uncertainty in the reference reflector values is the largest error source in absolute calibration. The total error estimate is 3.5 dB based on the parameter values given. If a number of independent measurements are made, the standard deviation will be reduced, but the absolute error will not be changed, due to the "bias" in the

absolute σ references. Errors in the RCS value of the absolute reference reflectors can be reduced by increasing the number of independent measurements made on each reflector.

Case II

The second scenario considered again requires that the calibration reflectors and test site be imaged at the same range and depression angle, but the test site is now remotely located. The time delay between reflector imaging and data gathering could extend to over a week. The geometry parameters of the system transfer function cancel (within the error bounds that we define as identical geometry), but now long-term variations in H_R become important and the calibration signal generator is used to relate the calibration results to the data obtained from the test site. Four sets of measurements on SAR output imagery are required: (1) calibration reflectors, (2) calibration signals obtained from a calibration reflector pass; (3) test-area sites, and (4) calibration signals recorded during a test-area pass. System and operating parameters must be recorded for all calibration and test-area passes. The two sets of measurements of the calibration signals are used to relate the calibration reflector power values P_I to the output values obtained from the test site (e.g., Figure 5.2).

Measurements (1) and (2) from the reflector array and signal generator provide the calibration of the signal generator power. Measurements of the calibration signals recorded during data gathering provide a measure of system response H_R during data gathering to account for any long-term variations.

Errors that contribute to the total uncertainty in reflectivity measurements as shown in Table 7.4 are due to uncertainties in σ, P_{cal}, P_T, and output-power measurements. Also, although it is specified that the geometry is constant, there will be errors in altitude, heading, and range used in calculating the geometry.

Variations in H_R are assumed to be compensated within the error of the calibration signals and measurements.

Case III

The relationship given for Case I is modified to include the geometry factors and the antenna response $G(\theta)$ when the reflector site and test site are imaged at different ranges and depression angles, but during a single pass. Measured output (image) powers for the reference reflectors and test site are given by Eq. (5.1). For this single-pass situation, the reflectors are located at or near the test site, so that H_R is constant during the total period (short-term stability). Errors that contribute are (1) the error associated with the measurement of the output powers, (2) the geometry as determined from aircraft altitude and slant range, (3) the antenna response, and (4) the error in the reference reflector.

Case IV

The imaging scenario which results in the largest value of uncertainty is associated with SAR measurements at a test site remote from the calibration reflectors, as Case II described, but with the data taken at a variety of ranges and depression angles. Calibration generator power levels are calibrated with the reference reflector array at a range R_1 and depression θ_1, as given by Eq. (5.4). Power measurements from the test-site area and calibration signals recorded during data gathering at the remote test site must be related to the calibration using Eq. (5.4). In addition to the error sources described in Case II, the following additional errors will contribute: (1) uncertainty in antenna response and (2) determination of the geometry constant using altitude and range information.

7.4.2 RELATIVE CALIBRATION

Measurements of RCS differences or ratios are comparison measurements to obtain relative values of RCS. Measurements of the relative

value of RCS may be made using (1) various areas or reflectors on a single image, (2) identical areas or reflectors as imaged during separate passes, (3) identical areas or reflectors as imaged on separate SAR channels (but during a given pass), and (4) identical or various areas as imaged during separate passes. The temporal separation between passes can range from minutes to days or months.

Several possible conditions for which relative measurements may be required are illustrated in Table 7.4. The single-channel expression for the received power is given by Eq. (7.1). Consider a very short time elapsing between the measurements of the two data sets to be compared, for example, on a given image within a single pass. If measurements are made of areas that have been imaged at the same depression angle, all system parameters are identical and (assuming negligible short-term system variation) the comparison of the power P_I for the two scenes provides a measure of the relative values of RCS. Again, for the short time interval situation, but considering areas imaged at different depression angles θ_1 and θ_2 and ranges R_1 and R_2, a comparison of power received must be weighted by antenna gain response and range, as illustrated in Eq. (5.3), to obtain a relative measurement of the two RCS values σ_1 and σ_2.

Considering relative measurements to be made on SAR data obtained over long time intervals, variations in the total system response must be considered. Comparison of RCS values from areas imaged at identical depression angles and range minimizes error, in that corrections for antenna response and differences in range (use of imaging geometry parameters) are not required. Relative measurements made on data from different SAR channels (frequency or polarization) requires absolute calibration on each channel.

8
REVIEW OF PREVIOUS CALIBRATION PROGRAMS

During the past 15 years or so, there have been a number of programs that have considered various aspects of calibration applied to imaging radar systems. Some of the major efforts are given in Refs. [57-65]. Most calibration approaches suggested for application to SAR systems include the use of reference reflectors and a calibration signal generator. These approaches differ in the methods of utilizing the reference reflectors and in the design and implementation of the calibration signal generator. The following discussion reviews the results from several programs directed toward the calibration of imaging radar systems.

1. The NRL four-frequency radar was operational during the 1966-1973 time period [57]. Calibration was achieved by utilizing two approaches: (1) receiver transfer functions for each channel were measured and (2) calibrated sphere reflectors were imaged on each data-gathering day. The spheres were dropped from the aircraft (Super Constellation) and the signal return was recorded during the period that the sphere could be manually tracked. Major error sources are identified as (1) receiver instabilities and (2) tracking error during sphere measurements. Estimates for the magnitude of these errors are approximately 1 dB for receiver stability and 2 dB maximum for sphere-tracking error. A maximum error estimate of ±3 dB is given in [57]. However, the error is less for relative measurements made between channels for which simultaneous sphere calibrations are obtained.

2. Goodyear Aerospace Corporation conducted a program to obtain calibrated data with an AN/APS-79 radar set in 1966 [58]. Calibration signals were recorded as density wedges on the signal film. These signals include phase and amplitude information identical to that received from individual targets

or terrain scatterers during the period of signal recording. A particular approach involves utilizing a sample of the coherent radar reference frequency and amplitude modulating this signal with noise. The noise is band-limited to match the Doppler spectrum width and amplitude weighted to match the antenna response (two-way). This signal is injected into the receiver at the antenna terminals. The band-limited noise is equivalent to the signal return from homogeneous terrain. Using this approach with a fixed PRF results in a calibration that matches the received signal spectrum only at one velocity. Variations in reference power are obtained with a calibrated attenuator. Signal wedges are recorded across the signal film, each wedge corresponding to a different input power level from the calibrated noise generator.

A number of radar parameters must be monitored during data gathering missions to obtain calibrated data. These include:

(1) range delay calibration references,
(2) altitude AGL,
(3) Power transmitted,
(4) receiver gain (if any),
(5) antenna angle,
(6) drift angle,
(7) roll,
(8) yaw, and
(9) transmitted pulse shape.

Antenna patterns were measured, but his did not include in-flight measurements which are required to account for the effects of the proximity of the aircraft frame. Measurements were made on film transparencies; these included the calibration power wedges and test areas of particular fields. Averages were taken over a measurement aperture that included an area of approximately 1000-ft diameter.

Data reduction utilizes the measured range and altitude to compensate for the depression angle and account for the range factor. The depression angle is used with the antenna response to obtain the antenna gain for each measurement. Corrections for roll, etc. (see above list) are utilized. The final measured output was a normalized scattering parameter from each field.

Data from several flight test programs are available. These data consist of radar imagery of various fields in the Phoenix area with values of scattering coefficients for each field.

Results from this program demonstrated that a useful quantitative measurement can be obtained from a calibrated SAR. This was based on measured values of precision for the SAR of about ±1 dB.

3. Another approach to the calibration of an imaging radar was taken by Westinghouse in 1970 [59]. This approach was applied to a noncoherent real-aperture system. The basic scheme follows, in general, other approaches. A reference signal is coupled into the radar receiver following the antenna and reference power is recorded as a function of input power level. The variations in calibration power are controlled by an attenuator which is automatically stepped through a range of values to provide the required output power calibration levels. Calibration signals are recorded over the entire range sweep to provide a measurement of range response.

   Here, the calibration power is provided by a sample of the transmitter power, which is suitably attenuated and mixed with the receiver L.O. signal. The power is not measured on an absolute scale, but is proportional to the transmitted

power level. Precise measurements of the antenna gain and the waveguide loss to the point of injection of the calibration signal are required.

Several options are available in the monitoring of the transmitted signal:

(a) separate monitoring and recording of absolute values,

(b) sampling and recording of transmitter signal,

(c) utilization of transmitter signal as calibration reference, and

(d) sampling of transmitter signal and use of sampled level to modulate a reference oscillator signal, which is recorded and used as the calibration signal.

4. A program, under AF sponsorship, was conducted by ERIM during the 1974-1976 period [60, 61]. This effort resulted in a calibration of the ERIM X-band SAR system. Reference reflectors were designed and used in two calibration arrays. Also, a calibration signal generator was utilized. This program is described in Appendix A.

   Conclusions and recommendations reached, based on results obtained from this effort, included: (1) measurements of the antenna pattern are required to verify any effects due to the proximity of the aircraft structure or to the antenna and (2) the calibration signal must be more flexible to provide suitable calibration signals for a greater range of operating parameters. This should include selectable values of range, vehicle velocities, and selectable amplitude sequences of signals. Also, automatic operation is recommended for calibration of future SAR systems.

5. Preliminary analysis of data obtained from the recent SEASAT L-band SAR has included evaluations of calibration [62].

Reflectors were located at several sites so as to be imaged during various passes of the SEASAT-SAR. Data were limited due to the untimely "death" of the SAR, but data available continue to be analyzed for various application studies and radar system evaluation. Calibration design considerations included: (1) stable receiver transfer function and measurements prior to launch and (2) sensitivity time control (STC) and reflector arrays. Also, detailed system parameter measurements (including the antenna pattern) were made prior to launch. Results of the preliminary analysis (2) verify the expected resolution of 10 meters, (2) measure the impulse response sidelobe level as -27 dB (somewhat higher than design value), and (3) measure the system response and dynamic range with imagery from the reflector array. However, the absolute calibration of the SAR was not realized.

Results from the SEASAT-SAR measurement are given in Reference 63. Again, the results are of a preliminary nature.

6. A very detailed calibration study is reported in Reference 64. This analysis is directed toward the calibration of the Shuttle Imaging Radar (SIR); the calibration approach proposed follows closely the previous calibration programs [58, 60, 61, 65] discussed. A calibration signal generator ("space calibrator" is defined for the space environment. Also, a reflector array (corner reflector form) is required. Tasks are outlined to define required reflectors, reflector sizes, mounting, and installation.

7. An approach to the calibration of SAR systems that utilizes calibrated ground-based and airborne scatterometer instruments is described by Fenner, et al. [34]. This approach is similar to the calibration verification methods prepared as a part of other calibration programs.

A well-documented ground test site in the Death Valley, California, area is identified for use as the calibration area. Two sets of measurements are described: (1) backscatter measurements using a calibrated ground based scatterometer system and (2) measurements of the identical area using calibrated airborne scatterometer instrumentation. Results are presented from measurements 1 and 2. These data are to be used as calibration references for SAR data obtained over the test site.

8. A calibration program, under DARPA sponsorship, was conducted at ERIM during the 1978-1981 period [65]. This program provided calibration capability for the four-channel X-L SAR system operated jointly by the Canada Centre for Remote Sensing CCRS and ERIM. The approach followed that utilized during the previous ERIM calibration program, but included the following additional tasks, as recommended:

   (a) measurements of the antenna pattern in the aircraft to provide in-flight measurements,

   (b) microprocessor-controlled calibration signal generator to provide the capability to generate calibration signals as a function of aircraft velocity, range, and amplitude values, and

   (c) improved reference reflectors for calibration verification and antenna pattern measurements.

   This effort has been recently completed; preliminary results from verification measurements show very good calibration capability. Values of reflectors located in areas imaged during subsequent flights have been determined using recorded calibration signals. Values obtained are within several dB of the measured RCS. Additional verification measurements are required to determine an error or calibration confidence bound.

In summary, calibration techniques applied to both SLAR and SAR systems utilize a calibration generator, reference reflectors, or both for the absolute calibration technique. Variations in the design and capability of the calibration signal generator are great. As discussed above, the simplified approach provides for a "step wedge" type calibration signal reference, applicable at one range only. A microprocessor-controlled calibration signal generator has been recently demonstrated that provides very great flexibility in providing calibration references applicable for a wide range of aircraft velocities, range, and amplitude values.

9
AdSAR SYSTEMS ANALYSIS SUPPORT

The objective of the joint (JSC/JPL) Advanced Synthetic Aperture Radar (AdSAR) Project was to develop and demonstrate technology for SAR systems with new functional and performance capabilities for missions planned for the 1985-1995 period. The technical goals of AdSAR included wide swath, selectable transmitter center frequency, selectable bandwidth and polarization, and absolute amplitude calibration.

As part of this project, the Radar and Optics Division of ERIM provided technical support by attending design review meetings, providing technical critiques and recommendations on the material presented at these meeting, and reviewing relevant SAR calibration technology.

During the early part of the project, ERIM reviewed the AdSAR specifications and design approach. The system description as documented in Reference 66 was an initial cut at the functional requirements for the system. Based on this description, the ERIM SAR Systems Analysis and Constraints (SARSAC) computer program was used to evaluate the predicted AdSAR system performance. Plots of ambiguities and terrain-to-noise ratio (equivalent to clutter-to-total noise ratio) as a function of range and azimuth distances for X- and L-band were generated. The results indicated that even through some of the parameter values given in Reference 66 were not optimized, the basic parametric design in terms of swath width, signal-to-noise ratio, ambiguity level, etc., was good.

The parameters assumed for this evaluation are given in Table 9.1. The ambiguity ratio, which is the ambiguous energy due to sampling of the radar signal divided by the energy received from an element in the desired scene, was the first factor considered. Figures 9.1 and 9.2 show the variation of ambiguity ratio as a function of distance along the range dimension for X- and L-band, respectively. Similarly, Figures 9.3 and 9.4 are plots of ambiguity

TABLE 9.1
PRELIMINARY DESIGN PARAMETERS FOR THE ADVANCED SAR SYSTEM

Parameters	X-band	L-band
Vehicle altitude	10 km	10 km
Squint angle	90°	90°
Ground range	10 km	10 km
Range resolution	7.5 m	7.5 m
Azimuth resolution	2.0 m	2.0 m
ISLR	-10.01 dB	-10.01 dB
Elevation beamwidth	35.0°	35.0°
Azimuth beamwidth	1.6°	12.0°
Peak elevational antenna sidelobes	-13 dB	-13 dB
Peak azimuth antenna sidelobes	-13 dB	-13 dB
Maximum power	1000 watts	1000 watts
Center frequency	9.6 GHz	1.275 GHz
System losses	4.3 dB	4.3 dB
Noise figure	7.9 dB	7.9 dB
Word size	6 bits	6 bits
Pulse length	20 μsec	20 μsec
PRF	1000 Hz	1000 Hz
Aircraft velocity	250 m/sec	250 m/sec

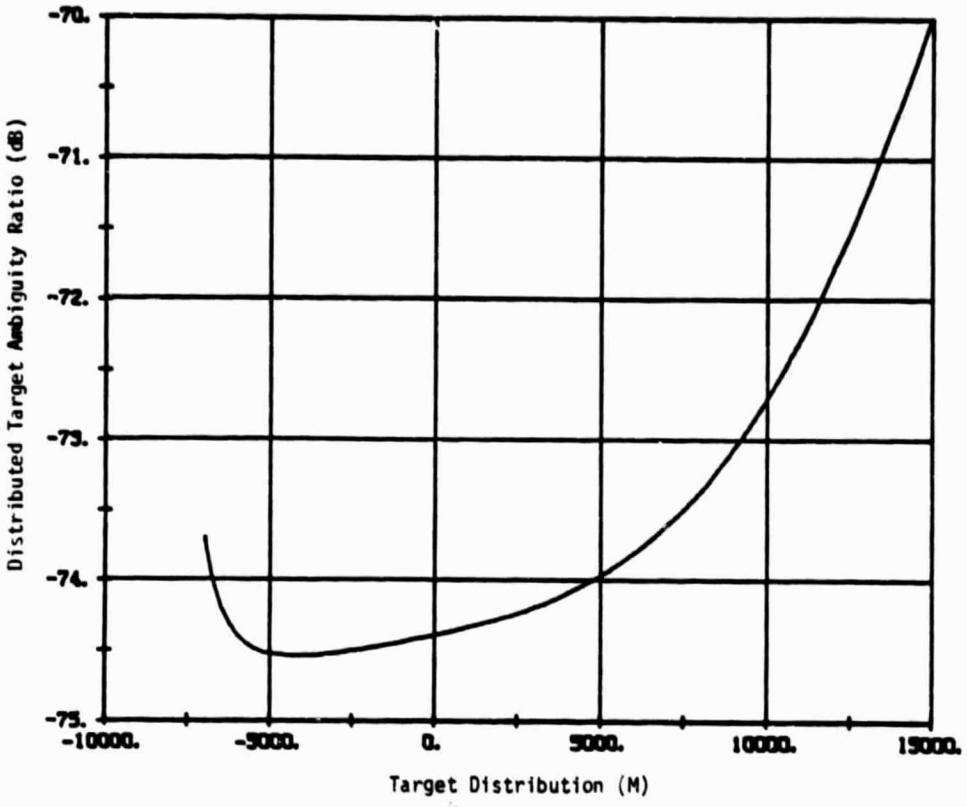

FIGURE 9.1. AMBIGUITY RATIO ALONG THE RANGE DIRECTION AT X-BAND.

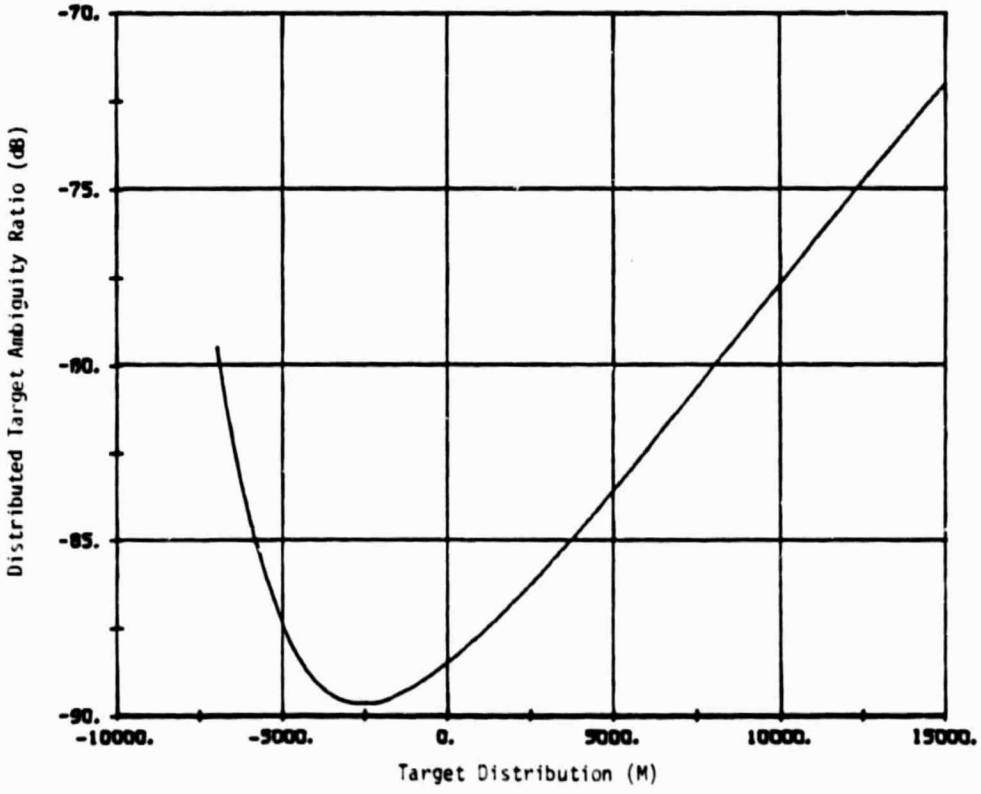

FIGURE 9.2. AMBIGUITY RATIO ALONG THE RANGE DIRECTION AT L-BAND.

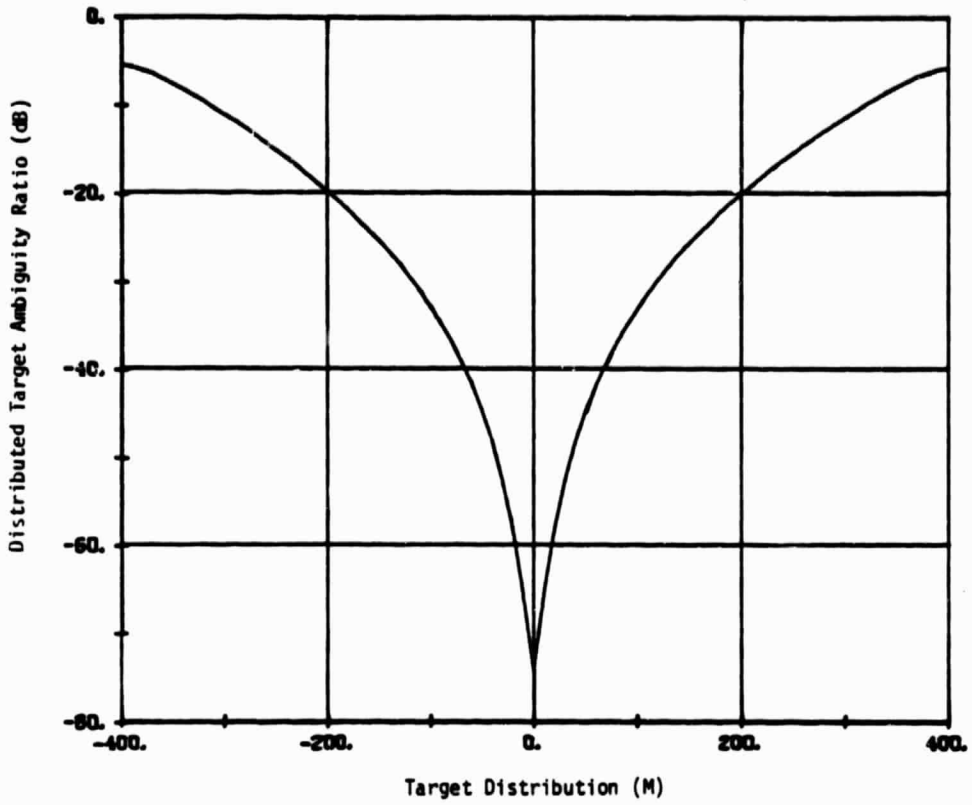

FIGURE 9.3. AMBIGUITY RATIO IN THE AZIMUTH DIRECTION FOR X-BAND.

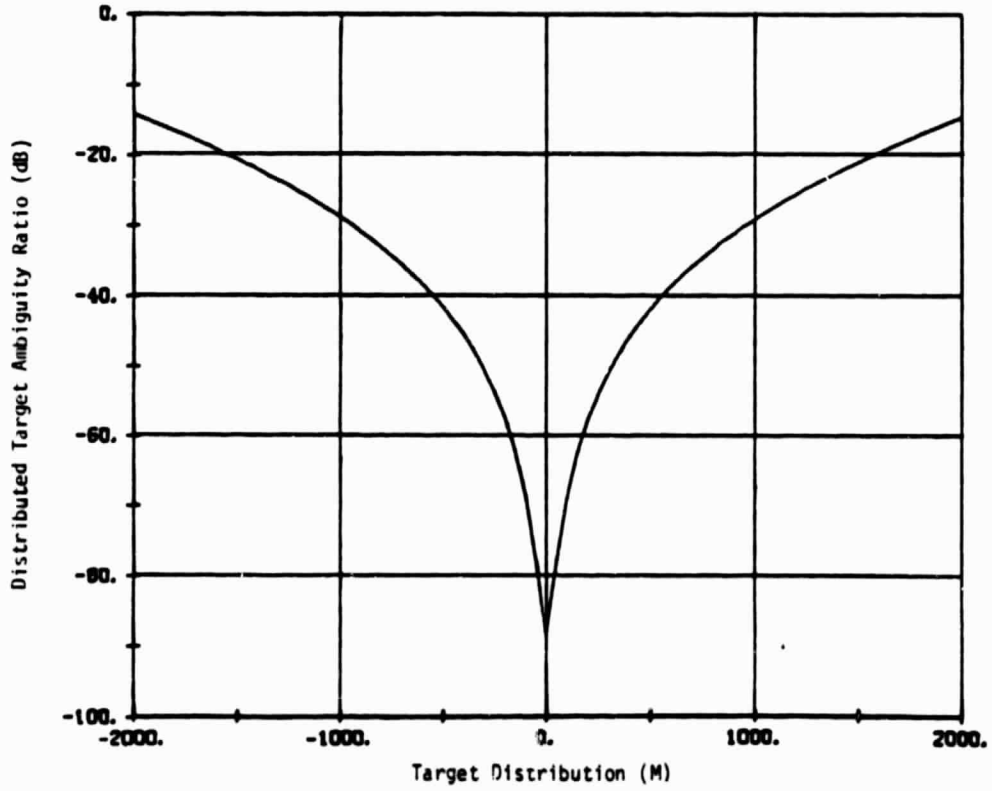

FIGURE 9.4. AMBIGUITY RATIO IN THE AZIMUTH DIRECTION FOR L-BAND.

ratio vs. target distance at X- and L-band along an azimuth cut through the center of the swath, i.e., at a ground range of 10 km. The -25 dB ambiguity level requirement can be seen from these curves to be consistent with the desired resolution and number of looks.

The terrain-to-noise ratio (TNR) as a function of backscatter coefficient σ° at X- and L-band is shown in Figures 9.5 and 9.6, respectively. These were plotted at a ground range of 23.5 km, which is considered to be the worst case. The additive noise was specified to be no worse than -30 dB, which is verified from these plots because TNR is equal or greater than 0 dB when σ° = -30 dB.

Figures 9.7 and 9.8 are plots of TNR along the range (line-of-sight) dimension. Since σ° = -30 dB for these curves, it follows that the total swath width is determined by the criterion than TNR is greater than 0 dB. The results indicate that the swath width is 19.02 km for X-band and greater than 20 km for L-band. This is consistent with the initial AdSAR system goal for a swath width of approximately 20 km.

The SARSAC capability used for this brief evaluation has been useful on a number of SAR system design studies in the past. We expect that this system analysis tool will also be useful for designing future multifunctional, calibrated SAR systems for various terrestrial and extra-terrestrial applications.

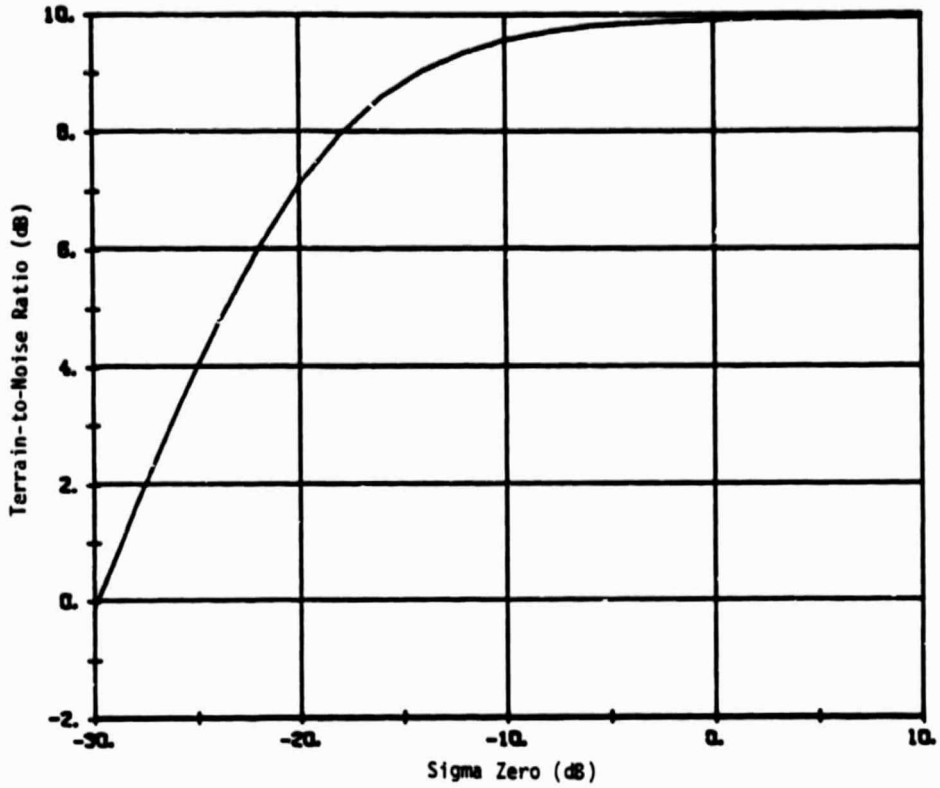

FIGURE 9.5. TNR VS σ_0 AT GROUND RANGE OF 23.5 KM AT X-BAND.

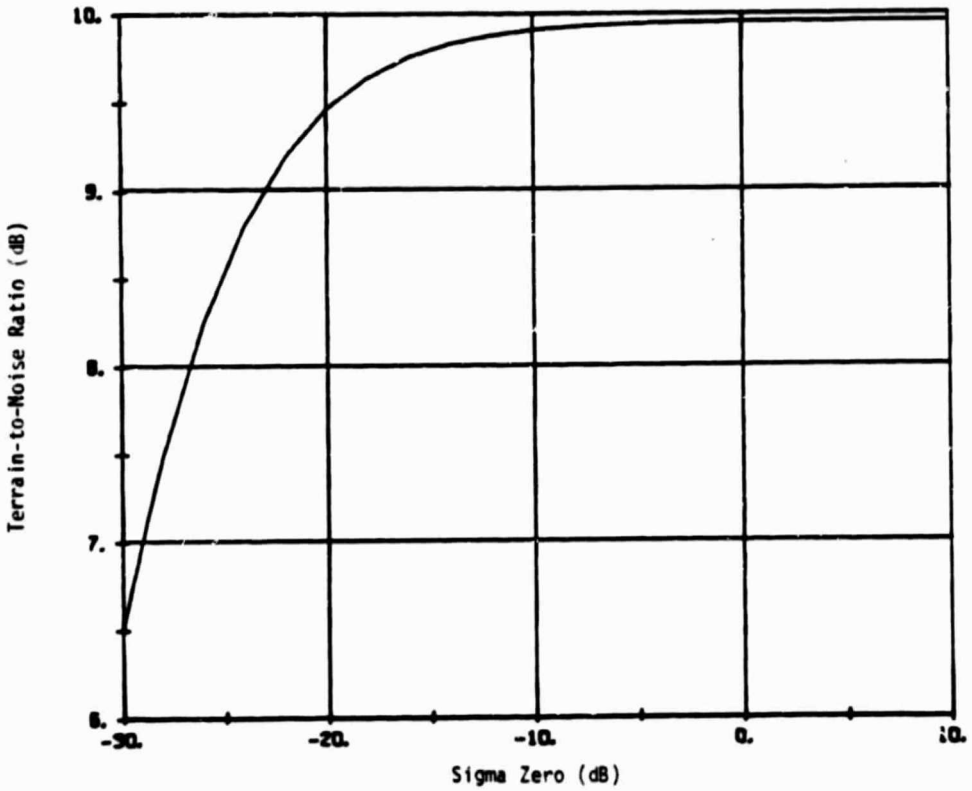

FIGURE 9.6. TNR VS σ_0 AT GROUND RANGE OF 23.5 KM AT L-BAND.

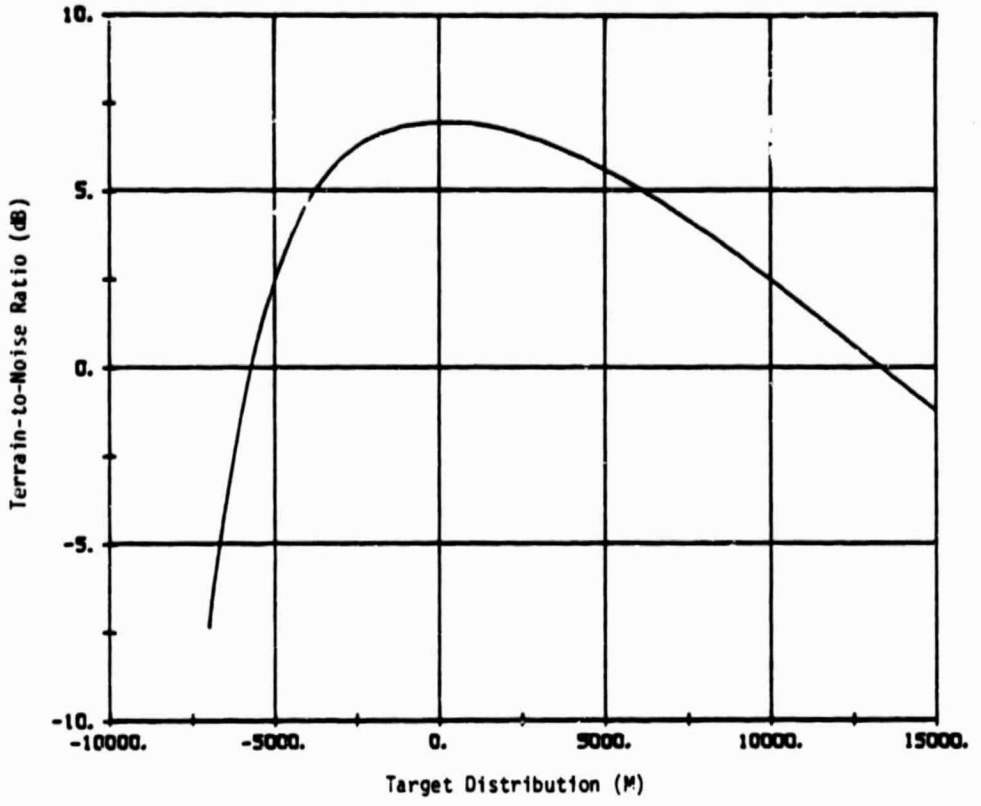

FIGURE 9.7. TNR ALONG THE RANGE DIRECTION WITH σ_o = -30 dB AT X-BAND.

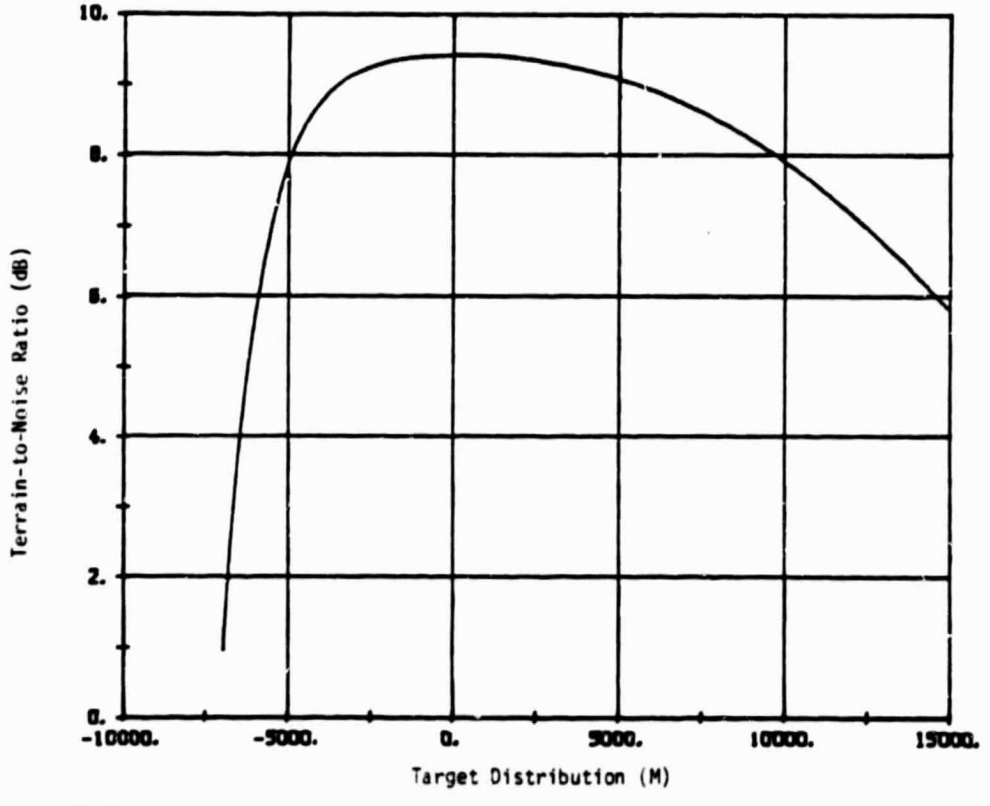

FIGURE 9.8. TNR ALONG THE RANGE DIRECTION WITH σ_o = -30 dB AT L-BAND.

10
CONCLUSIONS AND RECOMMENDATIONS

In this report, we have presented a review of SAR calibration technology, including a general description of the primary calibration techniques and some of the factors which affect the performance of calibrated SAR systems. The use of reference reflectors for measurement of the total system transfer function along with a calibration signal generator for monitoring of receiver to processor output temporal variation is a practical approach for SAR calibration. However, preliminary error analysis and previous experimental measurements indicate that reflectivity measurement accuracies of better than ±3 dB will be difficult to achieve. This is not adequate for many applications and, therefore, improved end-to-end SAR calibration techniques are required.

It is clear that a number of investigations should be performed to prepare for future designs and applications of calibrated SAR systems:

1. Results from a general review of available calibrated SAR data indicate a trend for the backscatter from terrain, as determined from SAR data, to be greater than results obtained using other reflectivity measurement instrumentation, such as scatterometer and ground-range facilities. This conclusion is based only on a comparison of "similar terrain types" as reported in the literature. Clearly, there are factors that could reconcile these differences, such as roughness effects, moisture, and others. However, since the trend seems to prevail, it is recommended that a careful verification experiment be defined and conducted to resolve this apparent discrepancy. The experiment should provide for the simultaneous gathering of data from a test area with a calibrated SAR system and with other instrumentation, such as a scatterometer, etc. The plan outlined by Fenner, et al. [34]

describes such an experiment. Adequate reference reflectors must be included so as to provide additional verification.

2. A detailed, systematic analysis of the factors that affect calibrated SAR performance has not been done. It is important to establish a complete, statistical SAR system amplitude model so that the relationships between (1) various errors, total system noise, and nonlinearities and (2) reflectivity measurement accuracy (RMA), reflectivity measurement resolution (RMR), and reflectivity measurement precision (RMP) can be determined.

3. There is also a need for a practical set of measurement procedures to assess SAR performance in terms of RMA, RMR, and RMP. This will involve the design of test sites with appropriate reflectivity standards that are well characterized.

4. Improved reflectivity references are needed. In many situations involving the measurement of terrain backscatter coefficients, distributed or diffuse reflectors would be advantageous.

5. The use of a calibration signal generator has been common practice in most previous SAR calibration programs. The signal generator can be considered as a monitoring device to assure that temporal variations of the receiver/processor portion of the system are within acceptable bounds and/or it can be used as a key element in a calibration approach by facilitating the data reduction process when making absolute reflectivity measurements. That is, rather than explicitly including various gain settings and processor amplitude parameters, e.g., laser power in the case of optical processing or digital processing normalization constants, it is often convenient to use the calibration signals as references in the image data. In either case, the trade-off study of

the alternate forms of calibration signals should be performed. The types range from point-like signals to a two-dimensional distributed signal with a "black hole" in the center for system noise monitoring.

6. As described in this report, it is important to be able to perform in-flight measurements of the antenna gain as a function of position across the swath. An error analysis of the five techniques reviewed herein along with the development of improved techniques is needed.

7. The degree of calibration needed for various applications is not very well known at the present time. Therefore, utility studies and experiments to establish realistic calibrated SAR performance requirements should be performed.

8. A significant effort in terms of calibrated SAR data collection and calibration instrumentation design investigation is needed to prepare for the development of future SAR systems for earth resource applications. In order to properly support these experiments, a reliable, stable, and well-characterized SAR system is required. The U.S. Air Force SAR Test Bed, which will be flight tested in 1982, is highly recommended for this role.

9. Large, high-quality calibration test sites should be established in three different regions in the United States. These quasi-permanent facilities would be used for performance verification and for any necessary recalibration of the future calibrated spaceborne SAR systems that will be required for earth resource applications.

10. Finally, increased emphasis should be placed on the development of improved terrain reflectivity models. Experimental measurements cannot be made for all combinations of the many variables which affect microwave backscatter. Therefore, calibrated SAR measurements should be used primarily to validate reflectivity models.

REFERENCES

1. Active Microwave Workshop Report, NASA SP-376, Lyndon B. Johnson Space Center, NASA, 22-26 July 1974.

2. Proc. of the Snowmass Radar Geology Workshop, Snowmass, CO, NASA/U.S. Geological Survey, July 1979 (Pub. Jan. 1981).

3. Tomlinson, P.G., A Model for Space Radar Clutter, RADC-TR-79-166, Rome Air Development Center, Griffiss Air Force Base, New York, June 1979.

4. Brindley, A.E., Overland Radar Technology Program: Analysis and Integration, ITT Research Institute, A.F. Systems Command, A.S.D., Final Report, Contract F33615-69-C-1387, AD 888 639L, June 1971.

5. Clutter Model for AEW Radar Design, NADC-AE-6633.

6. MacDonald, H.C., and W.P. Waite, "Imaging Radars Provide Terrain Texture and Roughness Parameters in Semi-Arid Environments," Mod. Geol., Vol. 4, No. 2, pp. 145-158, 1978.

7. Ulaby, F.T., J. Cihlar, and R.K. Moore, Active Microwave Measurement of Soil Water Content, CRES TR-177-46, Center for Research in Engineering Science, Univ. of Kansas, November 1973.

8. Newton, R.W., S.L. Lee, J.W. Rouse, Jr., and J.F. Paris, "On the Feasibility of Remote Monitoring of Soil Moisture with Microwave Sensors," Proc. of the Ninth International Symposium on Remote Sensing of Environment, Vol. I, Univ. of Michigan, April 1974, pp. 725-738.

9. Kauth, R.J., R.C. Cicone, and W.A. Malila, "Procedure M: A Framework for Stratified Area Estimation," 1980 Machine Processing of Remotely Sensed Data Symposium Record.

10. Fukunaga, K., Introduction to Statistical Pattern Recognition, Academic Press, New York, 1972.

11. DeLoor, G.P., and A.A. Jurrieens, The Radar Backscatter of Vegetation, AGARD, Propagation Limitations in Remote Sensing, pp. 12.1-12.7, June 1971.

12. Ulaby, F.T., T.F. Bush, P.P. Batlivala, "Radar Response to Vegetation--II: 8-18 GHz Band," Trans. IEEE, Vol. AP-23, September 1975, p. 608.

13. Bush, T.F., F.T. Ulaby, and T. Metzler, Radar Backscatter Properties of Milo and Soybeans, Univ. of Kansas Center for Research, Inc., RSL Tech. Memo 177-52, Lawrence, Kansas, October 1975.

14. Bush, T.F., and F.T. Ulaby, "Variability in the Measurement of Radar Backscatter," IEEE Trans. on Ant. and Prop., Vol. AP-24, No. 6, November 1976, p. 896.

15. Ulaby, F.T., and T.F. Bush, "Monitoring Wheat Growth with Radar," Photogrammetric Engineering and Remote Sensing, Vol. 42, No. 4, April 1976.

16. Hardy, N.E., J.C. Coiner, and W.O. Lockman, "Vegetation Mapping with Side-Looking Airborne Radar: Yellowstone National Park," AGARD Conf. on Prop. Limitations in Remote Sensing, Colorado Springs, CO, June 1971.

17. Flumerfelt, L.R., "Summary of Results of a Recent Sea Clutter Measurement Program," Trans. IEEE Ant. and Prop., Vol. AP-27, May 1979, p. 416.

18. BEal, R.C., P.S. DeLeonibus, and I. Katz (eds.), Spaceborne Synthetic Aperture Radar Imagery for Oceanography, Johns Hopkins Univ. Press, Baltimore, MD, 1981.

19. Gonzalez, F.I., R.C. Beal, W.E. Brown, P.S. DeLeonibus, J.W. Sherman, J.F.R. Gower, D. Lichy, D.B. Ross, C.L. Rufenach, and R.A. Shuchman, "Seasat Synthetic Aperture Radar: Ocean Wave Detection Capabilities," Science, 204, 1979, pp. 1418-1421.

20. Jones, W.L., and L.C. Schroeder, "Radar Backscatter from the Ocean: Dependence on Surface Friction Velocity," Boundary-Layer Meteorol., 13, 1978, pp. 133-149.

21. Ross, D.B., and W.L. Jones, "On the Relationship of Radar Backscatter to Wind Speed and Fetch," Boundary-Layer Meteorol., 13, 1978, pp. 151-163.

22. Shuchman, R.A., R.F. Rawson, and E.S. Kasischke, Analysis of Synthetic Aperture Radar Ocean Wave Data Collected at Marineland and Georges Bank, ERIM Report No. 123000-11-F, 1977.

23. Luther, C.A., and R.A. Shuchman, "Sea Ice Detectability as a Function of Resolution and Mixed Integration," To be published in the Proceedings of the SURSAT Workshop (held in Toronto, June 1980).

24. Hawkins, R.K., et al., "Single and Multiple Parameter Microwave Signatures of Sea Ice," Sixth Canadian Symposium on Remote Sensing, Halifax, May 1980 (to be published).

25. Deeker, C.V., R.G. Onstatt, and R.K. Moore, Radar Scatterometer Measurements of Sea Ice Remote Sensing Laboratory Center for Research Inc., The University of Kansas, RSL Technical Report No. TR 331-17, August 1980.

26. Gray, A.L., R.O. Ramsier, and W.J. Campbell, "Scatterometer and SLAR Results Obtained Over Arctic Sea-Ice and Their Relevance to the Problems of Arctic Ice Reconnaissance," Fourth Canadian Symposium on Remote Sensing, Quebec City, May 1977, pp. 424-443.

27. Onstott, R.G., et al., Radar Backscatter Study of Sea Ice, Remote Sensing Laboratory, Center for Research, Inc., The University of Kansas, RSL Technical Report No. RSL-TR-331-14, February 1980.

28. Larson, R.W., et al., "The Use of SAR Systems for Iceberg Detection and Characterization," Proceedings of the Twelfth International Symposium on Remote Sensing of Environment, ERIM, Ann Arbor, 1978, pp. 1127-1148.

29. Ketchum, R.B., An Evaluation of ERIM X-L Band Airborne Synthetic Aperture Radar Imagery of Sea Ice, NORDA Technical Note 28.

30. Larson, R.W., J.D. Lyden, R.A. Shuchman, and R.T. Lowry, Determination of Backscatter Characteristics of Sea Ice Using SAR Data, ERIM Final Report 142600-1-F, ONR, Arctic Programs, Contract No. N00014-79-C-0690, March 1981.

31. Harger, R.O., Synthetic Aperture Radar Systems, Academic Press, New York, 1970.

32. Larrowe, B.T., and R.W. Bayma, An Experiment to Show the Effects of Hardlimiting Video Signals in SAR, Report No. 37000-29-T, Radar and Optics Div., Willow Run Laboratories, University of Michigan, May 1972.

33. Held, D.N., and N.C. Mehta, "Amplitude Calibration of Synthetic Aperture Radars: The Effects of Nonlinearities," 1981 International Geoscience and Remote Sensing Symposium, June 1981.

34. Fenner, R.G., S.C. Reid, and G.G. Schaber, "An Unconventional Approach to Imaging Radar Calibration," Proc. of the 1978 Synthetic Aperture Radar Technology Conf., NMSU, Los Cruces, New Mexico, March 1978.

35. Stubenrauch, C.F., and A.C. Newell, "Some Recent Near-Field Antenna Measurements at NBS," Microwave Journal, Vol. 22, No. 11, November 1980, pp. 37-42.

36. Carver, K.R., and A.C. Newell, "SAR Antenna Calibration Techniques," Proc. of the Synthetic Aperture Radar Technology Conference, Los Cruces, NM, March 8-10, 1978, pp. II-3-1 to II-3-17.

37. Results reported in Section 6 of this report were obtained largely from work supported by (1) Air Force Avionics Laboratory, Contract AFAL-TR-44-239, November 1974 and (2) DARPA, with technical monitoring by MIT, Lincoln Laboratory, Purchase Order BX-309, February 1979-June 1980.

38. Brown, W.M., and C.J. Palermo, Random Processes, Communications, and Radar, McGraw-Hill, 1969, pp. 244-285.

39. Goldman, S., Frequency Analysis, Modulation, and Noise, McGraw-Hill, 1948, pp. 102-108.

40. Bayma, R.W., Development of a Statistical SAR IPR and Clutter Response Model, ERIM Report No. ASP-80-277, May 1980.

41. Max, J., "Quantizing for Minimum Distortion," IRE Transactions on Information Theory, Vol. IT-6, March 1960, pp. 7-12.

42. Bayma, R.W., Development of a Quantization Noise Model for SAR Video and Image Data, ERIM Report No. ASP-80-267, May 1980.

43. Kurtenbach, A.J., and P.A. Wintz, "Optimum Quantization," IEEE Transactions on Aerospace and Electronic Systems, (Supplement), Vol. AES-3, No. 6, November 1967, pp. 563-580.

44. Kurtenbach, A.J., and P.A. Wintz, "Quantizing for Noisy Channels," IEEE Transactions on Communications, Vol. COM-17, April 1969, pp 291-302.

45. Gray, G.A., and G.W. Zeoli, "Quantization and Saturation Noise Due to Analog-to-Digital Conversion," IEEE Transactions on Aerospace and Electronic Systems, Vol. AES-7, January 1971, pp. 222-223.

46. Gersho, A., "Quantization," IEEE Communications Society Magazine, Vol. II, No. 5, September 1977, pp. 16-29.

47. Li, F., D. Held, B. Huneycutt, and H. Zebku, "Simulation and Studies of Spaceborne SAR Image Quality with Reduced Bit Rate," 15th International Symposium on Remote Sensing of Environment, Ann Arbor, MI, May 1981.

48. Mood, Graybill, and Boes, Introduction to the Theory of Statistics, McGraw-Hill.

49. Reference Data for Radio Engineers, ITT, New York, Sixth Edition, 1968.

50. Bean, B.R., E.J. Dutten, and D.D. Warner, "Weather Effects on Radar," Chapter 24 from M.I. Skolnik's Radar Handbook, McGraw-Hill, New York 1970.

51. Precipitation, Clouds, and Aerosols, Chapt. 5 from Handbook of Geophysics and Space Environments, Cambridge Research Laboratories, U.S. Air Force, 1965.

52. Solomon, I., Estimated Frequencies of Specified Cloud Amounts Within Specified Ranges of Altitude, Tech. Rpt. 167, Air Weather Service, U.S. Air Force, 1963.

53. Povejsil, D.J., R.S. Raven, and P. Waterman, Airborne Radar, Boston Technical Publishers, Cambridge, MA, 1965.

54. Haddock, F.T., Scattering of Attenuation of Microwave Radiation through Rain, Report of NRL Progress, June 1956.

55. Nathanson, F.E., Radar Design Principles, McGraw-Hill, New York, 1969.

56. Radio Meteorology, U.S. National Bureau of Standards Monograph 92, U.S. Government Printing Office, 1966.

57 Guinard, N.W. The NRL Four-Frequency Radar System, NRL Report 6806, Naval Research Laboratory, Electronics Division, November 1968.

58. Calibration of an Airborne X-Band Radar for Measurements of Terrain Radar Returns, AN/APS-79 (XH-4) Radar Set, Goodyear Aerospace Corporation, Litchfield Park, Arizona, June 1966, AD 373 947 L.

59. Radar Calibration Study, Westinghouse Defense and Space Center, Aerospace and Electronic Systems Division, Baltimore, Maryland, prepared for U.S.A. Engineering Topographic Laboratory, February 1970, AD 508 966.

60. Amplitude Calibration Techniques Applied to the Environmental Research Institute of Michigan's Airborne Synthetic Aperture Radar System, ERIM, Radar and Optics Division, Ann Arbor, Michigan, Technical Report AFAL-TR-74-239, November 1974.

61. Radar Clutter Data Collection, Calibration, Digitization, and Analysis, ERIM, Radar and Optics Division, Ann Arbor, Michigan, Technical Report AFAL-TR-79-1232, December 1979.

62. Shuchman, R.A., A. Klooster, J.D. Lyden, and C.L. Liskow, Engineering Evaluation of ERIM-Generated SEASAT SAR Data, ERIM, Radar and Optics Division, Ann Arbor, Michigan, Report No. 151400-1-I, February 1981.

63. "Honeycutt Memos," Jet Propulsion Laboratory, Calif. Inst. of Tech., Pasadena, Calif., July 1979.

64. Shuttle Imaging Radar (SIR) Calibration Study, Final Report, Radar Systems Group, Hughes Aircraft Co., Culver City, California.

65. Calibration of the ERIM X-L SAR, Program Conducted 1978-1981, DARPA, Lincoln Laboratory Technical Monitor.

66. Preliminary Functional Requirements Document for Advanced SAR System, 20 June 1980 (prepared by JPL).

Appendix A

CALIBRATION OF SYNTHETIC APERTURE RADAR

R. W. Larson, R. E. Hamilton, and F. L. Smith
Environmental Research Institute of Michigan

Capt. J. C. Haynes
AFWL/ARAO Kirtland AFB
New Mexico 87117

Paper presented at the
1981 International Geoscience and Remote Sensing Symposium

June 8-10, 1981
Washington, D.C.

CALIBRATION OF SYNTHETIC APERTURE RADAR*

R.W. Larson, R.E. Hamilton, and F.L. Smith
Environmental Research Institute of Michigan
Ann Arbor, Michigan 48107

Capt. J.C. Haynes**
AFWL/ARAO Kirtland AFB
New Mexico 87117

Introduction

In the design of radar detection systems, an often-used measure of system performance is the probability of detection for a target of specified cross section. For most radar applications, cultural objects are the targets of interest. However, the energy scattered to the radar antenna from the target must compete with energy scattered from the terrain that is included within the resolution element surrounding the target. The latter energy is referred to as a clutter signal return and the probability of detection is a function of the magnitude and the statistics of this clutter return.

For other applications, the clutter return becomes the signal of interest. For example, in remote sensing work, it is the "clutter" energy scattered from the sea, ice, or land that must be received, classified, and interpreted to yield information.

For both areas of application, the characteristics of the radar clutter and the return from cultural targets, as measured with a synthetic aperture radar (SAR), become more valuable if the system is calibrated so as to provide absolute values of radar cross section.

Demonstration SAR Calibration Program

This paper briefly discusses a program whose objectives were to (1) calibrate a synthetic aperture radar (SAR), (2) collect amplitude-calibrated SAR clutter data from a variety of terrain areas, and (3) perform a statistical analysis on these data. This work was carried out by the Environmental Research Institute of Michigan (ERIM), under the sponsorship of the Air Force in cooperation with personnel of the Air Force Avionics Laboratory (AFAL). Additional details on the program can be found in References 1, 2, and 3.

---

*This effort was supported under Air Force Contract Nos. F33615-70-C-1433, F33615-72-C-1817, F33615-75-C-1034, and F33615-79-C-1820.

**WPAFB, Dayton, Ohio during the period this work was conducted.

ERIM's airborne X-band SAR system was calibrated and operated at 9.3 GHz for the data-collection phase of this program. This radar was flown in a C-131B aircraft on bailment to ERIM from the Air Force.

Calibration Techniques and System Design

The calibration techniques and instrumentation discussed here were developed under a program in which ERIM conducted an investigation to provide an amplitude calibration for ERIM's airborne SAR system; details of that program can be found in Reference 4.

Calibration of the radar system requires an accurate determination of the overall system transfer function K_n which relates radar cross section σ to output image intensity I_o, as follows:

$$\sigma = K_n I_o,$$

where K_n is the overall system transfer function applicable to each data set n (data flight or digital tape). Two techniques are used to measure K_n:

One of these techniques consists of imaging reference targets having various known values of backscattering cross section. The accuracy of this method depends upon the precision to which (1) the cross sections σ of the reference targets are known and (2) the output images of the targets can be measured [1, 4]. In this program, two identical arrays were used in order to provide calibrated references at different ranges; both arrays were located in the same vicinity (the Willow Run Airport area).

Using calibration reflectors, the complete system transfer function K_n is measured at the range and depression angle at which the reflectors are imaged. In each array, six values of σ were utilized which ranged from 0 dBsm (1 m^2) to 50 dBsm (10^5 m^2) in 10-dB steps. Three targets of each size, except for the single 50 dBsm reflector, were provided.

The other technique involves the use of a reference signal generator whose output signal simulates the radar return from a point target. This signal is generated by the same source that provides the chirp pulse to the radar transmitter and is injected into the receiver (Figure 1); it has the following characteristics: (1) the range (chirp) modulation, the pulse width, and the pulse repetition frequency (PRF) are identical to those transmitted, (2) the azimuth signal (Doppler history) is identical to that which would be received from the target at the selected range within the illuminated swath, and (3) the signal level at the injection point corresponds to that which would result from the target on the ground whose cross section is being simulated. Achievement of the correct power level requires accurate information about the measurement geometry, the antenna response, the transmitted power, and the values of

various system losses [1, 4]. The signal generator can be used to provide a measure of the system transfer function from the antenna's terminals to the output imagery. In this work, the signal generator provided signals to simulate received signals from two different ranges and two aircraft velocities only.

The reference-target technique has the advantage of providing a direct measurement of the overall radar system transfer function and the disadvantage that the reference targets must be set out on the ground and must be convenient to the areas being imaged by the radar. On the other hand, the reference-generator technique has the advantage of always being with the radar, but the disadvantage of measuring directly only a partial-system transfer function. With accurate measurement of the radar antenna pattern and the system transmission-line losses to the receiver, the reference-generator technique is satisfactory after verification of calibration using information from the reference-target measurements.

Note in Figure 1 that the receiver employs two channels; the reason is to increase the overall linear dynamic range of the system. The low-gain channel images strong targets without saturating while the high-gain channel images weak targets well above the noise.

Results from the calibration program [4] showed that the basic error in the amplitude calibration of the ERIM SAR system is 5 dB, which is one standard deviation for five independent measurements of a reference-target array. During the data-gathering program, one recording of the reference-target array was supplemented with three recordings of signal-generator calibrations on most of the signal films; this procedure resulted in a 7-dB standard deviation.

In addition, a mean-value shift of 9 dB was observed between the two calibration techniques, i.e., the reference targets produce lower output power than the signal generator for the same received power at the antenna. It is believed that the reference-target calibrations were correct and that the most probable source for this systematic error was the use of an incorrect value of antenna gain in the calculations related to the reference-generator calibration. Therefore, 9 dB have been subtracted from the signal-generator values used in plotting the calibration curves; in this way, the reference targets were used to calibrate the signal generator. The resulting values have standard deviations of 5 and 7 dB, as discussed above.

Collection and Analysis of Calibration Data

Both the reference-target and reference-generator calibration techniques were used on every data flight. The reference targets were imaged at the beginning and end of each flight; calibration signals from the reference signal generator were recorded at intervals during the flight.

The reference signal generator measures the partial-system transfer function K_R (from the receiver input through the output imagery). This can be converted to the overall-system transfer function K_η by considering the geometry, antenna response, etc. This function is defined by the following equation [1]:

$$K_n = \frac{(4\pi)^3 R^4 K_R}{P_t \lambda^2 G^2 L\, e^{-\alpha R}} \quad ,$$

where R = range,
P_t = transmitter power (peak),
λ = wavelength,
G = antenna gain,
L = system losses, and
α = propagation path attenuation factor.

The system transfer function K_R includes the system from the antenna terminals, where the calibration signal generator is mounted, to the output imagery. Thus, the factor K_R includes the following:

(1) transfer function for receiver antenna terminal to mixer output,

(2) transfer function for video amplifier,

(3) transfer function for recorder and film development process,

(4) transfer function for optical processor,

(5) range compression factor, and

(6) azimuth compression factor.

In addition, the calibration is a function of depression angle due to the antenna's elevation pattern [1, 4]. Therefore, to relate the calibration data to a specific depression angle, the values for the total power per resolution element, P_T, must be multiplied by an appropriate correction factor.

The calibrated SAR data were processed in the AFAL computer facilities to obtain distributions of backscatter for values of depression angle between approximately 7 and 20 degrees. Examples of the distributions or histograms are shown in Figures 2–4; examples for three depression angles are given. Figure 2 shows histograms for farmland areas in central Ohio. Figure 3 histograms are for snow-covered areas in central Michigan. Finally, an example of a combined histogram from the two receiver channels for an urban area is given in Figure 4.

Conclusions

Calibration of a SAR system has been demonstrated and limited data have been obtained with the calibrated X-band SAR system.

The major contributors to error are believed to be (1) uncertainties in absolute value of antenna response, (2) uncertainties in reference calibration reflection, and (3) variations in SAR signal processing. Values of σ_0 are in general agreement with data obtained from similar terrain types as reported in the literature. Best correlation occurs in the upper bounds of the average of 36 published data curves.

References

1. R.W. Larson and W. Carrara, Measurements of X-Band Clutter Statistics with Amplitude-Calibrated Radar, Report No. AFAL-TR-74-44, Environmental Research Institute of Michigan, Ann Arbor, June 1974, AD 530 492L.
2. R.W. Larson, A. Klooster, W. Bradford, and W. Carrara, Measurements of X-Band Clutter Statistics with Amplitude-Calibrated Radar, Supplement 1, Report No. AFAL-TR-74-44-Suppl. 1, Environmental Research Institute of Michigan, Ann Arbor, January 1976, AD B010 498L.
3. Capt. J.C. Haynes, R.W. Larson, et al., Radar Clutter Data Collection, Calibration, Digitization, and Analysis, Report No. AFAL-TR-79-1232, Environmental Research Institute of Michigan, Ann Arbor, December 1979.
4. R.W. Larson, et al., Amplitude Calibration Techniques Applied to the Environmental Research Institute of Michigan's Airborne Synthetic Aperture Radar System, Report No. AFAL-TR-74-239, Environmental Research Institute of Michigan, Ann Arbor, November 1974, AD 532 027L.

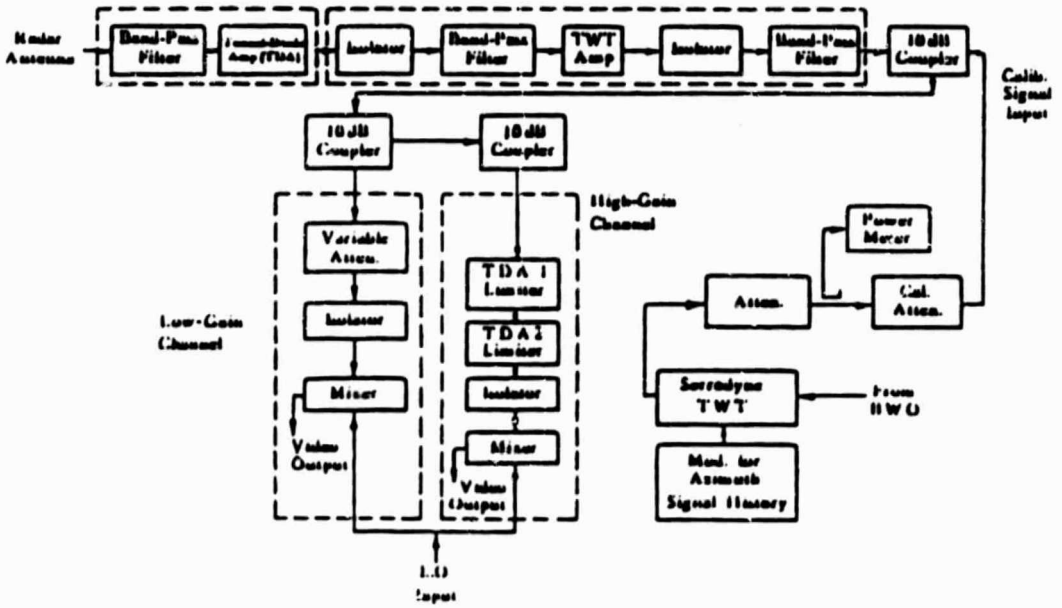

FIGURE 1. X-BAND SAR CALIBRATION RECEIVER.